Doctoral theses at NTNU, 2017:205

Mohammad Ostadi

New and Innovative Conceptual Designs of Gas-to-Liquid Processes

Doctoral thesis

Mohammad Ostadi

ISBN 978-82-326-2482-9 (printed ver.)
ISBN 978-82-326-2483-6 (electronic ver.)
ISSN 1503-8181

NTNU
Norwegian University of
Science and Technology

NTNU
Norwegian University of Science and Technology
Thesis for the Degree of
Philosophiae Doctor
Faculty of Natural Sciences
Department of Chemical Engineering

Doctoral theses at NTNU, 2017:205

NTNU
Norwegian University of
Science and Technology

Mohammad Ostadi

New and Innovative Conceptual Designs of Gas-to-Liquid Processes

Thesis for the Degree of Philosophiae Doctor

Trondheim, July 2017

Norwegian University of Science and Technology
Faculty of Natural Sciences
Department of Chemical Engineering

NTNU
Norwegian University of
Science and Technology

NTNU
Norwegian University of Science and Technology

Thesis for the Degree of Philosophiae Doctor

Faculty of Natural Sciences
Department of Chemical Engineering

ISBN 978-82-326-2482-9 (printed ver.)
ISBN 978-82-326-2483-6 (electronic ver.)
ISSN 1503-8181

Doctoral theses at NTNU, 2017:205

Printed by NTNU Grafisk senter

Abstract

A gas-to-liquid (GTL) process is one where natural gas is converted to synthetic fuels and other products. Our main focus is on the conversion of natural gas to liquid fuels by means of Fischer-Tropsch synthesis (FTS). In addition the possibility of integrating ammonia production with FT process is investigated. FTS is a commercial technology that allows converting synthesis gas, a mixture of CO and H_2, into fuels and chemicals.
The objective is to improve profitability by increasing the energy and carbon efficiencies through better process design, operation and integration. There is also a great incentive to reduce the investment cost in order to make such plants profitable at higher natural gas prices. This process could be one of the players in the reduction of our dependency on oil.
Conceptual design of a once-through GTL plant is performed which is suitable for placement on a Floating Production, Storage and Offloading (FPSO). Almost in all GTL plants that use autothermal reformer (ATR), pure oxygen is used as oxidant. In our design, enriched-air is proposed to be used instead. Two different membrane technologies are applied to produce enriched-air and separate H_2 from CO_2. FT reactor staging with product cooling and separation is performed in the design which resulted in increased production of heavy hydrocarbons. One of the distinguishing features of this design compared to other designs is that natural gas feed passes through two parallel paths: one for production of syngas and one for H_2 production. The produced H_2 is partly injected between stages and partly sent to product upgrading. H_2 injection between stages will increase the production of heavy hydrocarbons. The proposed process is self sufficient in terms of water and power, therefore can be used in remote locations.
In order to increase the profitability of the proposed GTL process, co-generation of ammonia with GTL products is investigated. In this process, without any change to the GTL process and with addition of a few extra equipment, co-generation of ammonia is achieved. This process is still self-sufficient with water and power. The estimated total capital investment of the combined GTL-ammonia process is about 900 million USD of which the ammonia process alone constitutes only 7%.
Having accurate kinetic models is very important in process simulation and results will depend on the choice of kinetic model used. Therefore it is vital to have kinetic models that correctly capture major variations in reaction rate subject to process conditions. In order to find a suitable model for the FT reaction, a kinetic model structure is regressed to microchannel experimental data of Yang et al. (2016). The fitted models for reaction rate and chain growth predict the reaction rate and selectivities to CH_4 and C_{5+} quite well.
The syngas production step is one of the most costly steps in a GTL plant. It is common practice to use oxygen as oxidant in the reforming step. However, by the introduction of microchannel reactors with their remarkable heat transfer characteristics, high active catalyst site exposure to reactants and therefore high once-through conversions, the use of enriched-air maybe justified. To test this hypothesis, comparison is done in the use of enriched-air versus pure oxygen in the reforming step of a GTL plant utilizing an ATR, while microchannel reactors are used in the once-through Fischer-Tropsch step. Pure oxy-

gen is provided by a cryogenic Air Separation Unit (ASU) and enriched-air by use of air separation membranes. By using pure oxygen less FT reactor volume is required which means lower reactor cost at the expense of having a costly cryogenic ASU. The estimated operating cost of ASU is lower than air membrane, while its installed cost is higher. Due to safety and space issues of having a cryogenic ASU offshore, the only viable option is the use of enriched-air, while in an onshore setting, the use of oxygen is more attractive.
Finally, systematic staging or the path optimization method of Hillestad (Hillestad, 2010) is applied on the Fischer-Tropsch synthesis with microchannel reactors. Optimization is done on the total reactor volume of the FT synthesis and the volume distribution between stages, in addition to hydrogen distribution and coolant temperature. The productivity is maximized subject to constraints on a maximum reactor temperature and a minimum conversion. Considerable reduction of reactor volume is obtained through path optimization.

To my parents and teachers for their love,
support and encouragement

Acknowledgements

This is not the end. It is not even the beginning of the end.
But it is the end of the beginning.
(Winston Churchill)

This thesis is submitted in partial fulfillment of the requirements for the degree of Doctor of Philosophy (PhD) at the Norwegian University of Science and Technology (NTNU). The research has been conducted at the Department of Chemical Engineering (IKP) from January 2014 to May 2017. The work has been funded by the Norwegian Research Council (GASSMAKS, 10403101), for which I am truly grateful.
I wish to express my sincere gratitude to my supervisor professor Magne Hillestad for his continuous support of my PhD study, for his patience, motivation, trust and guidance. His open door routine made him always available for discussions and help. I really enjoyed working with him in process simulation area where I gained from his knowledge and personal ethics. I have always been more inspired to continue my work after leaving his office.
I want to thank Dr. Erling Rytter for his insight, fruitful discussions during our meetings and his positive view on every problem. Thanks to Olaf Trygve Berglihn at SINTEF for his help with SUNDIALS (SUite of Nonlinear and DIfferential/ALgebraic Equation Solvers) and insightful comments.
I would like to thank professor Hilde Venvik and associate professor Jia Yang for their help with experimental data.
I had the privilege to work with master students for their master thesis which was a great learning experience: Kristoffer Moen, Martin Falkenberg, Marco Galimberti, Kristin Dalane, Morten Thomas Emhjellen, Mathias Lundgeren, Helene Florence Amndine Bour and Cathrine Ro Heuch.
Special thanks to my office mate Dr. Cristina Perinu for sharing the office and all the small chats and nice time.
My sincere thanks to my colleagues at the chemical engineering department for making my stay at NTNU memorable: Putta, Georgious, Eirini, Ida, Kristin, Ricardo, Seniz, Ardi, Sofia, Ingvild, Rosa, Hammad, Usman Shoukat, Usman Muhammad, Ram, Øystein, Luca, Diego and Gabreil.
At last but not least, I would like to thank my parents and my siblings for their unconditional love and support.

Mohammad Ostadi
Trondheim, May 2017

Contents

List of Tables

List of Figures

Notation

Acronyms

Symbol	Description
ACM	Aspen Custom Modeller
ASF	Anderson-Shultz-Flory distribution
ASU	Air Separation Unit
ATR	Auto-thermal Reformer
BCM	Billion Cubic Meters
C++	A general-purpose programming language
C#	A general-purpose programming language
CAER	Center for Applied Energy Research
COLaN	The organization for the management of the CAPE-OPEN standards
CSTR	Continuous Stirred-Tank Reactor
DLL	Dynamic Link Library
DME	Dimethyl Ether
EDF	Extension Definition File
FPSO	Floating Production, Storage and Offloading
FTS	Fischer-Tropsch Synthesis
GPU	Gas Permeation Unit
GTL	Gas to Liquid
HER	Heat Exchange Reformer
HP	High Pressure Steam
HTFT	High Temperature Fischer-Tropsch
LH	Langmuir-Hinshelwood
LHV	Lower Heating Value
LNG	Liquefied Natural Gas
LP	Low Pressure Steam
LPG	Liquefied Petroleum Gas
LTFT	Low Temperature Fischer-Tropsch
MeOH	Methanol
MP	Medium Pressure Steam
NPV	Net Present Value
PFR	Plug Flow Reactor
POX	Partial Oxidation
PRISM	Commercial name for a membrane product
PSA	Pressure Swing Adsorption
ROI	Return On Investment
RWGS	Reverse Water-Gas-Shift
SMR	Steam Methane Reforming
SQP	Sequential Quadratic Programming
SRK	Soave-Redlich-Kwong equation of state

USD	United States Dollar
VB	Visual Basic
WGS	Water-Gas-Shift reaction
WHSV	Weight Hourly Space Velocity

Symbols (Latin)

Symbol	Description	Dimention
a	Catalyst activity	–
a	Specific area of heat transfer	$\mathrm{m}^2/\mathrm{m}^3$
a_i	Component activity	–
A_R	Cross sectional area of tube	m^2
B	Dimensionless parameter	–
B_{bed}	Dimensionless parameter related to catalyst bed	–
B_c	Dimensionless parameter	–
B_p	Dimensionless parameter related to catalyst particle	–
C_5^+	Lump of hydrocarbon components containing 5 or more carbon atoms	–
$c_{p,i}$	Heat capacity at constant pressure of component i	$\mathrm{kJ}/(\mathrm{kg\,K})$
$\bar{c}_p$	Average heat capacity at constant pressure	$\mathrm{kJ}/(\mathrm{kg\,K})$
D_p	Particle diameter	m
D_t	Diameter of tube	m
diag()	Diagonal matrix	–
E	Activation energy	$\mathrm{kJ/mol}$
f_i^0	Reference fugacity taken to be 1 atm	atm
f_i	Component fugacity	atm
h	Enthalpy	$\mathrm{kJ/kg}$
$\mathscr{H}$	Scaling parameter for the lumps of components	–
h_{ext}	Heat transfer coefficient of cooling water	$\mathrm{kW}/(\mathrm{m}^2\,\mathrm{K})$
h_w	Heat transfer coefficient of boundary layer inside the tube	$\mathrm{kW}/(\mathrm{m}^2\,\mathrm{K})$
K_a	Equilibrium constant in terms of activities	–
K_i	Equilibrium constants	Varying
k_i	Kinetic constants	Varying
L	Length of channels	m
M_i	Molecular weight of component i	$\mathrm{g/mol}$
n	Carbon number	–
$\bar{n}$	Average carbon number of lump	–
N	Dimensionless parameter	–
N_c	Number of components	–
N_{chan}	Number of channels in microchannel reactor	–
Nu	Nusselt number	–
p_i	Partial pressure of component i	bar or MPa
Pr	Prandtl number	–
$\dot{Q}$	Heat flow	kW
R	Universal gas constant	$\mathrm{kJ}/(\mathrm{kmol\,K})$
$\widetilde{R}$	Reaction rate on mass basis	$\mathrm{kg}/(\mathrm{m}^3\,\mathrm{s})$

r	Reaction rate on molar basis	$\mathrm{kmol}/(\mathrm{m}^3\,\mathrm{s})$
r_p	Propagation rate of chain growth	–
r_t	Termination rate of chain growth	–
Re_p	Reynolds number of particle	–
S	Vacant site fraction	–
S_{c_i}	Selectivity to C_i	–
S/C	Steam to carbon ratio	–
s_w	Tube wall or channel wall thickness	m
T	Reactor temperature	K
$\bar{T}$	Average temperature	K
T_{NB}	Normal boiling point temperature	$^\circ\mathrm{C}$
U	Overall heat transfer coefficient	$\mathrm{kW}/(\mathrm{m}^2\,\mathrm{K})$
U_1	Stoichiometric usage ratios of hydrogen in paraffin production	–
U_2	Stoichiometric usage ratios of hydrogen in olefin production	–
u_{A}	Catalyst dilution design function	–
u_{c}	Catalyst type design function	–
u_{F}	Feed distribution design function	–
u_g	Gas velocity	$\mathrm{m/s}$
u_{H}	Heat exchange area distribution design function	–
u_{M}	Mixing design function	–
u_{p}	Pressure profile design function	–
u_{T}	Temperature of coolant design function	–
V	Volume	m^3
W	Mass flow rate	$\mathrm{kg/s}$
W_0	Mass flow rate at the inlet of reactor	$\mathrm{kg/s}$
w_i	Mass fraction of component i	–
X_{CO}	CO conversion	–
x_{F}	Extra feed composition/temperature distribution design function	–
x_n	Mole fraction of component n	–

Symbols (Greek)

Symbol	Description	Dimention
α	Propagation probability or chain growth probability	–
α_1	Propagation probability for paraffin production	–
α_2	Propagation probability for olefin production	–
α_{M}	Propagation probability for methane production	–
α_{H}	Highest value of α in reactor conditions	–
α_{L}	Lowest value of α in reactor conditions	–
β	Heat transfer area design function	$\mathrm{kg}/(\mathrm{m}^3\,\mathrm{s})$
γ	Dimensionless mass flow rate relative to the inlet ($W/W0$)	–
ϵ_{bed}	Bed's void fraction	–
θ	Dimensionless temperature	–
λ^0	Thermal conductivity at zero flow	$\mathrm{W}/(\mathrm{m}\,\mathrm{K})$
λ_f	Fluid thermal conductivity	$\mathrm{W}/(\mathrm{m}\,\mathrm{K})$
λ_G	Thermal conductivity of gas	$\mathrm{W}/(\mathrm{m}\,\mathrm{K})$
λ_p	Particle thermal conductivity	$\mathrm{W}/(\mathrm{m}\,\mathrm{K})$
λ_r	Effective radial thermal conductivity	$\mathrm{W}/(\mathrm{m}\,\mathrm{K})$
μ_g	Viscosity of gas	cP
$\nu_{i,j}$	Stoichiometric coefficient of component i in reaction j	–
ν_ℓ	Stoichiometric coefficient of a lump	–
ξ	Dimensionless volume of the path ($\frac{V}{V_{\mathrm{t}}}$)	–
ρ_g	Density of gas	kg/m^3
σ	Residence time or space time ($V_{\mathrm{R}}/W-0$)	$\mathrm{m}^3\,\mathrm{s}/\mathrm{kg}$
ϕ	Relative distribution between lumps of components	–

Chapter 1

Introduction

In this chapter a general introduction to GTL process is provided.

1.1 Gas to Liquid conversion

Huge amounts of associated gas are flared daily worldwide. The total gas volume flared yearly is estimated at 143 ($\pm$13.6) billion cubic meters (BCM), corresponding to 3.5% of global production (Elvidge et al., 2016). Figure 1.1 depicts the spatial distribution of natural gas (NG) flaring in 2012. Moreover, there are vast amounts of stranded gas reserves which are unused mainly because of being located in far away places. Converting NG to liquid products, such as liquified natural gas (LNG), FT products, ammonia, etc. is one option in utilizing these reserves (Figure 1.2). In this thesis, the main focus is on FT and ammonia processes. As shown in Figure 1.3, syngas, which is a mixture of H_2 and CO, is the main ingredient in the production of many chemicals such as Methanol (MeOH), Dimethyl ether (DME) and liquid fuels (C_nH_m).

1.2 Main steps in a GTL plant

There are three main steps in a GTL plant, which are shown in Figure 1.4: synthesis gas (syngas) production, FT synthesis and product upgrading. These steps are explained in the next sections.

1.3 Syngas production technologies

Syngas, a mixture of H_2 and CO, can be produced from any carbon-based feedstock (hydrocarbons, coal, petroleum coke, biomass). Among all, the lowest cost routes to syngas

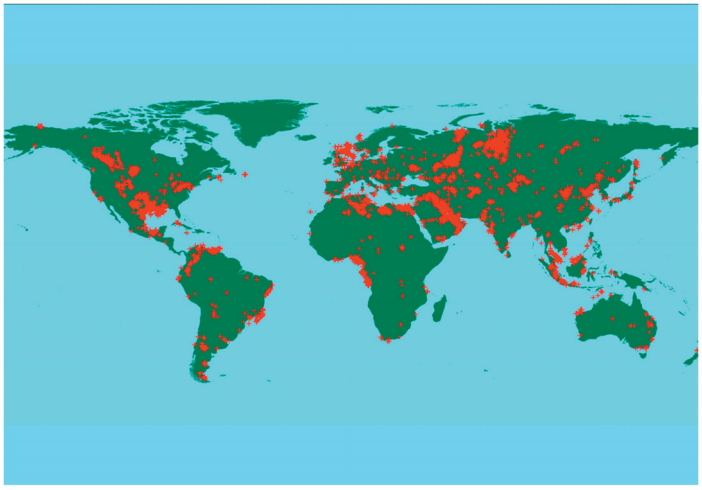

Figure 1.1: Spatial distribution of natural gas flaring in 2012 (Elvidge et al., 2016)

so far are based on natural gas (Wilhelm et al., 2001).

Sulfur removal, adiabatic pre-reforming and main reforming are the main steps in the syngas production. Depending on the carbonaceous feedstock and the applications of the syngas, there are different methods of producing syngas: catalytic steam methane reforming (SMR), two-step reforming, autothermal reforming (ATR), partial oxidation (POX), and heat exchange reforming. Advantages and disadvantages of each technology are shown in Table 1.1. Wilhelm et al. (2001) suggest that two-step reforming and ultimately ATR should be the technologies of choice for large-scale GTL plants. The choice of syngas production method influences the downstream equipment in terms of equipment sizes, compression requirement and heat integration of the plant. In our design, ATR and Heat Exchange Reformer (gas heated reformer) are used for syngas and hydrogen productions, respectively.

If there are heavier hydrocarbons present in the feed, a pre-reformer is used. In the pre-reformer all heavier hydrocarbons than methane are converted to CO, H_2, CH_4 and CO_2. Depending on the process that requires syngas, different H_2/CO ratios may be required. Table 1.2 shows the means and techniques to alter the syngas composition. Approximate variation in H_2/CO ratio that can be achieved by using these techniques are shown in Table 1.3.

1.4 Fischer-Tropsch synthesis

In Fischer-Tropsch synthesis, syngas is converted to a wide range of hydrocarbon products including paraffins, olefins, oxygenates, etc.

Table 1.1: Comparison of syngas generation technologies with natural gas feed (Wilhelm et al., 2001)

Technology	Advantages	Disadvantages
SMR	Most extensive industrial experience Oxygen not required Lowest process temperature requirement Best H_2/CO ratio for hydrogen production applications	H_2/CO ratio often higher than required when CO also is to be produced Highest air emissions
Heat exchange reforming	Compact overall size and footprint Application flexibility offers additional options for providing incremental capacity	Limited commercial experience In some configurations must be used in tandem with another syngas generation technology
Two-step reforming	Size of SMR is reduced Low methane slip favors high purity syngas applications Syngas methane content can be tailored by adjusting secondary reformer outlet temperature	Increased process complexity Higher process temperature than SMR Usually requires oxygen
ATR	Natural H_2/CO ratio often is favorable Lower process temperature requirement than POX Low methane slip Syngas methane content can be tailored by adjusting reformer outlet temperature	Limited commercial experience Usually requires oxygen
POX	Feedstock desulfurization not required. Absence of catalyst permits carbon formation and therefore operation without steam significantly lowering syngas CO_2 content Low methane slip Low natural H_2/CO ratio is an advantage for applications requiring ratio$<$2.0	Low natural H_2/CO ratio is a disadvantage for applications requiring ratio$>$2.0. Very high process operating temperatures Usually requires oxygen High temperature heat recovery and soot formation/handling adds process complexity Syngas methane content is inherently low and not easily modified to meet downstream processing requirements

Table 1.2: Techniques for adjusting syngas H_2/CO ratios (Wilhelm et al., 2001)

	Decreases ratio	Increases ratio
Recycle CO_2	*	
Import CO_2	*	
Remove H_2 via membrane	*	
Remove CO_2		*
Increase steam		*
Add shift converter		*

Table 1.3: Approximate variation in H_2/CO ratio for natural gas feed (Wilhelm et al., 2001)

	SMR	Two-step reforming*	ATR	POX
Import CO_2 or remove H_2 via membrane	$<$3.0	$<$2.5	$<$1.6	$<$1.6
Total CO_2 recycle	3	2.5	1.6	1.6
No CO_2 recycle	5	4	2.65	1.8
Increase steam	$>$5.0	$>$4.0	$>$2.65	$>$1.8
Add shift converter	∞	$>$5.0	$>$3.0	$>$2.0

* SMR followed by oxygen-blown secondary reforming

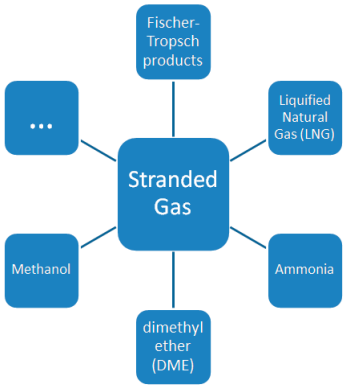

Figure 1.2: Monetization options of stranded gas reserves

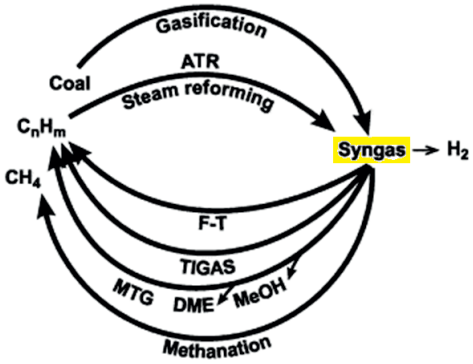

Figure 1.3: Syngas cycle (Rostrup-Nielsen, 2002)

1.4.1 Kinetics

Numerous reaction rate expressions are suggested for FTS in literature. In chapter 5, a review of some of these rate expressions is provided. In our process simulations, focus has been on rate expressions by Todic et al. (2014a, 2015) and Ma et al. (2014) which are described in chapter 3.

1.4.2 Catalysts

Some of the transition metals are active in FTS. The following order for transition metals is found by Vannice (1977) considering the average molecular weight of produced hydrocarbons: Ru $>$ Fe $>$ Co $>$ Rh $>$ Ni $>$ Ir $>$ Pt $>$ Pd. The last three metals, Pd, Pt, and Ir mainly produce methane. Ni is a methanation catalyst and does not have the broad selectivity of the other FT catalysts. Ru has very high activity and quite high selectivity for producing high molecular weight products at low temperatures. It is the most expensive

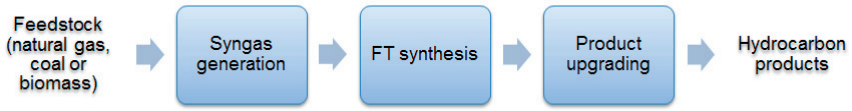

Figure 1.4: Three main sections in a GTL plant

FTS catalyst. Fe is very active and has water-gas-shift (WGS) activity. It has stronger tendency than Co and Ni to produce carbon deposits (Spath & Dayton, 2003). Co catalysts are used for Low temperature FTS. Our focus has been on cobalt catalyst, due to it's high selectivity towards heavier hydrocarbons and low WGS activity.

1.4.3 Chain growth

The product distribution from the Fischer-Tropsch synthesis is often described by the Anderson-Schulz-Flory (ASF) distribution (Figure 1.5), where the distribution is given by a single parameter; the chain growth probability or growth factor (α). According to ASF distribution, FTS product distribution can be mathematically represented by the following equations (Anderson et al., 1951):

$$x_n = (1-\alpha)\alpha^{n-1} \tag{1.1}$$

$$\frac{w_n}{n} = \frac{(1-\alpha)^2}{\alpha}\alpha^n \tag{1.2}$$

$$\ln\frac{w_n}{n} = \ln\frac{(1-\alpha)^2}{\alpha} + n\ln\alpha \tag{1.3}$$

where n is the number of carbon atoms in the product, x_n the mole fraction of product containing n carbon atoms, w_n the weight fraction of product containing n carbon atoms. The chain growth model, α, is described as:

$$\alpha = \frac{r_p}{r_p + r_t} \tag{1.4}$$

Where r_p is the chain propagation rate, and r_t is the chain termination rate. According to ASF distribution, the plot of $\ln(w_n/n)$ versus n is linear. However, methane and ethylene tend not to follow the ideal ASF distribution, and must be given special attention. In addition, the distribution may be characterized by two different values of α, which can be explained by two different active sites on the catalyst. The usual deviations from ASF distribution are (Todic et al., 2014b): a higher-than-expected yield of methane, a lower-than-expected selectivity to ethylene and a higher-than-expected yield of heavy hydrocarbons due to an increase in chain growth probability with carbon number. The propagation probability is a function of the reactor temperature, pressure and concentrations. In order to reduce the production of light products, it is desirable that the propagation probability be as high as possible.

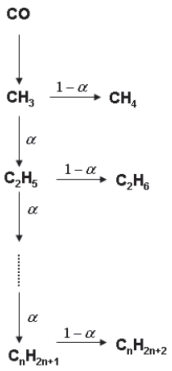

Figure 1.5: Chain growth to hydrocarbons in FT reaction

Table 1.4: Properties for different reactor types for Low-Temperature Fischer-Tropsch synthesis (Rytter & Holmen, 2015)

Reactor	Conversion per path (%)	Capacity per reactor (bbl/day)	Characteristics
Tubular fixed bed	30-35	6000	30,000 tubes with catalyst pellets or extrudates
Slurry bubble column	55-65	25000	Internal heat exchanger and optional product filter
Microchannel	65-75	1000	Metal block with $<$2 mm diameter channels

1.4.4 Reactors for Fischer-Tropsch Synthesis

There are two main types of FT reactors in commercial use today:

1. Tubular fixed bed
2. Slurry bubble column

Microchannel reactors are not in commercial use yet, but are gaining more and more attention in academia and industry. If this technology fully come into practice, it will make today's small natural gas reserves as well as stranded gas reserves a viable option for small scale GTL plants. Velocys and Compact GTL are leading companies in commercializing microchannel technology.

There are two main approaches for doing Fischer-Tropsch synthesis: High Temperature Fischer-Tropsch (HTFT) and Low Temperature Fischer-Tropsch (LTFT). In HTFT, there is no liquid outside the catalyst and in case of using fluidized bed reactors, formation of liquid will cause loss of fluidization and serious problems for catalyst particles. In HTFT, CO_2 can be consumed in the Reverse-Water-Gas-Shift (RWGS) reaction, which is an advantage. In LTFT, iron catalysts or supported cobalt catalysts may be used while for HTFT only fused iron catalysts are used (Jager, 1997). The properties of different reactor types used for LTFT are shown in Table 1.4. In fixed bed reactors once-through conversion is limited to 30-35% to avoid the danger of temperature runaway (Rytter & Holmen, 2015).

In slurry reactors, catalyst particles are suspended in the liquid hydrocarbon product of the FT process. Gaseous components leave from the top of the reactor. Heavier products have to be separated from the bottom of the reactor. Methods of separating products from the catalysts can be classified into several categories: Use of filtration, settling devices, magnetic separation and hydrocyclones (Rytter & Holmen, 2015). A major challenge to the catalyst in a slurry operation is any upset in production such as a sudden reduction in syngas flow which can lead to catalyst settling and serious overheating (Rytter & Holmen, 2015). The slurry bubble column reactor has a better heat transfer capacity, while the separation of liquid from the solid catalyst may be a problem. Fixed bed reactors are not suitable for HTFT operations. This is because of the danger of tube blockage by carbon deposition at higher temperatures. Large number of tubes and therefore heavy weight of the reactor can be considered a disadvantage for fixed bed reactor. The largest production capacity proposed for a tubular reactor is about 6000 bbl/day of product while for fluidized bed reactors it is 25000 bbl/day. This can also be considered a disadvantage for fixed bed. On the othe side, there is no need for extra equipment to separate heavy wax from catalysts because the liquid trickles down the catalyst bed. In slurry reactors, wax must be separated by fine catalyst particles by additional equipment. Another important advantage with fixed bed reactor is that the performance of commercial reactors can be predicted based on the performance of a single tube pilot plant reactor. In case of catalyst poisons in the syngas, slurry reactor is more prone to the danger of catalyst deactivation than the fixed bed reactor. Catalyst replacement in fixed bed reactors is more challenging than in slurry reactors in the sense that it needs to be offline and lengthy downtime is required. Other advantages of slurry reactors over fixed bed reactors include (Steynberg et al., 2004):

1. Lower cost compared to fixed bed;
2. Lower pressure drop;
3. Lower catalyst consumption compared to fixed bed;
4. Near to isothermal operation;
5. The possibility of online addition of catalyst.

1.4.5 Product upgrading

The upgrading unit is made to crack and isomerize the linear hydrocarbons from the FT synthesis. Moreover, saturation of alkenes to alkanes will take place. Due to cracking there will be a production of lighter components. Separation of the different products is by distillation where a stream of light gas, mainly LPG (Liquefied Petroleum Gas), will be recycled. The isomerized products have very high quality fuel and lubrication properties (Bouchy et al., 2009). A separate hydrogen plant will normally be required for hydrogen used by the hydro-treating reactor and the sulphur removal unit. One reason for having a separate hydrogen plant is flexibility of operation.

Chapter 2

Thesis Overview

In this chapter an outline of the thesis including motivation and scope is presented. The contributions and a list of publications are given.

2.1 Motivation and contribution

Vast amounts of associated gas are flared daily and huge amounts of stranded gas reserves are untapped due to technical or economical reasons. Transforming Gas to Liquid (GTL) fuel is one option in monetizing stranded gas reserves or reduction of flaring. The main objective of the thesis is to increase profitability of the GTL process by increasing carbon and energy efficiencies of the process. There is also great incentive to reduce the investment cost of the process because it is a very capital intensive process. To monetize stranded gas reserves, reduce flaring and investment cost, a novel process concept utilizing microchannel FT reactors is proposed (**paper I**) which is suitable for placement on a Floating Production, Storage and Offloading (FPSO) vessel. The process is autonomous in the sense that it is self sufficient with power and water. The process concept is simple and inexpensive since cryogenic air separation and fired heaters are not required. For the Fisher-Tropsch synthesis, both the conventional shell and tube fixed bed reactors and microchannel reactors are considered and compared.

To have a correct kinetic model for the FT reaction in microchannel reactor, model fitting is performed (**paper II**) on microchannel FT experimental data. This data is taken from Yang et al. (2016). As a result, suitable kinetic and chain growth models are obtained. Since these models are fitted to microchannel experimental data, therefore they are specifically suited to microchannel reactors. These new models are implemented in the same process proposed in **paper I** while the reactor volume distribution is optimized by means of path optimization method of Hillestad (2010) and the results are reported in **paper III**. As a result considerable reduction of reactor volume is obtained.

To increase the profitability of the GTL process, cogeneration of ammonia is proposed in **paper IV**. Addition of ammonia production increased the investment cost by 7%, however, the revenue of the process can increase by as much as 50%.

Syngas production step is one of the most costly steps in a gas to liquid plant. It is a common practice to use oxygen as oxidant in the reforming step. However, by the introduction of microchannel reactors with their remarkable heat transfer characteristics, high active catalyst site exposure to reactants, and therefore high once-through conversions, the use of enriched-air maybe justified. In **paper V**, the merits of using enriched-air versus pure oxygen in the reforming step of the GTL plant is analysed.

Last paper is the application of the path optimization method of Hillestad (2010) on the FT process. The total reactor volume of the FT synthesis and the volume distribution between stages, in addition to hydrogen distribution and coolant temperature are optimized. The productivity is maximized subject to constraints on a maximum reactor temperature and a minimum conversion. Considerable reduction of reactor volume is obtained by path optimization.

2.2 Outline of the thesis

In chapter 1, a general introduction to GTL process is provided. In chapter 3, details of reactor modelling and reaction rate expressions used in the thesis are given. Papers produced in the course of the PhD work are provided in chapters 4 through 9. In the last chapter (chapter 10), conclusions of the thesis and some directions for future work are given.

2.3 Summary of the papers

2.3.1 Paper I

A novel process concept is proposed for converting natural gas to liquid Fischer-Tropsch products. An autothermal reformer with enriched air as oxidant is applied for synthesis gas (syngas) production, and because of the inert nitrogen a once-through Fischer-Tropsch synthesis is the preferred option. In order to maximize the syngas conversion and the production of heavy hydrocarbons, a staged reactor path with distributed hydrogen feed and product withdraw is proposed. The hydrogen is produced by steam methane reforming in a heat exchange reformer (gas heated reformer), heat integrated with the hot effluent stream from the autothermal reformer. Tail gas from the last Fischer-Tropsch stage is sent to a gas turbine for power production. The hot exhaust gas from the gas turbine is used for natural gas preheating. The process is autonomous in the sense that it is self sufficient with power and water, and therefore well suited for production in remote locations such as a floating production unit. The process concept is simple and inexpensive since cryogenic air separation and fired heaters are not required. For the Fischer-Tropsch synthesis, both the conventional shell and tube fixed bed reactors and microchannel reactors are considered and compared. The highlights of the paper are:

- A once-through design with staged FischerTropsch synthesis and with distributed hydrogen feed;
- Two parallel paths: one for syngas with slightly under-stoichiometric hydrogen and one for hydrogen;
- Comparing fixed bed and microchannel reactors for FT synthesis.

2.3.2 Paper II

In order to do a good and realistic design of a GTL plant, it is necessary to have kinetic models that correctly capture major variations of reaction rates and selectivities subject to changes in process parameters. In this paper, a review of published kinetic rate models is done and twelve of them are analyzed based on different criteria, such as their behaviour at high conversions, high water partial pressure, sensitivity to added water, selectivity to C_{5+} products, etc. The rate models are implemented in a plug flow reactor model. Both fixed bed and microchannel reactors can quite accurately be represented by such a model. Here, the main purpose is to see the kinetic effects with changing composition along the reactor. In order to predict the product distribution, we have proposed our own chain growth model and fitted parameters to experimental data from Yang et al. (2016). The chain growth model includes the effect of water and predicts the C_{5+} and methane selectivities quite well. The highlights of the paper are:

- A review of published kinetic rate models for cobalt catalyst is done;
- Twelve kinetic rate models are analyzed based on different criteria in a plug flow model;
- A new chain growth model is proposed and fitted to microchannel experimental data;
- The proposed chain growth model includes the effect of water and predicts C_{5+} and CH_4 selectivities quite well.

2.3.3 Paper III

Converting remote natural gas to liquid fuel is one possible solution to the problem of transporting remote gas to the energy market. However, the high investment cost of GTL plants prevents large scale exploitation of remote gas reserves. A lean GTL process, which is cost effective and less complex, is suggested based on an autothermal reformer with enriched air as oxidant and a once-through Fischer-Tropsch synthesis. In order to maximize the syngas conversion and the production of heavy hydrocarbons, a staged microchannel reactor path with distributed hydrogen feed and product withdraw is proposed. The hydrogen is produced by steam methane reforming in a heat exchange reformer (gas heated reformer). A verified kinetic model for the Fischer - Tropsch reactor is used. This kinetic model was fitted to kinetic data of a 40 %CO/Al_2O_3 catalyst which was used in a microchannel reactor. A new chain propagation model was also fitted to the data. The

new kinetic and chain propagation models are believed to be specifically suitable for microchannel reactors. The chain propagation model in the process yields high C_{5+} selectivities. The process is autonomous in the sense that it is self-sufficient with power and water. The highlights of the paper are:

- The verified kinetic and chain propagation models are implemented in FT reactor;
- Reactor volume distribution is optimized;
- Considerable reduction of volume is achieved compared to **paper I**.

2.3.4 Paper IV

A novel process concept is proposed for cogeneration of Fischer-Tropsch products and ammonia. An autothermal reformer with enriched air as oxidant is applied for synthesis gas production, and because of the inert nitrogen, a once-through Fischer-Tropsch synthesis is necessary. In order to maximize the synthesis gas conversion and the production of heavy hydrocarbons in Fischer-Tropsch reactors, a staged reactor path with distributed hydrogen feed and product withdraw is applied. Hydrogen is produced by steam methane reforming in a heat exchange reformer (gas heated reformer), heat integrated with the hot effluent stream from the autothermal reformer. Part of this hydrogen stream is used in Fischer-Tropsch reactors and the rest is sent to product upgrading and ammonia synthesis. Part of the nitrogen produced from the air membrane is used as feed to the ammonia process. The proposed ammonia process is simple as it does not require separate shift reactors and a CO_2 capture unit. The process is autonomous in the sense that it is self sufficient with power and water, and therefore well suited for production in remote locations such as a floating production unit. The total investment of 12000 bbl/d (57 tonnes/h) GTL plant combined with 24 tonnes/h ammonia plant is estimated to be around 900 million USD, of which the ammonia process counts only for 7 %. The extra ammonia production will increase total revenues by 50 %, which makes the combined process commercially attractive. The highlights of the paper are:

- The proposed process consists of a once-through and staged Fischer-Tropsch synthesis together with ammonia process;
- Two parallel paths; one for syngas with slightly under-stoichiometric hydrogen and one for hydrogen production;
- Nitrogen feed to ammonia process from air membrane while hydrogen feed is from hydrogen production path;
- Comparing the combined GTL and ammonia process with the GTL process alone, the total investment is increased by 7% while the plant revenue is increased by 50%.

2.3.5 Paper V

The syngas production step is the most costly step in a gas to liquid plant. It is common practice to use oxygen as oxidant in the reforming step. However, by the introduction of

microchannel reactors with their remarkable heat transfer characteristics, high active catalyst site exposure to reactants and therefore high once-through conversions, the use of enriched-air maybe justified. The purpose of this paper is to analyse the merits of using enriched-air versus pure oxygen in the reforming step of a gas to liquid plant utilizing an autothermal reformer (ATR), while microchannel reactors are used in the once-through Fischer-Tropsch (FT) step. Pure oxygen is provided by a cryogenic Air Separation Unit (ASU) and enriched-air by use of air separation membranes. To make the two cases comparable, the total once-through CO conversion is kept the same. By using pure oxygen less FT reactor volume is required which means lower reactor cost at the expense of having a costly cryogenic ASU to produce pure oxygen. The operating cost of ASU is lower than that of the air membrane, while its installed cost is higher. Due to safety and space issues of having a cryogenic ASU offshore, the only viable option is the use of enriched-air, while in an onshore setting, the use of oxygen is more attractive. The highlights of the paper are:

- Analyse the merits of using enriched-air or pure oxygen in the reforming step of a once-through GTL process which utilizes microchannel reactors for Fischer-Tropsch Synthesis;
- Cost estimation of the two cases;
- Conclusion regarding which oxidant to use in onshore and offshore settings.

2.3.6 Paper VI

In **paper I** we proposed a new process configuration for a once-through GTL plant suited for a floating production unit. In that work we did not optimize the reactor path of the Fischer-Tropsch synthesis. Here, we have optimized the total reactor volume of the FT synthesis and the volume distribution between stages, in addition to hydrogen distribution and coolant temperature. The productivity is maximized subject to constraints on a maximum reactor temperature and a minimum conversion. Considerable reduction of reactor volume is obtained by path optimization. The highlights of the paper are:

- Path optimization method of Hillestad (2010) is applied on the FT synthesis section of a GTL plant
- Considerable reduction of FT reactor volume is obtained by path optimization

2.4 Publications

2.4.1 Journal publications

I Ostadi, M, Dalane, K, Rytter, E, Hillestad, M, Conceptual design of an autonomous once-through gas-to-liquid process Comparison between fixed bed and microchannel reactors, *Fuel Processing Technology* , vol. **154**, (2015), pp. 186 - 195.

II Ostadi, M, Rytter, E, Hillestad, M, Evaluation of kinetic models for FischerTropsch cobalt catalysts in a plug flow reactor, *Chemical Engineering Research and Design*, vol. **114**, (2016), pp. 236 - 246.

III Ostadi, M, Hillestad, M, Conceptual design of an autonomous once-through gas-to-liquid process with microchannel Fischer-Tropsch reactors, *Chemical Engineering Transactions*, vol. **52**, (2016), pp. 523-528.

IV Ostadi, M, Hillestad, M, Combined gas-to-liquid and ammonia production, *Under review in journal of Natural Gas Science and Engineering*

V Ostadi, M, Hillestad, M, Enriched air or oxygen as oxidant for an onshore gas-to-liquid process with microchannel reactors, *Submitted to Chemical Engineering & Technology*

VI Ostadi, M, Hillestad, M, Path optimization of the Fischer-Tropsch synthesis with cobalt catalyst and microchannel reactors, *Planned for submission to Chemical Engineering Science*

2.4.2 Conference presentations

I Ostadi, M, Hillestad, M, Conceptual Design of an Autonomous Once-through Gas-to-Liquid (GTL) Process with Microchannel Fischer-Tropsch Reactors. 19th Conference on Process Integration, Modelling and Optimisation for Energy Saving and Pollution Reduction (PRES), Prague, Czech Republic, 2016.

II Ostadi, M, Hillestad, M, Verification of a macro kinetic model and development of a product distribution model for a commercial Co/Re/-Al2O3 Fischer-Tropsch catalyst in microchannel reactor. 22nd International Congress of Chemical and Process Engineering (CHISA), Prague, Czech Republic, 2016.

III Ostadi, M, Rytter, E, Hillestad, M, Conceptual design and cost estimation of an offshore autonomous once-through gas-to-liquid process combined with ammonia synthesis. 2017 AIChE Spring Meeting and 13th Global Congress on Process Safety, San Antonio, Texas, 2017.

Chapter 3

Reactor Modelling and Kinetics

In this chapter, reaction rate expressions used in the process simulations are presented. Details of reactor modelling and implementation in process simulator are also discussed.

3.1 Kinetic models

Having a correct kinetic model is vital for the development and simulation of a chemical process. The model should be able to explain the effects of temperature and composition on the reaction rates and selectivities. Considering the Fischer-Tropsch reaction, there are numerous kinetic models in the literature. In paper 2 in chapter 5, a review of the reaction rate expressions are provided and 12 rate expressions are compared. In paper 1 in chapter 4, reaction rate expression by Todic et al. (2014a, 2015) is used. In the rest of the papers, reaction rate expression by Ma et al. (2014) is used.

3.1.1 The Todic rate expression

This is a rigorous model that is based on experiments done in a stirred tank slurry reactor with a Re-promoted Co catalyst supported on alumina (25%Co /0.48%Re /Al_2O_3) over a range of operating conditions (T = 478, 493, 503 K; P = 1.5, 2.5 MPa; H_2/CO = 1.4, 2.1; WHSV = 1.022.5 NL/gcat/h) which fits to our design conditions (Todic et al., 2014a, 2015). Todic model describes individual rates for each component and introduces different growth factor for each polymerization step. In general the growth factors are functions of the vacant site fraction, S ,which again is a function of changing growth factors, making the model implicit. This makes the model complex and many iterations maybe required to reach the solution. Hillestad (2015) simplified the model without much loss of accuracy. The simplified model provides an accurate description of the overall consumption of CO and H_2 without calculating very many individual reaction rates. The production of alkanes

and alkenes are described by two chain growth probabilities and both increases slightly with the carbon number. The selectivities of methane and ethene are given by specific rate equations. In the Todic et al. (2014a, 2015) model and the simplified model, it is assumed that there is no chain limitation, which implies an infinite dimensional model. To implement a description of an infinite distribution of components, it is necessary to group components into lumps of components. The implementation of such a model is not straight forward and a method for handling infinite number of reactions and components is described by Hillestad (2015). Lumps of components and their average molecular weights are accurately described without violating the element balances. The FTS reaction with lumped components are given as:

$$\mathrm{CO} + U_1 \cdot \mathrm{H_2} \xrightarrow{r_1} \mathrm{H_2O} + \nu_{1,1}\mathrm{CH_4} + \nu_{2,1}\mathrm{C_2H_6} + \nu_{3,1}\mathrm{C_3H_8} + \nu_{4,1}\mathrm{C_4H_{10}} + \nu_{[5,\infty],1}\mathrm{C^p_{5+}} \quad (3.1)$$

$$\mathrm{CO} + U_2 \cdot \mathrm{H_2} \xrightarrow{r_2} \mathrm{H_2O} + \nu_{1,2}\mathrm{CH_4} + \nu_{2,2}\mathrm{C_2H_4} + \nu_{3,2}\mathrm{C_3H_6} + \nu_{4,2}\mathrm{C_4H_8} + \nu_{[5,\infty],2}\mathrm{C^o_{5+}} \quad (3.2)$$

$$\mathrm{CO} + 3 \cdot \mathrm{H_2} \xrightarrow{r_3} \mathrm{H_2O} + \mathrm{CH_4} \quad (3.3)$$

$$\mathrm{C_2H_4} + 2 \cdot \mathrm{H_2} \xrightarrow{r_4} 2\mathrm{CH_4} \quad (3.4)$$

r_1 and r_2 are paraffin and olefin production rates, respectively. r_3 and r_4 are to account for heigh yield of methane and low yield of ethylene, respectively. U_1 and U_2 are stoichiometric usage ratios of $\mathrm{H_2}$ in r_1 and r_2 and are given in Equations 3.5 and 3.6, respectively. The stoichiometric coefficients of products, $\nu_{i,1}$ and $\nu_{i,2}$, are given in Equations 3.7 and 3.8, respectively. The stoichiometric coefficients of lumps of components in r_1 and r_2 are given in Equations 3.9 and 3.10, respectively.

$$U_1 = 3 - \alpha_1 \quad (3.5)$$

$$U_2 = 2 + (1 - \alpha_2)^2 \quad (3.6)$$

$$\nu_{i,1} = (1 - \alpha_1)^2 \alpha_1^{(i-1)} \quad (3.7)$$

$$\nu_{i,2} = (1 - \alpha_2)^2 \alpha_2^{(i-1)} \quad (3.8)$$

$$\nu_{[5,\infty],1} = (1 - \alpha_1)\alpha_1^4 \quad (3.9)$$

$$\nu_{[5,\infty],2} = (1 - \alpha_2)\alpha_2^4 \quad (3.10)$$

The reaction rate expressions for the above reactions are given as (Hillestad, 2015):

$$r_1 = k_7 \sqrt{K_2 p_{\mathrm{H_2}}}[S]^2 \frac{\alpha_M}{(1 - \alpha_1)^2} \quad (3.11)$$

$$r_2 = k_8[S]\frac{\alpha_M}{(1-\alpha_2)^2} \tag{3.12}$$

$$r_3 = k_{7,M}\sqrt{K_2 p_{\mathrm{H_2}}}[S]^2\alpha_M - r_1\nu_{1,1} - r_2\nu_{1,2} - 2r_4 \tag{3.13}$$

$$r_4 = r_2\nu_{2,2} - k_{8,E}[S]\alpha_M\alpha_2 \tag{3.14}$$

$$[S]^{-1} = 1 + K_1 p_{\mathrm{CO}} + \sqrt{K_2 p_{\mathrm{H_2}}} + (\frac{1}{K_2^2 K_4 K_5 K_6}\frac{p_{\mathrm{H_2O}}}{p_{\mathrm{H_2}}^2} + \sqrt{K_2 p_{\mathrm{H_2}}})\frac{\alpha_M}{(1-\alpha_1)} \tag{3.15}$$

Where S is the vacant site fraction, k_i are reaction rate constants, K_i is the equilibrium constants and p_i is the partial pressure of component i. The reaction rate and equilibrium constants are calculated with the use of the Arrhenius equation with the estimated values from Todic et al. (2014a, 2015). The oxygenates products in the FTS are neglected in the model. The growth factor for alkanes, α_1, and for alkenes, α_2, are given in Equations 3.16 and 3.17, respectively. α_M is the growth factor for the methanation reaction.

$$\alpha_1 = \frac{1}{1 + \frac{k_7\sqrt{K_2 p_{\mathrm{H_2}}}}{k_3 K_1 p_{\mathrm{CO}}}} \tag{3.16}$$

$$\alpha_2 = \alpha_1 e^{-0.27} \tag{3.17}$$

$$\alpha_M = \frac{1}{1 + \frac{k_{7,M}\sqrt{K_2 p_{\mathrm{H_2}}}}{k_3 K_1 p_{\mathrm{CO}}}} \tag{3.18}$$

3.1.2 The Ma rate expression

The second reaction rate expression that is used in our process modelling is the CAER (Center for Applied Energy Research) empirical kinetic model. Ma et al. (2014) employed this kinetic model to study their experimental data over a 25%Co/Al_2O_3 catalyst using a 1 L continuously stirred tank reactor (CSTR) under the conditions of 205 °C - 230 °C, 1.4 - 2.5 MPa, H_2/CO = 1.0 - 2.5 and 3 - 16 NL/g-cat/h (X_{CO} = 7 - 54%). The model with their estimated parameters is given as:

$$-r_{\mathrm{CO}} = \frac{k(T)P_{\mathrm{CO}}^{-0.31}P_{\mathrm{H_2}}^{0.88}}{1 - 0.24\frac{P_{\mathrm{H_2O}}}{P_{\mathrm{H_2}}}} \tag{3.19}$$

The rate constant is given as:

$$k(T) = 0.0133\exp(-\frac{104000}{R}(\frac{1}{T} - \frac{1}{483})) \tag{3.20}$$

As is explained in more detail in chapter 5, this model is used for model fitting to the microchannel experimental data. The reason for using this model is because it made a good fit to the experimental data.

Table 3.1: Effects of an increase in process parameters on α

Parameter	α
Temperature	$\downarrow$
Pressure	$\downarrow$
H_2/CO	$\downarrow$
H_2O	$\uparrow$

3.1.3 Chain growth model

In order to perform an FT reactor design with realistic evaluation of the products produced, there is need for a way to quantify the product distribution. Some kinetic models include a description of product distribution. However, most of them need a chain growth model to account for that. Hydrocarbon selectivities depend on local conditions like temperature, pressure and species concentrations, in particular of carbon monoxide and hydrogen, but also on produced water. Therefore a suitable chain growth model should include these variables. The effect of some of the most important parameters affecting product selectivity are discussed thoroughly in literature by for example Van Der Laan & Beenackers (1999). In chapter 5, a new chain growth model is proposed which includes the effect of water and predicts the C_{5+} and methane selectivities quite well. The fitted model is:

$$\alpha = \frac{1}{1 + k_2(T)\frac{P_{\mathrm{H_2}}^{1.45}}{P_{\mathrm{CO}} P_{\mathrm{H_2O}}^{0.253}}} \tag{3.21}$$

$$k_2(T) = 0.0233 \exp(-1959(\frac{1}{T} - \frac{1}{483})) \tag{3.22}$$

The effects of temperature, partial pressures of H_2O, H_2 and CO are taken into account in this model as shown in Figure 3.1. The growth probability decreases slightly with increasing total pressure, and increases with increasing H_2O partial pressure. With an increase in the H_2/CO ratio, the growth factor decreases. The same behaviour is observed with increase in temperature.

3.1.4 Lumping of components

In theory, FTS can produce hydrocarbon chains with infinite number of carbon atoms. An appropriate method of handling this infinite number of components is to introduce lumps of components. We have chosen to model alkane components individually up to C_{10} and a lump C_{11+}^{p} describing the tail distribution. While for alkenes, with less heavier components, we have chosen to model individual components up to C_4 and a lump C_{5+}^{o}. The reason for having that many individual components is to get the phase equilibrium calculations more accurate.

In flowsheeting software, lumps are described as hypothetical components. These software expect hypothetical components to have fixed properties, like molecular weight, and it is not allowed to have changing properties which is the case for the lumps here. To overcome this problem, two different approaches were taken:

Table 3.2: Properties of lumps in the first approach

alpha	Carbon number	MW	T^*_{NB} (°C)
$\alpha_{1\mathrm{H}}$ =0.97	43.33	608.67	606.9
$\alpha_{1\mathrm{L}}$=0.9	20	282	343
$\alpha_{2\mathrm{H}}$=0.74	13.84	195.84	251.1
$\alpha_{2\mathrm{L}}$=0.68	13.25	185.75	237.7

* Normal boiling point temperature

First approach

In the first approach, each of the paraffin and olefin lumps was defined with two hypothetical components with fixed properties and a coefficient to define the relative distribution between them (Hillestad, 2015). For example, C^{p}_{11+} which represents the hypothetical group for paraffins with carbon numbers greater than 10, is defined by C^{pH}_{11+} and C^{pL}_{11+}. For olefin lump, C^{o}_{5+} is described by C^{oH}_{5+} and C^{oL}_{5+}. Carbon numbers of these new components are calculated with highest and lowest possible α values in the reactor conditions. Therefore the distribution of lumped components are related to the known components (namely C^{pH}_{11+}, C^{pL}_{11+}, C^{oH}_{5+}, C^{oL}_{5+}). Molecular weights are calculated according to the following relations:

$$\bar{M}_{C^{p}_{11+}} = 14.027 \cdot (11 + \frac{\alpha_1}{1-\alpha_1}) + 2.016 \tag{3.23}$$

$$\bar{M}_{C^{o}_{5+}} = 14.027 \cdot (5 + \frac{\alpha_2}{1-\alpha_2}) \tag{3.24}$$

By use of Asymptotic Behavior Correlations presented by Marano & Holder (1997), boiling point temperatures for these components were estimated which are shown in Table 3.2. In this table average carbon numbers for paraffins and olefins are calculated by Equations 3.25 and 3.26, respectively.

$$\bar{n}_{n,[11,\infty]} = 11 + \frac{\alpha_1}{1-\alpha_1} \tag{3.25}$$

$$\bar{n}_{n,[5,\infty]} = 5 + \frac{\alpha_2}{1-\alpha_2} \tag{3.26}$$

The conservation of mass requires that the stoichiometric coefficient of the lump, ν_ℓ, multiplied by the molecular mass of the lump remains the same. This is a simplification, but maybe a necessary simplification to be able to implement the model in a flowsheeting software.

$$\nu_\ell(\alpha)\bar{M}_n(\alpha) = \phi\nu_\ell(\alpha_{\mathrm{L}})\bar{M}_{n,\mathrm{L}}(\alpha_{\mathrm{L}}) + (1-\phi)\nu_\ell(\alpha_{\mathrm{H}})\bar{M}_{n,\mathrm{H}}(\alpha_{\mathrm{H}}) \tag{3.27}$$

From the above equation, the relative distribution, ϕ, can be calculated. This approach is used in chapters 4, 6 and 7.

Second approach

In the second approach, which is more accurate, the varying lump is defined with at least three different lumps with fixed properties. To clarify this point better, let's consider the general Fischer-Tropsch reaction:

$$\mathrm{CO} + U \cdot \mathrm{H_2} \xrightarrow{r_{\mathrm{FT}}} \nu_1 \mathrm{C}_1 + \nu_2 \mathrm{C}_2 + \nu_3 \mathrm{C}_3 + \nu_4 \mathrm{C}_4 + \bar{\nu}_{N+} \mathrm{C}_{N+} + \mathrm{H_2O} \tag{3.28}$$

Where:

$$\nu_i = (1-\alpha)^2 \alpha^{i-1} \tag{3.29}$$

$$\bar{\nu}_{N+} = (1-\alpha)\alpha^{N-1} \tag{3.30}$$

In this approach, the varying lump with varying properties, C_{N+}, is described with three different lumps with fixed properties: one lump from C_N to C_M, $\mathrm{C}_{[N-M]}$, the second lump from C_{M+1} to C_P, $\mathrm{C}_{[(M+1)-P]}$, and the third lump contains hydrocarbons with more than P number of carbon atoms, $\mathrm{C}_{[(P+1)-\infty]}$. The choice of N, M and P are arbitrary and can be different for paraffins and olefins. The conservation of mass requires that the stoichiometric coefficient multiplied by the molecular weight of the lump remains the same:

$$\bar{\nu}_{\mathrm{N+}}(\alpha)\bar{M}_{\mathrm{N+}}(\alpha) = \nu'_{[N-M]}(\alpha)M_{[N-M]} + \nu'_{[(M+1)-P]}(\alpha)M_{[(M+1)-P]} + \nu'_{[(P+1)-\infty]}(\alpha)M_{[(P+1)-\infty]} \tag{3.31}$$

where the stoichiometric coefficients of the new lumps are given as:

$$\nu'_{[N-M]} = \mathscr{H}(1-\alpha)(\alpha^{(N-1)} - \alpha^M) \tag{3.32}$$

$$\nu'_{[(M+1)-P]} = \mathscr{H}(1-\alpha)(\alpha^M - \alpha^P) \tag{3.33}$$

$$\nu'_{[(P+1)-\infty]} = \mathscr{H}(1-\alpha)\alpha^P \tag{3.34}$$

$\mathscr{H}$ is a scaling parameter and must be present to ensure mass balance. This is because of the simplification used for the molecular weight of the new lumps which are assumed constant. The average carbon number and consequently the molecular weight of the new lumps are calculated by assuming an average chain growth factor according to the reactor conditions. Average carbon numbers are calculated by the following relations (Hillestad, 2015):

$$\bar{n}_{n,[N,M]} = \frac{\sum_{i=N}^{M} i\alpha^{i-1}}{\sum_{i=N}^{M} \alpha^{i-1}} = \frac{N\alpha^{N-1} - (N-1)\alpha^N - (M+1)\alpha^M + M\alpha^{M+1}}{(1-\alpha)(\alpha^{N-1} - \alpha^M)} \tag{3.35}$$

$$\bar{n}_{n,[(P+1),\infty]} = (P+1) + \frac{\alpha}{1-\alpha} \tag{3.36}$$

Table 3.3: Properties of lumps in the second approach

Component Lumps	Carbon number	MW	T^*_{NB} (°C)
Paraffin1$_{[6-10]}$	7.834	111.672	121.25
Paraffin2$_{[11-20]}$	14.820	209.480	267.79
Paraffin2$_{[21-\infty]}$	32.500	457.0	470.44
Olefin1$_{[6-10]}$	7.323	102.525	103.32
Olefin2$_{[11-20]}$	13.043	182.597	233.69
Olefin3$_{[21-\infty]}$	23.333	326.667	385.55

* Normal boiling point temperature

By substituting Equations 3.32, 3.33 and 3.34 into 3.31, the unknown $\mathscr{H}$ will be calculated. In chapter 8, this approach is used and each of the lumps for paraffins and olefins is represented by three lumps of components with fixed properties. The properties of these lumps are calculated by use of Asymptotic Behavior Correlations presented by Marano & Holder (1997), which are shown in Table 3.3.

3.2 Plug flow reactor (PFR) model

In order to formulate the mathematical model for the PFR model, a short section of the reactor tube is analysed (Figure 3.1).

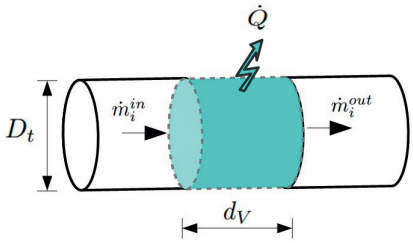

Figure 3.1: Control volume for a tubular reactor

The resistances to the inter-phase heat and mass transport are neglected, i.e. there are no fluid-to-particle heat and mass transfer resistances, and the plug flow model is described with a pseudo-homogeneous model. The reaction rates are expressed in terms of fluid-phase partial pressures and temperature. No axial and radial diffusion of mass and temperature is considered. The material balance over section dV in Figure3.1 is:

$$W(\omega_i^{in} - \omega_i^{out}) = \tilde{R}dV \tag{3.37}$$

Where $\tilde{R} = \Sigma_{j=1}^{N_r}(\nu_{i,j} r_j M_i)$, r_j is the reaction rate for reaction j on mole basis, N_r is the number of reactions taking place, $\nu_{i,j}$ is the stoichiometric coefficient, W is the total mass flow and ω_i is the mass fraction of component i. If the r_j is given based on the mass

of catalyst, it is necessary to multiply it with ρ_{bulk} which is the bulk density of the catalyst. The mass balance equation based on a differential volume will be:

$$W\frac{\mathrm{d}\omega_i}{\mathrm{d}V} = \tilde{R} \tag{3.38}$$

A heat balance is similarly derived to evaluate the temperature profile along the reactor. The energy conservation over a differential element dV of the reactor is:

$$\frac{\mathrm{d}Wh}{\mathrm{d}V} = -Ua(T - T_{cool}) \tag{3.39}$$

Where a is the specific area of heat transfer defined as $a = \frac{\mathrm{d}A}{\mathrm{d}V}$, U is the overall heat transfer coefficient and the enthalpy is defined as:

$$h = \Sigma_{i=1}^{N_c}(\omega_i h_i) = h^T\omega \tag{3.40}$$

where h and ω are vectors of component enthalpies and mass fractions, respectively and N_c is the number of components.

By applying the enthalpy definition into Equation 3.39:

$$\frac{\mathrm{d}Wh^T\omega}{\mathrm{d}V} = -Ua(T - T_{cool}) \tag{3.41}$$

By developing the differential:

$$h^T\frac{\mathrm{d}W\omega}{\mathrm{d}V} + W\omega^T\frac{\mathrm{d}h}{\mathrm{d}V} = -Ua(T - T_{cool}) \tag{3.42}$$

Knowing that component enthalpy is approximated by $h_i \sim c_{p,i}T$ and average heat capacity calculated by $\bar{c}_p = \Sigma\omega_i c_{p,i}$ and by substituting Equation 3.38:

$$h^T\tilde{R} + W\bar{c}_p\frac{\mathrm{d}T}{\mathrm{d}V} = -Ua(T - T_{cool}) \tag{3.43}$$

The first term is the heat of reaction and the second term is the sensible heat. The heat of reaction is defined as:

$$h^T\tilde{R} = \Sigma_i(H_i M_i)\Sigma_j(\nu_{i,j}r_j) = \Sigma_j(\Sigma_i\nu_{i,j}H_i M_i)r_j = \Sigma_j\Delta H_j r_j \tag{3.44}$$

The energy balance in the differential form will be:

$$W\bar{c}_p\frac{\mathrm{d}T}{\mathrm{d}V} = \Sigma_j(-\Delta H_j)r_j - Ua(T - T_{cool}) \tag{3.45}$$

For a cylindrical tube a is equal to $\frac{4}{D_T}$ where D_T is the tube diameter. Boiling water is used as coolant and its temperature is assumed to be constant.

3.2.1 Heat of reaction

Let's consider the following Fischer-Tropsch reaction:

$$\mathrm{CO} + U \cdot \mathrm{H_2} \xrightarrow{r_{\mathrm{FT}}} \mathrm{H_2O} + \nu_1 \mathrm{C_1} + \nu_2 \mathrm{C_2} + \nu_3 \mathrm{C_3} + \nu_4 \mathrm{C_4} + \nu_{5+} \mathrm{C_{5+}} \tag{3.46}$$

The heat of this reaction at 298 K is calculated by the sum of the heats of formation (ΔH_f^{298}) of products and subtraction of the heats of formation of reactants:

$$\Delta H_r^{298} = \Delta H_{f_{\mathrm{H_2O}}}^{298} + \nu_1 \Delta H_{f_{\mathrm{C_1}}}^{298} + \nu_2 \Delta H_{f_{\mathrm{C_2}}}^{298} + ... + \nu_n \Delta H_{f_{\mathrm{C_n}}}^{298} - \Delta H_{f_{\mathrm{CO}}}^{298} - U \Delta H_{f_{\mathrm{H_2}}}^{298} \tag{3.47}$$

$\Delta H_{f_{\mathrm{H_2}}}^{298}$ is zero because the standard enthalpy of formation of any pure element in its naturally occurring form is taken as zero. According to Chaumette et al. (1995), heat of formation of n-paraffins containing i number of carbon atoms at 298 K in (kcal/mol) can be expressed as:

$$\Delta H_{f_{\mathrm{C_i}}}^{298} = -4.89412i - 10.8527 \tag{3.48}$$

We can write it as:

$$\Delta H_{f_{\mathrm{C_i}}}^{298} = -ai - b \tag{3.49}$$

By substituting Equation 3.49 in Equation 3.47, we will have:

$$\Delta H_r^{298} = \Delta H_{f_{\mathrm{H_2O}}}^{298} + \Sigma_{i=1}^{\infty} \nu_i (-ai - b) - \Delta H_{f_{\mathrm{CO}}}^{298} \tag{3.50}$$

$$\Delta H_r^{298} = \Delta H_{f_{\mathrm{H_2O}}}^{298} + a\Sigma_{i=1}^{\infty} (\nu_i i) - b\Sigma_{i=1}^{\infty} \nu_i - \Delta H_{f_{\mathrm{CO}}}^{298} \tag{3.51}$$

The term $\Sigma_{i=1}^{\infty}(\nu_i i)$ is equal to one because of the carbon mass balance. Moreover, the term $\Sigma_{i=1}^{\infty}\nu_i$ can be shown to be equal to $(1-\alpha)$. Therefore the heat of reaction equation reduces to :

$$\Delta H_r^{298} = \Delta H_{f_{\mathrm{H_2O}}}^{298} + a - b(1-\alpha) - \Delta H_{f_{\mathrm{CO}}}^{298} \tag{3.52}$$

The heat of reaction at any temperature, T, can be found as the heat of reaction at 298 K plus the integral of the heat capacity as follows:

$$\Delta H_r^T = \Delta H_r^{298} - U \Delta H_{f_{\mathrm{H_2}}}^T + \int_{298}^{T} c_p(T) dT \tag{3.53}$$

where c_p are the heat capacities at constant pressure. Heat capacities of components involved in the reaction are taken from Perry's Chemical Engineers' handbook (Perry & Green, 2008) which are functions of temperature and are in the following form:

$$c_p = C_1 + C_2 [\frac{\frac{C_3}{T}}{\sinh(\frac{C_3}{T})}]^2 + C_4 [\frac{\frac{C_5}{T}}{\cosh(\frac{C_5}{T})}]^2 \tag{3.54}$$

Since the average reaction temperature in the reactor is assumed to be 220 °C (493 K), Equation 3.53 will result in:

$$\Delta H_{r_{\mathrm{paraffins}}}^{493} = -49.740231 + 12.053277\alpha_1 \tag{3.55}$$

Which has the units of (kcal/mol).

The heat of formation of olefins equation will result in the following form which also has the units of (kcal/mol):

$$\Delta H^{493}_{r_{\text{Olefins}}} = -18.18 - 18.516446\alpha_2 - 1.289277\alpha_2^2 \tag{3.56}$$

The reason for the difference in the structure of equations 3.55 and 3.56 is the difference in the stoichiometric coefficient of consumption of hydrogen in paraffin and olefin production, which are $(3-\alpha_1)$ and $(2+(1-\alpha_2)^2)$ for paraffins and olefins, respectively.

The heat of reaction for reactions 3.3 and 3.4 in (kcal/mol) are calculated as: $\Delta H^{493}_{r_3} = -51.383231$ and $\Delta H^{493}_{r_4} = -49.578134$, respectively.

3.2.2 Pressure drop

The most common pressure drop equation for flow through packed beds is that of Ergun & Orning (1949). It expresses the pressure drop along a fixed bed of particles as a function of gas properties such as density, ρ_g, viscosity, μ_g, and velocity, u_g, plus the bed's void fraction, ϵ_{bed} and particle diameter, D_p.

$$\frac{\mathrm{d}p}{\mathrm{d}V} = -(1.75 + 150\frac{(1-\epsilon)\mu_g}{\rho_g u_g D_p})\frac{\rho_g u_g^2}{D_p}\frac{1-\epsilon}{\epsilon^3}\frac{1}{A_R} \tag{3.57}$$

Where A_R is the cross sectional area of the tube.

3.2.3 Effectiveness factor

Due to diffusion there are concentration gradients and to some extent temperature gradient, inside a pellet. The effectiveness factor of a pellet, defined as the ratio between the integrated reaction rate over the pellet volume and the rate at bulk gas conditions, is normally less than unity. For a catalyst pellet of 3 mm diameter with homogeneous distribution of active sites, and with Todic et al. (2014a, 2015) kinetic model applied and diffusivities found by Erkey et al. (1990), the effectiveness is calculated to be 0.20-0.25 on average along the reactor for the main reaction formation of alkanes (reaction 3.1).

3.2.4 Heat transfer correlation

The system of resistances to heat transfer from catalyst bed to cooling water is shown in Figure 3.2. The overall heat transfer coefficient is calculated as the inverse summation of resistances:

$$\frac{1}{U} = R_{catalystbed} + R_{boundarylayer} + R_{metalwall} + R_{coolingwater} \tag{3.58}$$

$$\frac{1}{U} = \frac{D_T}{8\lambda_r} + \frac{1}{h_w} + \frac{s_w}{\lambda_w} + \frac{1}{h_{ext}} \tag{3.59}$$

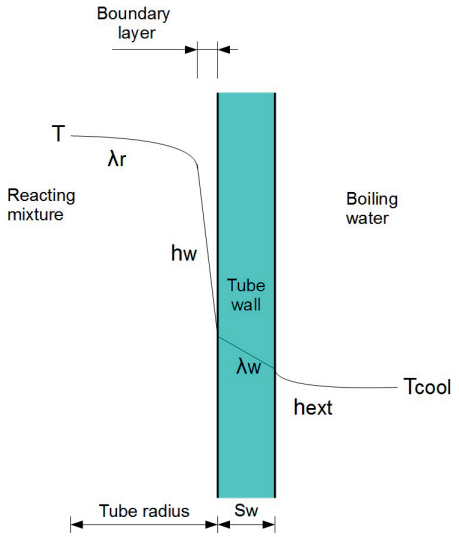

Figure 3.2: Heat transfer resistances for a tube

Resistances due to metal wall and cooling water are neglected, since they are considered to be negligible compared to the other terms. Therefore, the overall heat transfer coefficient is calculated as:

$$\frac{1}{U} = \frac{D_T}{8\lambda_r} + \frac{1}{h_w} \tag{3.60}$$

where λ_r and h_w are calculated with correlations found in Wen & Ding (2006).

$$Nu_w = 2.4\frac{\lambda^0}{\lambda_f} + 0.054(1 - \frac{D_p}{D_T})Re_p Pr^{\frac{1}{3}} \tag{3.61}$$

$$Nu_w = \frac{h_w D_p}{\lambda_f} \tag{3.62}$$

Where λ^0 is the thermal conductivity at zero flow and it is calculated with the following equation by Krupiczka (1967):

$$\frac{\lambda^0}{\lambda_f} = (\frac{\lambda_p}{\lambda_f})^n \tag{3.63}$$

Where λ_p is the particle thermal conductivity and n is an experimental constant related to the bed voidage, ϵ_{bed}, particle and fluid thermal conductivities by the following correlation:

$$n = 0.28 - 0.757 \log \epsilon_{bed} - 0.057 \log(\frac{\lambda_p}{\lambda_f}) \tag{3.64}$$

Fluid thermal conductivity (λ_f) is calculated by calling the built-in function of process simulator. Finally, the effective radial thermal conductivity, λ_r, is found by the following

correlation from Bey & Eigenberger (2001):

$$\frac{\lambda_r}{\lambda_f} = \frac{\lambda^0}{\lambda_f} + 0.1 Re_p Pr \tag{3.65}$$

3.2.5 Radial heat conduction

The radial temperature profile in the reactor tubes can be approximated by a quadratic polynomial of the form: $T(r) = a + br + cr^2$. In order to find the coefficients in the above polynomial expression, boundary conditions are required:

$$\left.\frac{\mathrm{d}T}{\mathrm{d}r}\right|_{r=0} = 0 \tag{3.66}$$

$$\left.\frac{\mathrm{d}T}{\mathrm{d}r}\right|_{r=R} = \frac{h_w(T_{r=R} - T_{cool})}{-\lambda_r} \tag{3.67}$$

Where λ_r is the effective radial conductivity, h_w is the heat transfer coefficient of the boundary layer between the core of the tube and its inner wall and R is the tube radius. From the first boundary condition, parameters b is found to be zero: $b = 0$ and the temperature equation reduces to:

$$T(r) = a + cr^2 \tag{3.68}$$

From the second boundary condition:

$$2cR = \frac{h_w(T_{r=R_T} - T_{cool})}{-\lambda_r}$$

$$2cR = \frac{h_w(a + cR^2 - T_{cool})}{-\lambda_r}$$

$$T_{cool} = a + (R^2 + \frac{2\lambda_r R}{h_w})c \tag{3.69}$$

Now by using the expression for average radial temperature:

$$\bar{T} = \frac{\int_0^R 2\pi r T(r) dr}{\int_0^R 2\pi r dr}$$

$$\bar{T} = \frac{2\pi \int_0^R r(ar + cr^2) dr}{\pi R^2}$$

$$\bar{T} = a + \frac{1}{2}cR^2 \tag{3.70}$$

By comparing Equation 3.70 and Equation 3.68, it is found that the average temperature is at $r = \frac{R}{\sqrt{2}}$. By subtracting Equation 3.69 from Equation 3.70, coefficient c is calculated:

$$\bar{T} - T_{cool} = c(\frac{1}{2}R^2 - (R^2 + \frac{2\lambda_r R}{h_w}))$$

$$c = -\frac{2}{R^2}\frac{\bar{T} - T_{cool}}{1 + \frac{4\lambda_r}{Rh_w}}$$

and from Equation 3.70, coefficient a is calculated:

$$a = \bar{T} + \frac{\bar{T} - T_{cool}}{1 + \frac{4\lambda_r}{Rh_w}}$$

The average temperature, $\bar{T}$, is used in the reactor model.

3.3 Microchannel reactor model

The mass and heat balances used for the microchannel model are the same as those for the PFR model, except for the heat transfer correlations. In our model, particles with diameter of 0.2 mm are applied in the reaction channels. Because of the small diameter a reasonable assumption is that there will be no mass transfer limitation inside the particles, equivalent to setting the effectiveness factor equal to unity for all reactions (Rytter et al., 2007). All catalyst sites are exposed to the syngas, and that is one reason to why system volumes can be reduced up to 10 times compared to conventional reactors (Leviness et al., 2011).

3.3.1 Heat transfer correlation

The system of resistances to heat transfer from catalyst bed to cooling water is shown in Figure 3.2. The overall heat transfer coefficient is calculated as the inverse summation of resistances:

$$\frac{1}{U} = R_{catalystbed} + R_{boundarylayer} + R_{metalwall} + R_{coolingwater} \tag{3.71}$$

$$\frac{1}{U} = \frac{D_T}{8\lambda_r} + \frac{1}{h_w} + \frac{s_w}{\lambda_w} + \frac{1}{h_{ext}} \tag{3.72}$$

Resistances due to metal wall and cooling water are neglected, since they are considered to be negligible compared to the other terms. Therefore, the overall heat transfer coefficient is calculated as:

$$\frac{1}{U} = \frac{1}{h_w} + \frac{D_T}{8\lambda_{\mathrm{r,eff}}} \tag{3.73}$$

Heat transfer correlation between fluid and reactor wall is taken from VDI (2010). Guettel & Turek (2010) have also used in their modelling of microchannel reactor.

$$\lambda_{\mathrm{r,eff}} = \lambda_{\mathrm{bed}} + \lambda_G \frac{Pe}{8} \tag{3.74}$$

$$Nu_w = \frac{h_w D_p}{\lambda_G} = (1.3 + \frac{5D_p}{D_T})B_{\mathrm{bed}} + 0.19Re^{0.75}Pr^{0.33} \tag{3.75}$$

$$B_{\mathrm{bed}} = \frac{\lambda_{\mathrm{bed}}}{\lambda_G} = 1 - \sqrt{1-\epsilon_{\mathrm{bed}}} + B_c\sqrt{1-\epsilon_{\mathrm{bed}}} \tag{3.76}$$

$$B_c = \frac{2}{N}(\frac{B}{N^2}\frac{B_p - 1}{B_p} ln\frac{B_p}{B} - \frac{B+1}{2} - \frac{B-1}{N}) \tag{3.77}$$

$$B_p = \frac{\lambda_p}{\lambda_G} \tag{3.78}$$

$$N = 1 - \frac{B}{B_p} \tag{3.79}$$

$$B = 1.25(\frac{1-\epsilon_{\mathrm{bed}}}{\epsilon_{\mathrm{bed}}})^{\frac{10}{9}} \tag{3.80}$$

3.4 Path optimization

A systematic way of doing an optimal staging of reactor path is described by Hillestad (2010). A path is a line of production or part of it, and represents the process from starting material to final or intermediate products. A model that describes the rate at which the phenomena take place, must be available or made. Most importantly, a model describing the reaction kinetics and product distribution is necessary. Phenomena like reaction, heat transfer, phase separation and mixing may take place on the path. In addition to the size of each stage, design functions representing mixing (dispersion), heat transfer, additional feeds, separation of products, catalyst dilution are defined on the path which are presented in Table 3.4. An objective function is optimized with respect to the design functions and the result is a sequence of reactor stages, separators, heat exchangers, etc. The optimization determines the volume distribution among units, in addition to the distribution of extra feeds, separation of products, catalyst activity, distribution of heat transfer area and coolant temperature distribution. As with this method, the design functions contain both structural and parametric information. Structural information is e.g. the sequence of units and location of extra feeds. Parametric information is e.g. the size of each unit. The production of heavy components is maximized, but other versions of the objective function may be defined such as a combination with energy efficiency and product quality. Since the FT reactor can be very large, there will be a need to divide the volume into several reactor volumes. The idea is that instead of having these volumes only in parallel, they may also be arranged in series as stages. This gives us freedom to improve the operating conditions. Application of this method on FT process is explained in chapter 9.

Table 3.4: Mapping of basic operations and design functions (Hillestad, 2010)

Basic operation	Design function	Symbol
Fluid mixing	Mixing	u_{M}
Chemical reaction	Catalyst dilution	u_{A}
	Different catalyst types	u_{c}
Heat exchange	Exchange area distribution	u_{H}
	Temperature of coolant	u_{T}
Extra feeding	Feed distribution	u_{F}
	Feed composition/temperature	x_{F}
Pressure change	Pressure profile	u_{p}

3.4.1 Staging of the reactor path

The reactor path is divided into a number of stages and the design functions are optimized in order to maximize an objective function. The flow model, Equation 3.81, represents the change of state variables along the path (Hillestad, 2010):

$$[\gamma \mathrm{I} - u_{\mathrm{M}} \sigma \tilde{J}] \frac{\mathrm{d}x}{\mathrm{d}\xi} = \sigma u_{\mathrm{A}} \tilde{R}(x) + u_{\mathrm{F}} \mathrm{K}(x_{\mathrm{F}} - x) - u_{\mathrm{H}} \mathrm{E}(x - x_w) \tag{3.81}$$

Where:
γ is the dimensionless mass flow rate relative to the inlet (W/W_0)
u_{M} is the mixing design function
σ residence time or space time, (V_{R}/W_0)
$\tilde{J}$ is the partial derivative of component reactions with respect to x, which is:
$\tilde{J} = \frac{\partial \tilde{R}(x)}{\partial x}$+diag$(0, 0, ..., 1)[\alpha(1 - \frac{C_{\mathrm{p,F}}}{C_p}) - \beta \frac{C_{\mathrm{p,ref}}}{C_{\mathrm{p},0}}]$
α is the feed distribution in $\mathrm{kg}/(\mathrm{m}^3\,\mathrm{s})$
β is the heat transfer area design function, $\beta = \frac{Ua}{C_{\mathrm{p,ref}}}$ in $\mathrm{kg}/(\mathrm{m}^3\,\mathrm{s})$
ξ is the dimensionless volume of the path (independent variable), ($\frac{V}{V_{\mathrm{t}}}$)
u_{A} is the catalyst dilution function
u_{F} is the feed distribution design function, $u_{\mathrm{F}} = \sigma\alpha$
K is a diagonal matrix, K =diag$(1, 1, ..., \frac{C_{\mathrm{p,F}}}{C_{\mathrm{p}}})$
u_{H} is the heat transfer area distribution function, $u_{\mathrm{H}} = \sigma\beta$
E is a diagonal matrix, E =diag$(0, 0, ..., \frac{C_{\mathrm{p,ref}}}{C_{\mathrm{p}}})$
x is the vector of mass fractions augmented with dimensionless temperature
$x = [\omega_{\mathrm{CO}}, \omega_{\mathrm{H_2}}, \omega_{\mathrm{H_2O}}, \omega_{\mathrm{N_2}}, \omega_{\mathrm{C_1}}, \omega_{\mathrm{C_2}}, \omega_{\mathrm{C_3}}, \omega_{\mathrm{C_4}}, \omega_{\mathrm{C_{5+}}}, \theta]$
θ is the dimensionless temperature, $\theta = \frac{T - T_{\mathrm{ref}}}{T_{\mathrm{ref}}}$
$\tilde{R}(x)$ is the reaction rate vector in mass basis, $\mathrm{kg}/(\mathrm{m}^3\,\mathrm{s})$
$\tilde{R}(x) = [\tilde{R}_{\mathrm{CO}}, \tilde{R}_{\mathrm{H_2}}, \tilde{R}_{\mathrm{H_2O}}, \tilde{R}_{\mathrm{N_2}}, \tilde{R}_{\mathrm{C_1}}, \tilde{R}_{\mathrm{C_2}}, \tilde{R}_{\mathrm{C_3}}, \tilde{R}_{\mathrm{C_4}}, \tilde{R}_{\mathrm{C_{5+}}}, \tilde{R}_{\theta}]^{\mathrm{T}}$
$\tilde{R}_{\theta}$ is defined as:
$\tilde{R}_{\theta} = \frac{-\Delta_{\mathrm{r}}\mathrm{H}}{C_{\mathrm{p}} T_{\mathrm{ref}}} r_{\mathrm{CO}}$

To explain the terms in Equation 3.81: The first term on the right is mass consumption or production due to reactions, the second term accounts for extra feed stream and the last

term accounts for the heat added or removed from the reactor path. A brief explanation to different design functions are given here and more details can be obtained in Hillestad (2010).

Mixing: This design function is denoted by u_{M} and it can have values between zero and one. When it is zero, Equation 3.81 represents a plug flow model and when it is one, it represents a completely mixed reactor (CSTR). For values between zero and one, the mixing structure will be a plug flow with recycle.

Heat transfer: The design function $u_{\mathrm{H}} = \frac{Ua\sigma}{C_{\mathrm{p,ref}}}$ defines the heat transfer area distribution along the path. The function is dimensionless, where U is the overall heat transfer coefficient and a is the heat transfer area density in $\mathrm{m}^2/\mathrm{m}^3$.

Distributed feed: the design function $u_{\mathrm{F}} = \alpha\sigma$ represents the distribution of extra feed along the path.

Chemical reactions: The design function u_{A} is the relative catalyst activity or catalyst dilution and it can vary between zero and one.

The optimal reactor configuration can be found by solving the following optimization problem:

$max\ J$

[σ,u]$\in \mathcal{U}$

$s.t\ \frac{\mathrm{d}z}{\mathrm{d}\xi} = f(z,u);\ z(0) = z_0$

where:

$z = [x^{\mathrm{T}}, \gamma]^{\mathrm{T}}$

$\mathcal{U}$ is the design space. The objective function (J) considered here is the maximization of the mass fraction of heavy components at the end of the path. The model equations are discretized by orthogonal collocation method and formulated as nonlinear equality constraints and the optimization problem is solved through infeasible path optimization. Path constraints on the state variables are represented by nonlinear inequality constraints.

$h(z,u) \leqslant 0$

3.5 Model implementation in process simulator

Two critical challenges were faced during the implementation of the FT synthesis reactor in a process simulator, such as Aspen HYSYS: the first one is related to the reaction rate expression. Most process simulators, like Aspen HYSYS, accept reaction rate expressions in specific forms and if a rate expression does not fit in that form, their implementation will not be with ease. The second challenge is about the implementation of lumps. In most process simulators, components are not allowed to have changing properties, such as molecular weight, etc. This makes it challenging to implement lumps since they have changing molecular weights. Several methods were investigated to overcome these challenges, which are introduced in this section. In the rest of the thesis, the term "HYSYS" will refer to "Aspen HYSYS". This is just for simplification of the text.

3.5.1 HYSYS extensibility (unit operation extension)

This is a powerful feature of HYSYS which enables users to add additional unit operations, kinetic reactions, and other tools to the software. However developing and implementing

a model is not easy as it requires a good understanding of HYSYS program and an object-oriented programming language (VB or C++ or C#). A HYSYS extension consists of two separate files: ActiveX server DLL (Dynamic Link Library) and the EDF (Extension Definition File). DLL contains the compiled code and the EDF acts as the link between DLL and the HYSYS program. The DLL file is written in an object oriented programming language (VB or C++ or C#). The EDF file is created using the Extension View Editor (supplied with HYSYS program). The relationship between the HYSYS program, the EDF and the DLL can be represented as in Figure 3.3 which shows that HYSYS communicates with DLL through the EDF file. More details about HYSYS extensibility can be found in extensibility manual (AspenTechnology, 2011). Unit operations built with this method can only be used in HYSYS. This method worked well, however with some serious drawbacks. The programming part was not robust, especially the debugging of the code. Each of the DLL files needed to be registered on the computer, which was troublesome at times. Although this method worked, but it was not robust and therefore did not meet our expectations.

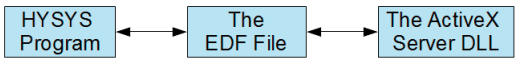

Figure 3.3: HYSYS extensibility structure (AspenTechnology, 2011)

3.5.2 User-Unit operation in HYSYS

User-unit operation, like the unit operation extension, allows the user to build custom unit operations for their simulations. Unit operation extension and the user-unit operation differ mainly in the location of the defining code. With a user-unit operation the defining code is written and exists within the HYSYS simulation. The other difference is that the code is not in compiled form and the user-unit operation code is available to everyone which may distribute confidential information. The disadvantages of using this method is the same as making unit operation extension. Although this method worked, it was not robust and therefore did not meet our expectations. More details about adding user unit operation can be found in manual (AspenTechnology, 2011).

3.5.3 Aspen custom modeler (ACM)

Aspen Custom Modeler (ACM) is a powerful tool to make customized unit operation models. These models can be used in process simulator software such as Aspen Plus or HYSYS. ACM uses an object-oriented modelling language and Microsoft Visual Basic for scripts to build simulation applications. In this way a block can be built, where the appropriate design equations are introduced and the input/output variables are defined and linked dynamically with other available process equipment (AspenTechnology, 2011). ACM can cope with different kinds of problems such as dynamic, steady state, parameter estimation and optimization using an equation-oriented approach (AspenTechnology, 2011). An important feature of ACM is that it provides the possibility of using Aspen

Plus property database which makes it possible to calculate properties of components with different fluid packages. One disadvantage of ACM is that many equations must be solved simultaneously and even the explicit variables are treated as equations. Another disadvantage is related to initialization of all the variables. If the variables have values that are away from the solution, the model will not converge. In general, main steps that must be followed in order to implement a unit operation model into Aspen Plus or HYSYS using ACM are:

- The governing equations such as mass and energy should be written for the equipment and input and output variables must be decided. The system of equations must have zero degree of freedom which means that the number of equations and unknowns must be equal.

- The components that are involved in the simulation model should be declared. After exporting the model to the process simulator software, the exact components that are used during development of ACM model must be defined in the process simulator, meaning that the components must have identical names in the process simulator and in the ACM model.

- The model input and output streams must be declared and assigned to an input or an output port, respectively. These ports are added to enable the module to exchange information with other blocks in the process simulator. In order to be able to export the new model to Aspen Plus or HYSYS, C++ compiler must be installed on the computer. After exporting the model to HYSYS and in case it converges, it would look like Figure 3.4.

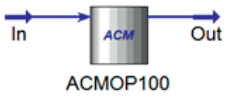

Figure 3.4: ACM model in HYSYS

3.5.4 MATLAB CAPE-OPEN unit operation

CAPE-OPEN is a collection of open software interface standards that describe the interaction between flowsheet software components (Douglas, 1988). These set of standards facilitate interoperability between process simulators and they cover most aspects of process simulation activities: Unit operations, Thermodynamics, Physical properties, Numerics, etc. COLaN is responsible for setting the standards and is a non-profit organization (COLaN, 2017). If a unit operation is CAPE-OPEN compliant, it can be used in any process simulation software that are CAPE-OPEN compliant. Typical setup for simulation environments supporting CAPE-OPEN models is shown in Figure 3.5. End-user can plug any CAPE-OPEN compliant property package or unit operation into any CAPE-OPEN

compliant process modelling environment. Most of process simulation software (like Aspen HYSYS, Aspen Plus, VMGsim, etc) have CAPE-OPEN sockets which means they accept CAPE-OPEN unit operations and property packages.

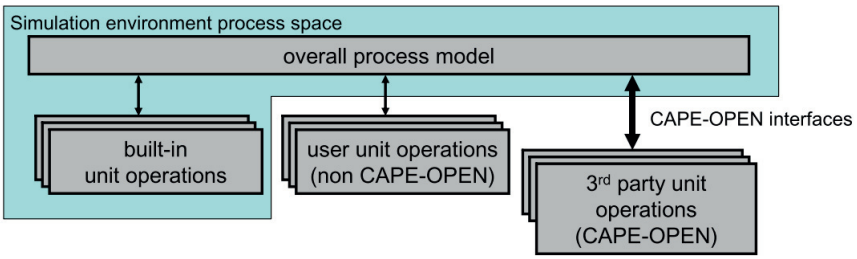

Figure 3.5: Typical setup for simulation environments supporting CAPE-OPEN models (Van Baten, 2009)

MATLAB CAPE-OPEN unit operation is a CAPE-OPEN compliant unit operation (AmsterChem, 2017). By using this unit operation, MATLAB code can be directly used within HYSYS or any other CAPE-OPEN compliant software. All functions from MATLAB library can be used within the simulation software. This is a great advantage of this unit operation. The running time of this method is also remarkable compared to the other methods mentioned before. This is the preferred method for building a new unit operation in any CAPE-OPEN compliant software. More information in use of CAPE-OPEN in process simulation can be found in published literature (Van Baten & Pons, 2014; Baten & Szczepanski, 2011; Morales-Rodriguez et al., 2008). In Appendix I, a brief introduction on how to simulate a unit operation by use of MATLAB CAPE-OPEN unit operation (AmsterChem, 2017) in HYSYS is provided.

Chapter 4

Conceptual Design of an Autonomous Once-through Gas-to-Liquid Process - Comparison Between Fixed Bed and Microchannel Reactors

This chapter is based on the published paper "Conceptual design of an autonomous once-through gas-to-liquid process - comparison between fixed bed and microchannel reactors" in journal: Fuel Processing Technology , vol. ***154****, (2015), pp. 186 - 195.*

A novel process concept is proposed for converting natural gas to liquid Fischer-Tropsch products. An autothermal reformer with enriched air as oxidant is applied for synthesis gas (syngas) production, and because of the inert nitrogen a once-through Fischer-Tropsch synthesis is the preferred option. In order to maximize the syngas conversion and the production of heavy hydrocarbons, a staged reactor path with distributed hydrogen feed and product withdraw is proposed. The hydrogen is produced by steam methane reforming in a heat exchange reformer (gas heated reformer), heat integrated with the hot effluent stream from the autothermal reformer. Tail gas from the last Fischer-Tropsch stage is sent to a gas turbine for power production. The hot exhaust gas from the gas turbine is used for natural gas preheating. The process is autonomous in the sense that it is self sufficient with power and water, and therefore well suited for production in remote locations such as a floating production unit. The process concept is simple and inexpensive since cryogenic air separation and fired heaters are not required. For the Fisher-Tropsch synthesis, both the conventional shell and tube fixed bed reactors and microchannel reactors are considered

and compared.

4.1 Introduction

Due to the depletion of easily accessible oil, and steadily increasing energy consumption worldwide, focus is turned on untapped resources that are unused for technical or economic reasons, such as associated and stranded gas reserves. One of the biggest challenges in exploiting remote gas reserves is transportation of the gas. Converting natural gas to liquid fuels, gas-to-liquids, is one possibility to bring remote natural gas reserves to the market.

If a floating production vessel is to be used for gas-to-liquid processing, there are several requirements that are not necessarily equally restrictive for an onshore plant. There are restriction with respect to space and the total weight of equipment. The floating production vessel need to be autonomous in the sense that all production utilities, such as water and power, need to be available onboard the unit. Due to safety issues a cryogenic air separation unit may be problematic onboard a floating production vessel because of the possibility of presence of pure oxygen in the vicinity of hydrocarbons. Also high columns with liquid inventory on board a rolling vessel may create problems.

There has been some investigations looking at the feasibility of installing a gas-to-liquid (GTL) process on a floating production storage and offloading (FPSO) vessel. Daewoo Shipbuilding & Marine Engineering together with RES Group Incorporated, have completed conceptual design package of GTL process for FPSO application producing 20000 bbl/day of a Fischer-Tropsch liquid syncrude product. They considered steam-CO_2 combined reforming for syngas production and slurry bubble column as Fischer-Tropsch (FT) synthesis (Kim et al., 2014a). Velocys, which is one of the pioneers of commercializing microchannel technology, propose the use of microchannel technology on FPSO (Leviness et al., 2011; Tonkovich et al., 2008). Velocys together with Toyo Engineering and Mitsui Ocean Development & Engineering Co are working on commercializing Micro-GTL technology which is applicable for small scale gas reserves. CompactGTL is another leading company in modular small scale GTL. Together with Petrobras, they built a fully integrated small scale GTL facility using associated gas. SBM Offshore together with CompactGTL is cooperating on offshore projects to increase productivity and to reduce flaring. The concept utilizes CompactGTL technology for conversion of associated gas into syncrude. Loenhout et al. (2006) proposed to use air instead of pure oxygen in the reforming step. Three-phase slurry bubble column reactors were used for the two stages of the FT reaction. Use of air in the reformer resulted in very large equipment downstream the reformer. Masanobu et al. (2004) proposed to use oxygen blown autothermal reformer (ATR), which requires an air separation unit onboard the ship. Syntroleum Corporation has developed an offshore gas-to-liquid conversion process that uses air in a reforming process step to produce syngas (Hutton & Holmes, 2005). The feasibility assessment of utilizing associated gas and converting it into Fischer-Tropsch liquids on the FPSO was studied by Chevron Research and Technology in cooperation with Fluor Daniel, Inc. and Air Products and Chemical (Lowe et al., 2001).

Fonseca et al. (2012) used steam methane reformer to produce syngas. In their design, they considered microchannels for the steam methane reforming and FT reactors. Kim

et al. (2014b) considered process design and simulation of a methanol plant on an FPSO. They used steam-CO_2 reforming and plug flow reactor model in their design. The overall process was set in a high pressure environment to comply with the spatially constrained off-shore condition. Tonkovich et al. (2008) considered methanol production on an FPSO using multiple microchannel unit operations. These unit operations include reactors, phase separation, and distillation.

In our proposed design, the FT reactor path is staged with distributed hydrogen feed and products withdrawal between the stages. A slightly under-stoichiometric H_2/CO will increase the production of C_{5+} products. To compensate for the consumption, hydrogen is added between the stages. The hydrogen is produced by the use of a heat exchange reformer (HER), a high temperature shift reactor and a membrane unit to separate H_2 from CO_2. Part of the hydrogen will be used for product upgrading. Syngas is produced by an autothermal reformer with enriched air as as oxidant. High once-through conversion over the FT reactors, more than 90%, is possible even with inert nitrogen in the syngas. The tail gas, being unconverted syngas, nitrogen, and lighter hydrocarbons, is used as fuel for the gas turbine for necessary power production. Furthermore, the use of enriched air instead of air to the ATR will increase the production of C_{5+} enough to compensate for the extra investment of an air membrane and extra compressors. A comparison between conventional fixed bed reactors and microchannel reactors is made. With fixed bed reactors three stages are applied, while with microchannel reactors two stages are sufficient to obtain high CO conversion with a once-through configuration. A comparison of the two reactor types indicates that microchannel will require less space, but the total weight is larger.

The selected capacity of the proposed GTL plant utilizes 120 MMscfd of natural gas and produces about 58 tonne/h or more than 12000 bbl/day of hydrocarbon products. Natural gas specifications are given in Table 4.1. The natural gas NG1 is used throughout this chapter as the base case, while NG2 is only applied to see the effect of a heavier natural gas. The wax products need to be upgraded by hydrocracking in order to keep the oil liquified and prevent the product viscosity from becoming too high, but also to saturate the alkenes. If the GTL plant is integrated with oil production, the products may be blended with the conventional oil. A simplified block flow diagram of the proposed process concept is shown in Figure 4.1.

4.2 The proposed process concept

A more detailed process flow diagram of the proposed GTL process concept is shown in Figure 4.2. The main areas shown here are syngas production, hydrogen production, Fischer-Tropsch synthesis, in addition to gas turbine power generation, while the product upgrading process and the steam utility system are not shown. After sulfur removal, the natural gas is mixed with steam and preheated to 480 °C before entering the pre-reformer. The outlet of the pre-reformer is further heated to ca 650 °C. These heat exchangers will be located inside the exhaust gas duct from the gas turbine. Stream 100 is split into two streams, 101 and 102, the former to the ATR and the latter to the HER. The energy required for the steam reforming reactions in the HER is provided by the hot outlet stream from the ATR. The outlet of the HER is cooled down to 350 °C before entering the high temperature

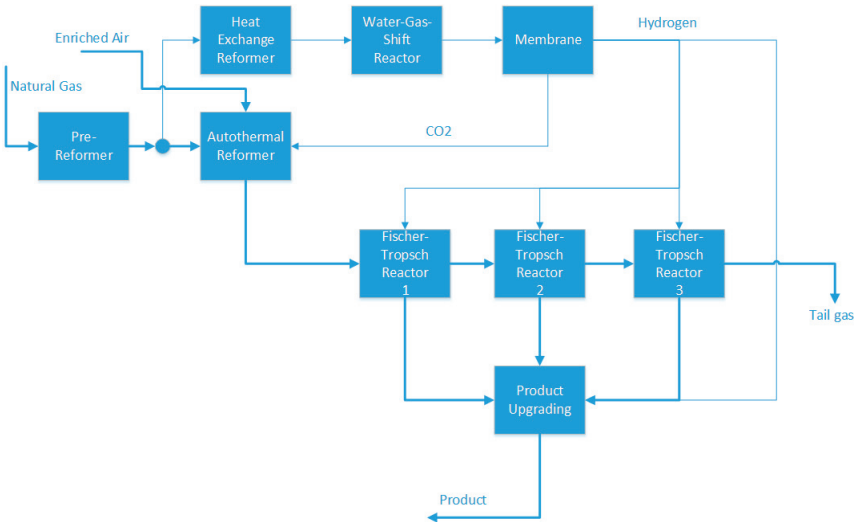

Figure 4.1: Block flow diagram of the proposed process concept; water and steam are not shown.

water gas shift (WGS) reactor, shifting CO to CO_2 and H_2. After the WGS reactor, the stream is cooled to ca 30 °C and water is knocked out before entering the membrane unit for separation of H_2. The hydrogen rich stream with 99 % purity is then compressed and distributed between the Fischer-Tropsch stages. The CO_2 rich stream, which also contains some H_2, CO and CH_4, is compressed and recycled to the ATR. By adding this stream the H_2/CO ratio out of the ATR will be reduced, which is beneficial for the FT synthesis. The effluent stream from ATR after heat exchange with the HER, is further cooled to 30 °C to knock out water from the syngas. Without further compression the syngas stream is heated to 210 °C before entering the first Fischer-Tropsch stage. The approximate inlet pressure to the first stage is about 26 bar. In order to increase the rate of the FT reactions, and also suppress catalyst deactivation, the gas outlet from FT reactors are cooled down and partly condensed where water and hydrocarbon products are separated from the gas. The tail gas, consisting of unconverted syngas, nitrogen and light gas components produced in the Fischer-Tropsch reactors, is used as fuel in the gas turbine to supply power to consumers.

Simulations were carried out using HYSYS V8.6 process simulator. Modeling of Fischer Tropsch reactor and HER are done using Aspen Custom Modeler. The other reactors (WGS, Pre-reformer and ATR) are simulated using the Gibbs reactor model present in HYSYS. Soave-Redlich-Kwong (SRK) equation of state is used as the thermodynamic model to calculate thermodynamic properties. All chemical properties were provided by Aspen Properties V8.6.

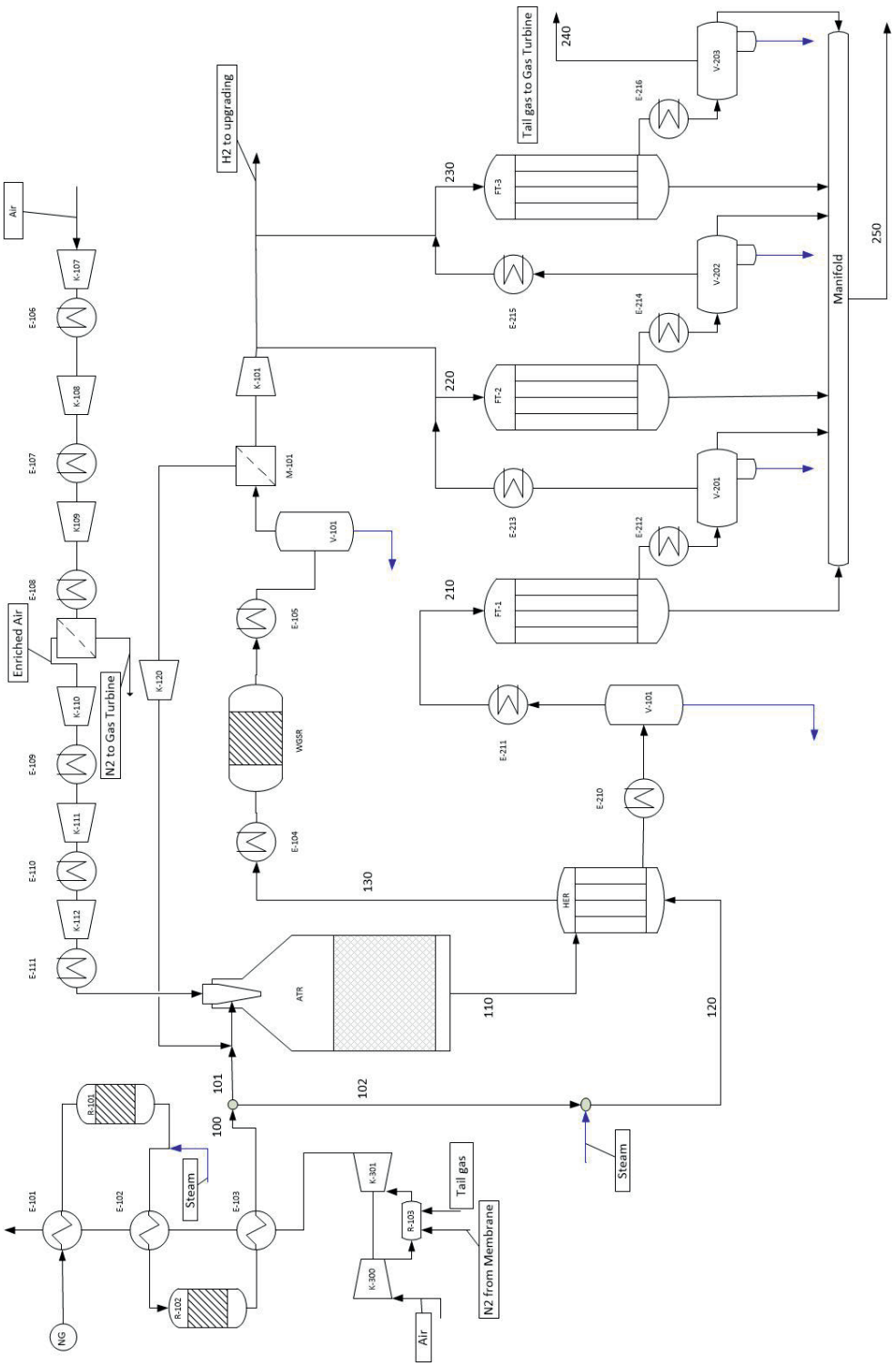

Figure 4.2: Process flow diagram of the proposed GTL plant. Heat integration and the steam system are not shown here.

Table 4.1: Specifications of the natural gas feeds; NG1 is used for all the results produced here, while NG2 is used to see the effect of heavier natural gas.

	NG1	NG2
Temperature [°C]	50	50
Pressure [bar]	30	30
Flow [MMscfd]	120.2	120.2
Molar flow [kmol/h]	6000	6000
Mole fraction		
CH_4	0.95	0.85
C_2H_6	0.02	0.067
C_3H_8	0.015	0.033
$n{-}C_4H_{10}$	0.01	0.022
$n{-}C_5H_{12}$	0.005	0.011
CO_2	0	0.017

4.2.1 Syngas production

An autothermal reformer is selected for syngas production. The main reasons are that the H_2/CO ratio can be adjusted to be close to the optimal ratio and the ease of scalability. The ATR is a relatively simple piece of equipment with a burner and a catalyst bed in a brick-lined pressure vessel (Rostrup-Nielsen, 2002). A pre-refomer is used in front of the ATR to prevent coke formation on the ATR catalyst. Pre-reforming is usually operated adiabatically at $400 - 550$°C, and almost all higher hydrocarbons are converted to methane and carbon oxides. The pre-reformer is an adiabatic fixed bed reactor and the outlet condition is calculated by assuming equilibrium.

With an air-blown ATR, it is practically impossible to recycle the unconverted syngas because of very high nitrogen concentrations. This is also the case with enriched air, and a once-through synthesis scheme is the only option to avoid high accumulation of nitrogen. However, by using enriched air instead of air, an increased production of 7.8 and 15.5 % can be obtained with fixed bed and microchannel reactors, respectively. PRISM membrane separators from Air Products are considered (AirProducts, 2015). With these membranes, enriched air with oxygen concentrations ranging from 25 to 50% can be obtained. Considering the large air flow through the membrane and therefore avoiding a very large membrane modules, a PRISM membrane is chosen to have 34% oxygen purity. Long durability and simple startup of the separator are highlighted by the producer. Air is fed to the membrane at 16 bar and 100 °C. The enriched air is on the permeate side at a pressure of 1 bar, and needs to be re-pressurized before entering the ATR. Three compressors are used before the air membrane and three compressors are used after the air membrane. Inter-coolers are used between the air compressors in order to avoid excessive air temperatures and compressor work.

An alternative to air or enriched air is to use pure oxygen. Pure oxygen from cryogenic air separation poses significant safety challenges offshore, in addition to large investment costs.

4.2.2 Hydrogen production

As demonstrated here, slightly under-stoichiometric H_2/CO ratios to the Fischer-Tropsch reactors result in higher C_{5+} production. With under-stoichiometric H_2/CO feed ratios, this ratio will naturally decrease along the reactors. The stoichiometric consumption H_2/CO ratio can be calculated as described by Hillestad (2015). There are four reactions to take into account, but the predominant reaction is the formation of alkanes. When the product distribution follows the Anderson-Schulz-Flory distribution, the consumption ratio is $3 - \alpha$, where α is the propagation probability. The propagation probability will change with the H_2/CO ratio and the temperature, but a typical value of α is 0.94 giving a stoichiometric H_2/CO consumption ratio of 2.06. When H_2/CO ratio is slightly under-stoichiometric, more C_{5+} products can be obtained (Rafiee & Hillestad, 2012; Rytter, 2010) and in order to compensate for the consumption, hydrogen is added between the stages.

Steam reforming with the use of a heat exchange reformer is applied to produce hydrogen with H_2/CO ratios of more than three. Heat exchange reformers are now commercially available and the technology is becoming mature. Kellogg Brown and Root (KBR) started using this technology in 1994 (Malhotra et al., 2004), Haldor Topsøe in 2003 (Thomsen et al., 2006), and Johnson Matthey/Davy Technologies has solid experience with this technology (Carson et al., 2010). Apart from being a hydrogen generator, the HER provides efficient heat integration and avoids the use of a waste heat boiler. Here, the steam to carbon ratio (S/C) of the feed to the HER is chosen to be two. The heat exchange reformer is counter current and consists of 1000 steam reformer tubes of 10 cm diameter and 10 m long. Modelling of the heat exchange reformer is described in detail by Falkenberg & Hillestad (2015).

The remaining CO is converted to CO_2 by the use of a water gas shift reactor. The CO reacts with water to produce CO_2 and H_2. The WGS inlet gas is cooled to approximately 350°C in E-104. Because of exothermic nature of WGS reaction, the temperature increases along the reactor. For simulation purposes chemical equilibrium (Gibbs reactor) is assumed at the outlet of the WGS and the operating conditions are 450°C and 28 bar. The WGS effluent is cooled down to 30°C to remove most of the water before entering the membrane.

With the use of a membrane, a hydrogen rich and a CO_2 rich stream are produced. 85.5 % of the H_2 is separated and ends up in the hydrogen rich stream. The CO_2 rich stream is recycled back to the ATR to decrease the H_2/CO ratio at the outlet of the ATR. The membrane used here is a carbon membrane. It is ceramic tubes covered with membrane surface and tailored pores so that mainly hydrogen will pass through. The permeance of hydrogen is 200 GPU and for CO_2 it is 2 GPU, while for methane it is negligible (He, 2011). The membrane is countercurrent and there is no sweep gas on the permeate side. This will produce very pure hydrogen on the permeate side.

4.2.3 Fischer-Tropsch Synthesis

Cobalt catalysts are more selective to higher hydrocarbons, more active at lower temperatures, considerably less shift active and less selective to alkenes than iron catalysts and is therefore chosen for this process. On the other hand, the cost ratio between cobalt and iron catalysts is 230 (Rao et al., 1992) based on the relative price of metals. Although a

number of kinetic models have been proposed in the literature, we have chosen to apply a rigorous kinetic model developed by Todic & al. (Todic et al., 2015, 2014a). The model is based on experiments done in a stirred tank slurry reactor with cobalt catalyst over a range of operating conditions which fits to our design conditions. The production of alkanes and alkenes are described by two chain growth probabilities and both increases slightly with the carbon number. The selectivities of methane and ethene are given by specific rate constants. A method for handling infinite number of reactions and components, suggested by Hillestad (2015) is used, where lumps of components and their average molecular weight are accurately described without violating the element balances. The method provides an accurate description of the overall consumption of CO and H_2 without calculating very many individual reaction rates. We have chosen to model alkane components individually up to C_{10} and a lump C^{p}_{11+} describing the tail distribution. While for alkenes, with less heavier components, we have chosen to model individual components up to C_4 and a lump C^{o}_{5+}. The reason for having that many individual components is to get the phase equilibrium calculations more accurate. For the sake of brevity the lumps C^{p}_{5+} and C^{o}_{5+} are reported here, but they are made by adding individual components and the modeled lumps. The molecular weight of the lumps C^{p}_{11+} and C^{o}_{5+} will change as the propagation probability changes. However, components in a process simulation system are normally described by constant molecular weights, so also in Hysys. A way of handling this is to let a lump with varying molecular weight be represented by two lumps with constant but different molecular weight. This is described in detail by Hillestad (2015).

The Fischer-Tropsch synthesis is staged with product withdrawal and hydrogen addition between the stages. This enables high conversion of syngas and high selectivity to higher hydrocarbons. The Fischer-Tropsch reactors are shell and tube fixed bed or microchannel fixed bed reactors. Since water is the main byproduct, the partial pressure of water vapor increases along the reactor. This can cause hydro-thermal sintering of many FT catalysts (Baxter, 2010; Tsakoumis et al., 2010). Once-through conversion in one stage is limited to 80% to have the maximum C_{5+} selectivity and also preserve catalyst life (Schanke et al., 2001). Studies of the effect of low amounts of water during FTS for cobalt catalysts show that a low partial pressure of water ($p_{H_2O}/p_{H_2} < 1$) may have a positive kinetic and selectivity effect during FTS (Lögdberg et al., 2011). However, at high water partial pressures, oxidation of some cobalt to irreducible oxidized cobalt compounds may occur (Schanke et al., 1995).

Studies on the kinetics of FT synthesis show that nitrogen only dilutes syngas and therefore has no influence on the kinetics if the partial pressures of carbon monoxide and hydrogen are kept constant (Jess et al., 1999). Moreover, nitrogen plays an important role in the operation of multi-tubular reactors by facilitating removal of generated heat.

Fixed bed reactor

Considering the robustness against marine motion, and in particular inclination and inertia effects, fixed bed reactors are considered a good option for installation on a FPSO. Slurry bubble column reactors, having many favorable properties such as better heat transfer properties, have large volumes of liquid inventory and may be sensitive to wave motion. For the fixed bed reactor we assume a two-dimensional homogeneous reactor model with no axial dispersion. Boiling water is used as the coolant and the coolant temperature

is assumed to be constant along the axial direction. Three fixed bed reactor stages are considered. The number of tubes at each stage is chosen such that the superficial gas velocities in all stages are approximately 0.4 m/s. Table 4.2 shows the chosen design parameters of the fixed bed model.

Table 4.2: Design parameters of fixed bed and microchannel reactors.

	Fixed bed	Microchannel
Catalyst bulk density [kg/m^3]	1200	1200
Catalyst particle diameter [mm]	3	0.2
Catalyst void fraction	0.40	0.40
Cooling water temperature [°C]	220	220
Diameter of tube / channel side [mm]	25	2×2
Length of tube / channel [m]	12	2

Due to diffusion, there are concentration gradients, and to some extent a temperature gradient, inside a pellet. The effectiveness factor of a pellet, defined as the ratio between the integrated reaction rate over the pellet volume and the rate at bulk gas conditions, is normally less than unity. For a catalyst pellets of 3 mm diameter with homogeneous distribution of active sites, and with a kinetic model as applied here (Todic et al., 2015, 2014a) and diffusivities found by Erkey et al. (1990), the effectiveness is calculated to be 0.20-0.25 on average along the reactor for the main reaction formation of alkanes. Due to different diffusion rates of reactants, a pellet will affect the selectivity compared to the intrinsic kinetics. Here, however, we assume the catalyst pellets have a thin layer of active catalyst sites only on the external surface; eggshell catalyst. On the external surface we may neglect the diffusion resistance. The volume fraction of active layer on a pellet is here chosen to be 8 %. The catalyst loading can be increased beyond 8 % without running into problems of temperature runaway since the syngas consists of more than 27 % nitrogen, which helps mitigate temperature profile. Even with a homogeneous distribution of active sites throughout the pellet and with our diluted syngas, the calculations indicate that the temperature peak will be moderate. By increasing the catalyst loading on the pellet to 100 %, an effectiveness factor of 0.20-0.25 has to be applied. However, in the sequel we have assumed 8% catalyst loading and no diffusion resistance.

Microchannel reactor

Microchannel technology, with numerous parallel channels of small dimensions, enhances heat transfer because the specific heat transfer area is much larger. With microchannel technology heat transfer rates are accelerated 10 to 1000 times (Leviness et al., 2011). Reactors with microchannels are suited for reactions that are highly exothermic or highly endothermic. Channels filled with FT catalyst powder and channels with coolant water are arranged in a cross flow configuration. Our simulations are based on channels with a dimension of 2×2 mm^2 and a length of 2 meter. Considering the thickness of the channel wall, the outer dimensions of each channel will be 3×3 mm^2. An illustration of a repeating unit of microchannels is shown in Figure 4.3. The reactor consists of several

thousands of these repeating units. We assumed a two-dimensional homogeneous model with no axial dispersion. Boiling water is used as coolant and its temperature is assumed to be constant along the axial direction. Particles with diameter of 0.2 mm are applied in the reaction channels. Because of the small diameter a reasonable assumption is that there will be no mass transfer limitation inside the particles, equivalent to setting the effectiveness factor equal to unity for all reactions (Rytter et al., 2007). All catalyst sites are exposed to the syngas, and that is why system volumes can be reduced up to 10 times compared to conventional reactors (Leviness et al., 2011). Table 4.2 shows the design parameters of the microchannel reactor model.

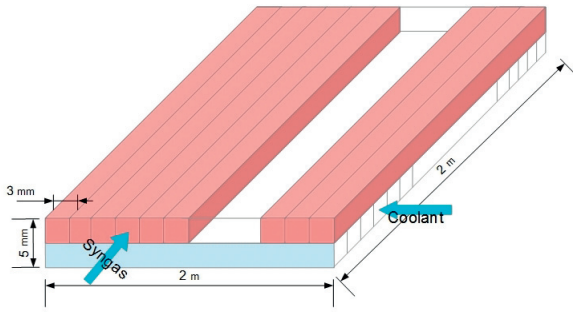

Figure 4.3: A repeating unit of a microchannel reactor.

Isothermal behavior of microchannel FT reactors has been demonstrated by Tonkovich et al. (Tonkovich et al., 2008). The hot-oil-cooled microchannel reactors are isothermal to within $\pm 1^{\circ}$ C (Deshmukh et al., 2010). This is also verified with our reactor model. With very high heat removal capability, single pass conversions near 80% can be realized. Unlike the fixed bed case, only two microchannel FT reactor stages are required due to the high CO conversion at each stage. The tail gas out of the second stage contains large amounts of nitrogen, 75 %, which makes it uneconomical to use a third stage. The tail gas is sent to the gas turbine for power generation.

4.2.4 Gas turbine for power production

The tail gas from the last Fischer-Tropsch stage is used as fuel to the gas turbine for power production. This gas consists of unconverted syngas, nitrogen, and lighter components formed in the synthesis reactors. The retentate stream from the air separation membrane is used as feed to the gas turbine. This stream is very useful as a feed to the gas turbine for several reasons; it does not need to be pressurized because the pressure is 16 bar, it keeps the turbine inlet temperature low, it contains nitrogen for cooling of the turbine blades, and since it contains 10 % oxygen less air needs to be compressed. The amount of oxygen to the gas turbine is adjusted to 15% more than the stoichiometric consumption, and there is about 1.3 % excess oxygen in the exhaust gas. If the inlet pressure to gas turbine is increased more power can be produced. However, to avoid two extra compressors, 16 bar pressure is chosen for power generation. With the high conversion obtained with microchannel reactors, the tail gas contains 73% nitrogen and 13% CO_2. This gas does

not contain enough energy and in this case 20% of the excess hydrogen is added to the tail gas as fuel to gas turbine. Still there is more than sufficient amount of hydrogen for product upgrading. With the fixed bed reactors the conversion is lower and the tail gas contains enough energy to produce sufficient power. The power production is sufficient to provide power for all the consumers accounted for in this process. Approximately 22.7 MW and 9.3 MW of excess power is produced with fixed bed and microchannel reactors, respectively. The temperature of the exhaust gas, after heat exchanged, is approximately 240 °C.

4.3 Results and discussion

To obtain a CO conversion of more than 90%, three fixed bed stages or two microchannel stages are required for the FT synthesis. The number of tubes or channels in each stage are selected so as to have approximately the same superficial gas velocity profile in all stages. The lengths are not changed. The simulations are done for both air-blown and enriched air-blown ATR, but only the results with enriched air are shown here. It is found that by using enriched air instead of air, on average 7.8% and 15.5% more C_{5+} can be produced in fixed bed and microchannel reactors, respectively.

In all simulations, the ATR outlet temperature is kept at 1060 °C and the steam-to-carbon ratio to the ATR is 0.6, while to the HER the steam-to-carbon ratio is 2.0. The feed composition to each stage is adjusted by hydrogen addition so that the H_2/CO ratios are the same and equal to the ratio from the ATR. Equal H_2/CO ratios to each stage need not be optimal, but is here chosen to be the case for convenience. Also the coolant temperatures are chosen the same for all stages, 220 °C, and furthermore the gas residence times at each stage are chosen the same. These parameters need not be optimal, and there is a potential of reducing the FT reactor volume without losing production. This will be studied further, and a methodology for systematic staging of reactor paths, described by Hillestad (2010), will be applied to find the optimal conditions for all parameters.

4.3.1 The effect of the split ratio between ATR and HER

As the split ratio to ATR is increased, more natural gas is sent to ATR and less to HER. Less gas to HER means less H_2 and CO_2 production, and therefore less CO_2 recycle to ATR inlet. This causes the H_2/CO ratio to increase. In all simulations, methane selectivity is higher in the next FT stage than in the previous one. The reason is that the applied kinetic model (Todic et al., 2015, 2014a) predicts that the growth factor decreases with decreasing pressure, and consequently more production of lighter hydrocarbons.

The effect of the split between the ATR and the HER for both FT synthesis reactor types are shown in Tables 4.3 and 4.4. The overall CO conversions for both microchannel and fixed bed simulations increases as the split ratio is increased. The reason for this trend is attributed to the kinetic model that dictates enhanced rates at increasing H_2/CO ratios. On the other hand, the chain growth probability, and thus the selectivity to higher hydrocarbons, decreases with increasing H_2/CO ratios. In Tables 4.3 and 4.4 the production rates of C_{5+} for both microchannel and fixed bed are seen to have a maximum, though relative flat for the fixed bed. For the microchannel case the maximum is at 85

% split and therefore this is chosen as the optimum split, while for the fixed bed 90% is chosen as the optimum split in terms of C_{5+} production. The optimum split will certainly depend on many parameters including temperature, the natural gas feed composition and steam-to-carbon ratio. We know that if the H_2/CO ratio at the inlet of the reactor is over stoichiometric, this ratio gradually increases along the rector length. In Table 4.3 for the 92 % split the H_2/CO ratio is over stoichiometric but this is not the case in Table 4.4. The reason is that hydrogen usage is a function of chain growth probability (α) and α is a function of temperature, pressure and H_2/CO ratio (Hillestad, 2015). For the same inlet H_2/CO ratio in microchannel and fixed bed, there is better temperature control in microchannel. The pressure drop in two reactors is also different which influence the value of α. Since we may have different α values in the two reactors for the same inlet H_2/CO ratio, we see this difference in Table 4.3 and Table 4.4.

Table 4.3: Simulations with fixed bed model and with different feed gas split ratios to ATR and S/C=0.6.

Split ratios to ATR	0.85	0.9	0.92	0.95	0.97	1.0
H_2/CO ratio to first stage	2.00	2.09	2.13*	2.18*	2.22*	2.28*
CO Conversion [%]	88.9	89.5	89.9	90.5	91.0	90.6
C_{5+} production [tonne/h]	53.3	53.5	53.5	53.3	53.2	52.8
CH_4 Selectivity in first stage [%]	6.4	6.9	7.1	7.4	7.6	7.7
CH_4 Selectivity in second stage [%]	8.7	9.3	9.7	10.4	10.8	11.0
CH_4 Selectivity in third stage [%]	13.1	14.2	14.9	16.9	18.4	19.4

* H_2/CO ratio increased along the reactor length

Table 4.4: Simulations with microchannel model and different feed gas split ratios to ATR and S/C=0.6.

Split ratio to ATR	0.82	0.85	0.87	0.9	0.92	0.95	0.97	1.0
H_2/CO ratio to first stage	1.97	2.00	2.04	2.09	2.13	2.18*	2.22*	2.28*
CO Convesion [%]	95.6	96.0	96.5	97.1	97.5	99.0	99.9	100.0
C_{5+} production [tonne/h]	57.2	57.3	57.2	57.1	57.0	56.5	55.8	55.3
CH_4 Selectivity in first stage [%]	7.0	7.3	7.7	8.3	8.8	9.5	10.0	10.7
CH_4 Selectivity in second stage [%]	14.0	14.9	15.9	17.6	18.7	26.8	36.3	44.9

* H_2/CO ratio increased along the reactor length

4.3.2 Steam-to-carbon ratio

The effect of the feed steam-to-carbon (S/C) ratio and the split ratio to the ATR on the H_2/CO ratio is shown in Figure 4.4. As the S/C ratio is increased, the H_2/CO ratio out of ATR increases. The effect of S/C ratio and the split ratio to the ATR on the C_{5+} production rates in both fixed bed and microchannel are shown in Figure 4.5. Lowering the S/C ratio,

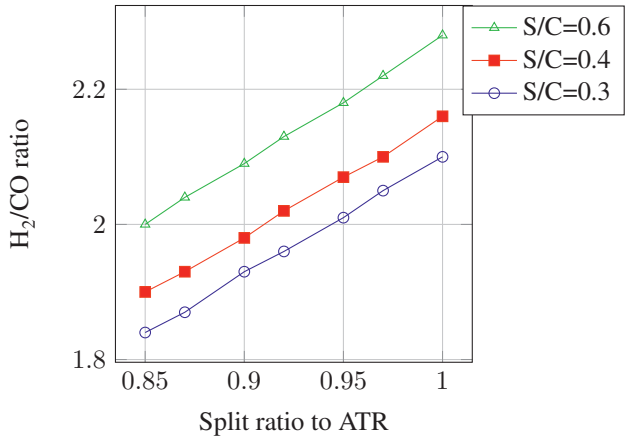

Figure 4.4: H_2/CO ratio out of the ATR as function of the split feed flow ratio to the ATR.

the H_2/CO ratio of the syngas becomes lower, and the production of C_{5+} has a maximum at a H_2/CO ratio which is slightly under-stoichiometric. By reducing the S/C ratio from 0.6 to 0.3, about 4 tonnes/h more C_{5+} products can be produced. Although a low S/C ratio is beneficial, a S/C ratio of 0.6 is chosen here because this ratio is industrially tested and proven. The risk of coke formation and catalyst deterioration increases with lower S/C ratios.

4.3.3 Design at the optimal split

The optimal ATR split with fixed bed FT synthesis reactors is 0.9 at a steam-to-carbon ratio of 0.6. At these conditions, a summary of the the result of the chosen design is given in Table 4.5. Similarly, the optimal ATR split with the microchannel FT synthesis reactors is 0.85 at the the same S/C ratio, and a summary of the results of the chosen design is given in Table 4.5. In the microchannel case, as much as 87.5% of the C_{5+} products are produced in the first stage.

Table 4.5: Fixed bed model results with a split to ATR of 0.9 and microchannel model with split to ATR of 0.85 and with S/C=0.6 for both cases.

	Fixed bed				Microchannel		
Stages	1	2	3	Total	1	2	Total
Catalyst volume [m^3]	286	225	179	690	96	64	160
CH_4 selectivity [%]	6.9	9.3	14.2	9.0	7.3	14.9	8.5
CO conversion [%]	42.5	53.2	60.9	89.5	81.3	79.0	96.1
C_{5+} production [tonne/h]	26.3	18.4	8.8	53.5	50.1	7.1	57.3

At these split ratios, an overview of some important process streams are given in Tables 4.6 and 4.7 for the fixed bed and the microchannel reactors. The stream numbers are

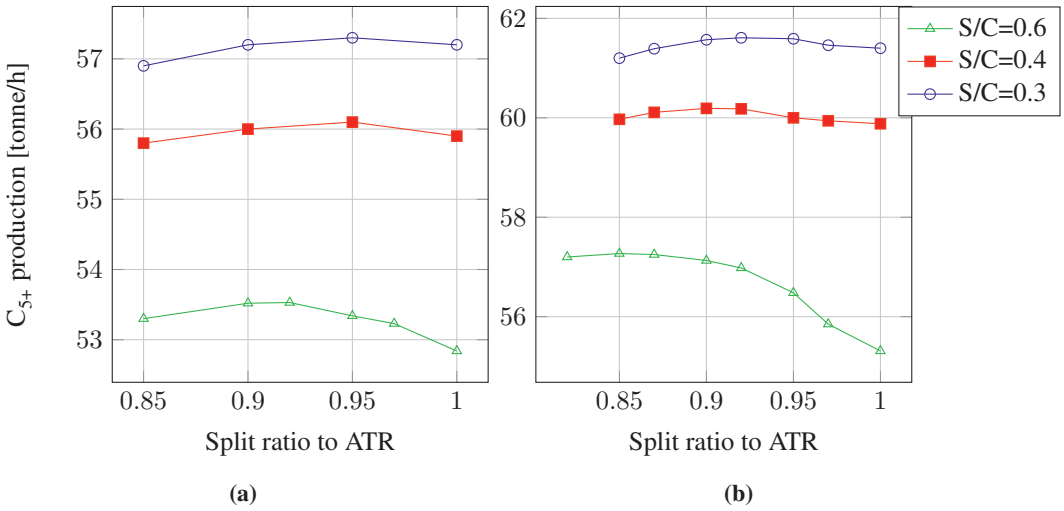

Figure 4.5: The production of C_{5+} with different S/C ratios and split ratios to the ATR, a) Fixed bed model b) Microchannel model

referred to the process flow diagram in Figure 4.2. Temperature, pressure, mass flows in addition to mass fractions of the important components are chosen to be shown. Stream 110 is the hot outlet stream from the ATR, while 120 and 130 are the feed and effluent streams on the tube side of the heat exchange reformer. Streams 210, 220 and 230 are the feed streams to stage 1,2 and 3 of the FT reactors, while stream 240 is the tail gas and 250 is the total product stream. As can be seen in stream 210 and 220, the pressure drop in the first fixed-bed reactor is lower than that of the microchannel reactor. Ergun equation is used to calculate pressure drop in both reactor types. Although we have lower superficial gas velocity in microchannel reactor, the particle diameter is 15 times smaller in microchannel case which results in higher pressure drop.

4.3.4 Water and power

If the process concept is to be deployed on a FPSO, it needs to be self sufficient with water and power. With the proposed process concept, there is no need to desalinate seawater or burn extra natural gas. Table 4.8 shows the water balance for the two reactor concepts. Water retrieved from the product may contain some oxygenates and small amounts of hydrocarbons but the water is perfect to be used as feed to the ATR or HER. These components will be reformed in the pre-reformer. Water retrieved from the syngas is much cleaner, mainly small amounts of CO_2 is present, and the water can easily be purified.

Table 4.9 shows the power balance. With fixed bed reactors the tail gas contains enough energy, whereas with the microchannel reactors 20 % of the hydrogen is added to the tail gas to obtain sufficient energy. In that respect the plant is autonomous in the sense that it produces more power and water than is consumed.

Table 4.6: Important stream information in the simulation with fixed bed model; the split to ATR is 0.9 and S/C = 0.6.

Stream	110	120	130	210	220	230	240	250
Temperature (°C)	1060	441	1050	210	210	210	30	175
Pressure (bar)	28.50	28.50	26.49	27.00	24.60	22.12	19.99	19.99
Mass flow (tonne/h)	485.31	42.44	42.44	407.74	339.63	291.39	266.53	54.02
Mass fractions								
CO	0.312	0	0.345	0.371	0.256	0.140	0.060	0.001
H_2	0.047	0.003	0.095	0.056	0.039	0.021	0.008	0
H_2O	0.161	0.726	0.425	0.002	0.001	0.001	0.001	0.002
CH_4	0.002	0.237	0.005	0.003	0.011	0.021	0.031	0
C_2-C_4	0	0	0	0	0.006	0.014	0.022	0.002
C_{5+}^{p} (alkanes)	0	0	0	0	0.005	0.008	0.010	0.891
C_{5+}^{o} (alkenes)	0	0	0	0	0	0	0	0.100
CO_2	0.100	0.033	0.130	0.119	0.143	0.167	0.182	0.003
N_2	0.377	0	0	0.449	0.538	0.627	0.686	0.002

4.3.5 Comparing fixed bed and microchannel reactors

The principal results for the two reactor types are given in Table 4.10. The reactor productivity in terms of catalyst volume, the microchannel reactor has 4.6 times larger productivity than the fixed bed. On the other hand, the total weight of the microchannel reactors are calculated to be greater that the fixed bed. Including the catalyst weight the microchannel reactors are 17 % heavier than with fixed bed reactors. The total weight includes cylindrical pressure shells that the microchannel modules are kept in.

The carbon efficiency is defined as the fraction of the carbon of components in the feed ending up as carbon of components in the product stream. Figure 4.6 shows the carbon distributions with the two synthesis reactor types. With fixed bed, the carbon efficiency is about 57 %, while with microchannel synthesis reactors is about 62 %. The main reason is that higher conversion, and thus less CO in the tail gas, is obtained with microchannel reactors. The rest of the carbon ends up in different components in the tail gas, including CO_2 produced in the ATR and lighter hydrocarbons produced in the Fischer-Tropsch synthesis reactors.

The carbon distribution is an important process descriptor, but energy distribution through the process is even more important. In the literature energy efficiency can be calculated in different ways so they may be difficult to compare. Here we look at the fraction of the total NG1 feed lower heating value (LHV) that is converted to LHV of the product and hydrogen streams, in addition to power export, energy of steam and finally lost energy. The tail gas and eventually some hydrogen are combusted to produce power that covers the compressor demands. The compressors are not included as input energy since their power demand is covered by the gas turbine. The excess power from the gas turbine, adjusted with the Carnot efficiency to be comparable to thermal energies, is reported as ”power export”. Lost energy includes external cooling and thermal energy of the exhaust

Table 4.7: Important stream information in the simulation with microchannel model; the split to ATR is 0.85 and S/C = 0.6.

Stream	110	120	130	210	220	240	250
Temperature (°C)	1060	441.2	1052	210	210	30	178.5
Pressure (bar)	28.50	28.50	28.10	26.93	22.80	19.15	19.15
Mass flow (tonne/h)	476.90	63.89	63.89	399.10	270.90	249.40	58.10
Mass fractions							
CO	0.314	0	0.343	0.375	0.104	0.024	0
H_2	0.045	0.003	0.095	0.054	0.015	0.002	0
H_2O	0.165	0.727	0.428	0.002	0.001	0.001	0.004
CH_4	0.002	0.236	0.005	0.003	0.023	0.032	0
C_2-C_4	0	0	0	0	0.017	0.027	0.002
C^p_{5+} (alkanes)	0	0	0	0	0.007	0.009	0.857
C^o_{5+} (alkenes)	0	0	0	0	0	0	0.130
CO_2	0.107	0.033	0.129	0.128	0.189	0.205	0.005
N_2	0.366	0	0	0.438	0.645	0.700	0.002

Table 4.8: Water balance.

Water Stream [tonne/h]	Fixed Bed	Microchannel
Steam demand	105.7	119.1
Retrieved water from syngas	89.8	96.4
Retrieved water from product	87.5	92.8
Excess water	71.5	70.1

Table 4.9: Power balance.

Category	Power source/ sink	Fixed bed [MW]	Microchannel [MW]
Power sinks	Aircompression	139	134.2
	H_2 compression	3.0	4.5
	CO_2 recycle to ATR	0.2	0.2
Power sources	Gas Turbine	164.9	148.2
Excess power production		22.7	9.3

gas from the gas turbine, in addition to pressure losses and loss of energy in compressors and turbine. Figure 4.7 gives a picture of the energy distribution with the two different synthesis reactor types. We should also bear in mind that part of the hydrogen energy will be transferred to the product after the product upgrading.

With fixed bed reactors 45 % of the natural gas LHV ends up in the product, while 9 % ends up as LHV of excess hydrogen, 26 % is steam produced from the FT reactors and hot

Table 4.10: Comparison between processes with fixed bed and microchannel reactors

	Fixed bed	Microchannel
Optimum feed split ratio to ATR	0.90	0.85
Total CO Conversion [%]	89.47	96.08
Total Methane Selectivity [%]	9.05	8.46
Carbon efficiency [%]	57.15	61.71
Catalyst volume [m^3]	690	160
Size of reactors [m^3]	3053	2115
Weight of empty reactors [tonne]	2141	3293
Weight of catalysts [tonne]	828	192
Reactor Productivity [tonne/(h m^3)]	0.078	0.358
Surplus hydrogen [tonne/h]	4.4	4.7

syngas, 4 % is power export, while 16 % is lost energy. With the microchannel alternative, 50 % (slightly less) of the natural gas LHV ends up in the product stream, while 9 % ends up as LHV of excess hydrogen. Less energy in steam production mainly due to less energy in the hot syngas, and less power export and slightly less lost energy.

Reaction heat generated in the Fischer-Tropsch reactors will be used for medium pressure steam production. This steam can be used in other parts of the process, however not considered here. The amount of steam from the FT reactors are estimated to be 289.5 and 311.4 tonnes/h for the fixed bed and microchannel reactors. The sensible heat generated from the FT reactors is calculated by integrating the heat transfer along the tubes, and the amount of steam generated is calculated by heating and evaporating water from 20 °C and 23.19 bar. However, there will be more steam produced with the fixed bed alternative, because of the higher split and thus the hot syngas after HER contains more energy.

4.3.6 The effect of heavier natural gas

The natural gas used so far, NG1 in Table 4.1, is relatively light. If the natural gas is somewhat heavier, as NG2 in Table 4.1, what will be the consequences? Notice that 6000 kmol/h of NG2 contains more carbon that NG1. Notice also that the split parameter is not optimized in this case.

With fixed bed reactors and with NG2 as the feed and the same conditions as described in Table 4.5, i.e same split and S/C ratio, the production of C_{5+} is increased to 60.3 tonnes/h, while the CO conversion is about the same, and the methane selectivity is decreased to 8.4 %. More hydrogen is distributed between the stages and excess hydrogen has dropped to 3.8 tonnes/h, while the excess power is about the same. The same tendency is also found with microchannel reactors. The methane selectivity drops to 7.6 %, the CO conversion drops to 93.6 %, while the C_{5+} production increases to 63.7 tonnes/h. There is a slight drop in the carbon efficiency, 61 %. The amount of distributed hydrogen is increased so the excess hydrogen is lower.

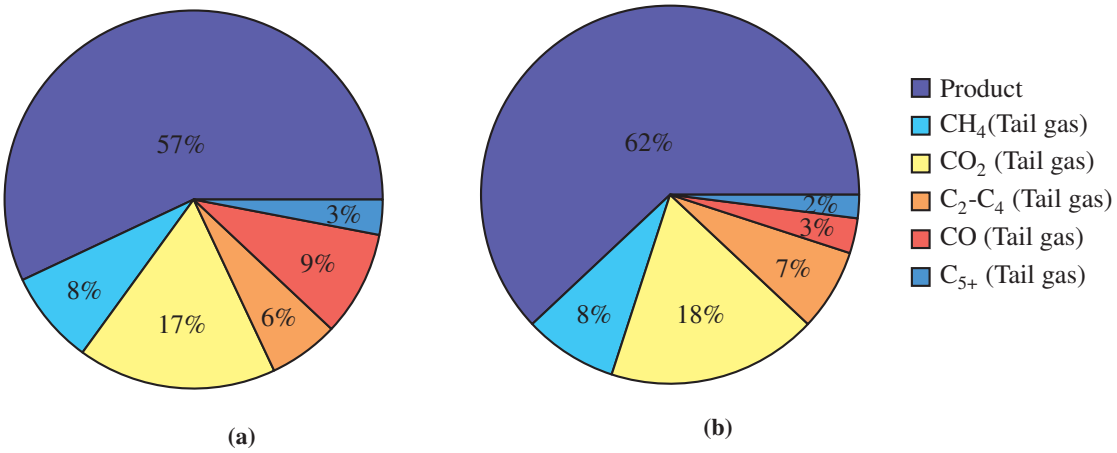

Figure 4.6: The relative distribution of carbon between the products stream and the tail gas, with a) fixed bed reactor and with b) microchannel reactors.

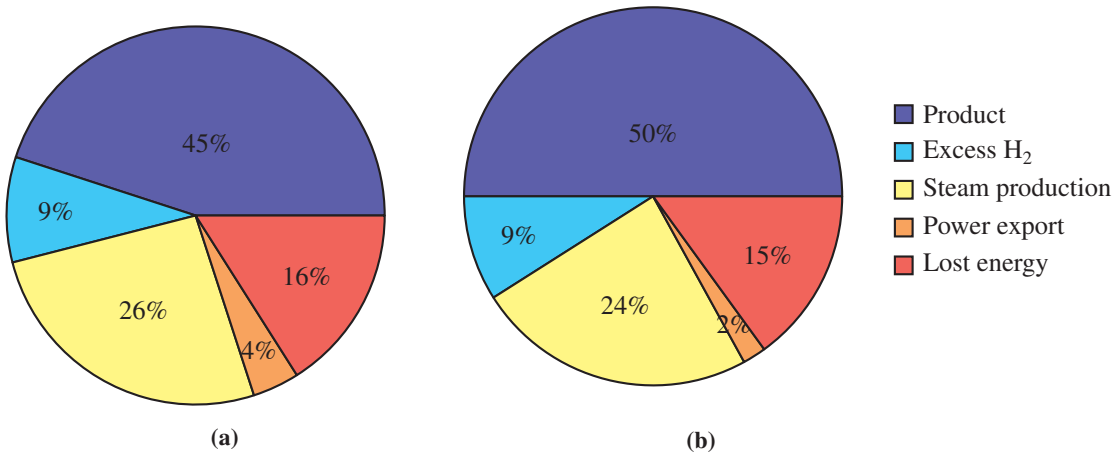

Figure 4.7: The relative distribution of energy content of the natural gas in different products streams of the GTL plant with a) fixed bed reactors and b) microchannel reactors.

4.3.7 Cost Estimation

The purchased cost for the fixed bed reactors is estimated based on different methods; different cost data of shell and tube heat exchanger extrapolated, the cost of material needed and the cost of pressure vessels plus the cost of one inch tubes. The latter is used here, and the cost of assembling the reactor is added, which is estimated equal to the material costs. There are 48500 tubes distributed in two shells at the first stage, 38200 tubes distributed in two shells at the second stage and 30500 tubes in one shell at the third stage. Purchased cost of the FT fixed bed reactors with catalyst is estimated to 42.6 million USD and installed cost to 100.9 million USD. Installed costs include piping, equipment erection, instrumentation and control, electrical and lagging and paint. The fixed bed FT reactors constitute 37 % of the total costs when civil, structure, buildings, the upgrading unit and the ship are not included. If the process is to be on a FPSO the upgrading process will be relatively simple because the oil need to be refined onshore.

The total fixed capital investment including offsites, design and engineering and contingency add up to approximately 500 million USD. Note that civil, structures, buildings, the upgrading unit and the FPSO are not included in this estimate. The main reason for the relatively low cost is that cryogenic air separation and conventional steam reformers are avoided.

The estimated cost of microchannel reactors is higher, but there is no historical data available to base concrete cost estimates on. It is higher because the microchannel reactors require more material and the cost of producing the microchannel reactors is relatively higher.

4.4 Conclusion

A novel process concept is proposed for converting natural gas to liquid hydrocarbon products. Syngas is produced in an enriched air-blown ATR at a slightly under-stoichiometric H_2/CO ratio. The synthesis section is staged and hydrogen is fed between the stages to make up for the hydrogen consumption. Products and water are removed between the stages. This enables a high CO conversion in a once-through configuration. The process produces syngas and hydrogen in two parallel paths. Hydrogen is produced in a heat exchange reformer, heat integrated with the hot outlet from the ATR. The process does not require cryogenic air separation or fired heaters. With the proposed configuration, high once-through CO conversion, in the order of 90 % and more, is achieved.

Conventional fixed bed and microchannel reactor models for the FT synthesis are developed and tested separately in process simulations. The carbon efficiencies for a once-through synthesis are calculated to be 57 and 62 % for the fixed bed and microchannel reactors, respectively. The part of the energy that ends up in the product is 45 and 50 % for the fixed bed and microchannel reactors. However, the fixed bed alternative produces more energy as steam and power for export.

A natural gas with heavier gas gives more products and less excess hydrogen. As long as there is sufficient excess hydrogen for upgrading, the heavier natural gas NG2 gives a more favorable energy distribution.

The process is autonomous as it is self-sufficient with power and water. The total in-

vestment of a 12000 bbl/day plant without considering the ship, buildings and structures or the upgrading unit is estimated to approximately 500 million USD with fixed bed reactors. Even when everything is not counted in the total cost, the proposed process concept is estimated to be less expensive than existing projects. The main reason for the low cost is that cryogenic air separation and the costly steam methane reformer are avoided.

Chapter 5

Evaluation of Kinetic Models for Fischer-Tropsch Cobalt Catalysts in a Plug Flow Reactor

This chapter is based on the published paper: "Evaluation of kinetic models for Fischer-Tropsch cobalt catalysts in a plug flow reactor" in journal: Chemical Engineering Research and Design, vol. ***114****, (2016), pp. 236 - 246.*

In order to do a good and realistic design of a Gas-to-Liquid (GTL) plant, it is necessary to have kinetic models that correctly capture major variations of reaction rates and selectivities subject to changes in process parameters. In this study, a review of published kinetic rate models is done and twelve of them are analyzed based on different criteria, such as their behaviour at high conversions, high water partial pressure, sensitivity to added water, selectivity to C_{5+} products, etc. The rate models are implemented in a plug flow reactor model. Both fixed bed and microchannel reactors can quite accurately be represented by such a model. Here, the main purpose is to see the kinetic effects with changing composition along the reactor. In order to predict the product distribution, we have proposed our own chain growth model and fitted parameters to experimental data from Yang et al. (2016). The chain growth model includes the effect of water and predicts the C_{5+} and methane selectivities quite well.

5.1 Introduction

There are numerous models available predicting reaction rates of the Fischer-Tropsch synthesis (FTS), and there is a diversity of different model structures. The reasons for the diversity may be assigned to different type of catalyst, type of support and promoters, cat-

alyst particle size and pore size, etc. In Table 5.1 a summary of 30 selected kinetic studies on cobalt catalysts is presented, dating back to 1949 to present, where different reactor types are applied, in addition to temperature, pressure and H_2/CO ranges. Some of the kinetic models give a detailed description of formation rates of individual components, while most models only describe the overall consumption rate of CO given as simple rate expressions. In Table 5.2 a summary of the latter type is listed. Some of the models (Yang et al., 1979; Pannell et al., 1980; Wang, 1987) are simple power law expressions:

$$-r_{\mathrm{CO}} = aP_{\mathrm{H_2}}^{b}P_{\mathrm{CO}}^{c} \tag{5.1}$$

In these expressions b is positive and c is negative, suggesting inhibition by adsorbed CO. Anderson (1956) found that the equation developed by Brötz (1949) to be inadequate for data over a wide range of inlet H_2/CO ratios and developed an equation by suggesting that the rate is proportional to the desorption of chains. The concentration of growing chains on the catalyst surface was related empirically to $P_{\mathrm{H_2}}^{2}P_{\mathrm{CO}}$. Zennaro et al. (2000) fitted their data fairly well by a simple power law expression of the form:

$$-r_{\mathrm{CO}} = aP_{\mathrm{H_2}}^{0.74}P_{\mathrm{CO}}^{-0.24} \tag{5.2}$$

However, they reported that the data are best fitted by a Langmuir-Hinshelwood (LH) rate model similar to that proposed by Yates & Satterfield (1991).

$$-r_{\mathrm{CO}} = \frac{aP_{\mathrm{CO}}P_{\mathrm{H_2}}^{0.74}}{(1+bP_{\mathrm{CO}})^2} \tag{5.3}$$

Yates & Satterfield (1991) proposed the following rate model:

$$-r_{\mathrm{CO}} = \frac{aP_{\mathrm{CO}}P_{\mathrm{H_2}}}{(1+bP_{\mathrm{CO}})^2} \tag{5.4}$$

They correctly pointed out that it is often a high degree of covariance between the estimated parameters, so that several terms in the denominator can barely be justified from a statistical perspective. In terms of Langmuir-Hinshelwood (LH) kinetics, one of these parameters would represent a surface rate constant while others are adsorption equilibrium coefficient. It is assumed that CO is the predominant surface species, which is justified by non-reacting, single component adsorption data on cobalt surfaces.

Botes et al. (2009), in their search for a suitable model, tested 16 different reaction models and came up with an LH kinetic model. Their preferred kinetic model is considered semi-empirical because it cannot be derived from an assumed reaction mechanism.

Keyvanloo et al. (2016) explored several mechanisms and LH rate models. Their proposed rate is:

$$-r_{\mathrm{CO}} = \frac{aP_{\mathrm{CO}}^{0.5}P_{\mathrm{H_2}}^{1}}{(1+bP_{\mathrm{CO}}+cP_{\mathrm{H_2}}^{0.5})^2} \tag{5.5}$$

In the denominator b is an activated rate constant and not an equilibrium constant. Therefore b increases with increasing temperature instead of decreasing. Ma et al. (2014) observed a positive kinetic water effect on Co/Al_2O_3 catalyst. It is consistent with the results of the effect of co-fed water on cobalt FTS in this work and the literature (e.g. Lögdberg

et al. (2011)) for Co/Al_2O_3 catalysts. Ma et al. (2014) employed their empirical model which has the effects of water:

$$-r_{\mathrm{CO}} = \frac{k_1(T) P_{\mathrm{CO}}^{-0.31} P_{\mathrm{H_2}}^{0.88}}{1 - 0.24 \frac{P_{\mathrm{H_2O}}}{P_{\mathrm{H_2}}}} \tag{5.6}$$

Some researchers have proposed more detailed kinetic models which are more complex and include a description of product distribution. The works of Storsæter et al. (2006); Visconti et al. (2007, 2011); Todic et al. (2013, 2014a, 2015); Mosayebi & Haghtalab (2015) and Mosayebi et al. (2016) are among this category.

The role of water on catalytic activity is a highly complex matter. Water is known to increase or decrease the catalytic activity. The influence of water on the cobalt-FT reaction kinetics has become an important topic in the literature and some authors have started to include water in their kinetic models (Withers et al., 1990; Van Steen & Schulz, 1999; Das et al., 2005; Bhatelia et al., 2011; Ma et al., 2014). The results of water co-feeding studies have not been very consistent, as some reported a positive effect on the reaction rate (Schulz et al., 1994; Krishnamoorthy et al., 2002; Li et al., 2002b) and some a negative influence of water on the reaction rate (Li et al., 2002c), while others have found no effect at all (Schulz et al., 1997; Li et al., 2002a). According to Ma et al. (2014), a positive water effect on the FT rate was observed on SiO_2 supported Co catalysts (Krishnamoorthy et al., 2002; Li et al., 2002b; Storsæter et al., 2005), a positive (Storsæter et al., 2005) or a slightly negative (Li et al., 2002a) water effect was observed on Co/TiO_2 catalysts, and a negative (Li et al., 2002c) or no significant effect (Schulz et al., 1997; Botes, 2009) or a positive water effect (Borg et al., 2006; Lögdberg et al., 2011) was observed on Co/Al_2O_3 catalysts. Dalai & Davis (2008) reviewed water effects on the performances of unsupported and supported Co catalysts. They concluded that the effects of water on FTS is quite complex and depends on the support and its nature, Co metal loading, its promotion with noble metals, and preparation procedure.

The product distribution from the Fischer-Tropsch synthesis is often described by the Anderson-Schulz-Flory (ASF) distribution, where the distribution is given by a single parameter; the chain growth probability or growth factor (α). In order to perform an FT reactor design with realistic evaluation of the products produced, there is a need for a way to quantify the product distribution. Some kinetic models include a description of product distribution. However most of them need a chain growth model to account for product distribution. Hydrocarbon selectivities depend on local conditions like temperature, pressure and species concentrations, in particular of carbon monoxide and hydrogen, but also on produced water. Therefore a suitable chain growth model should include these variables. The effect of some of the most important parameters affecting product selectivity are discussed thoroughly in literature by for example Van Der Laan & Beenackers (1999).

According to Ma et al. (2014), the effect of water on selectivities to C_{5+} and CH_4 for cobalt based catalyst has reached a consensus; indigenous or added water increase C_{5+} selectivity and decrease CH_4 selectivity (Schulz et al., 1997; Krishnamoorthy et al., 2002; Storsæter et al., 2005; Botes, 2009; Ma et al., 2011). Lögdberg et al. (2010) investigated the effect of adding water vapor to 20 cobalt-based supported catalysts. Although there was a large variation in selectivity, added water increased C_{5+} selectivity and decreased CH_4 selectivity for all catalysts. It is surprising however, that none of the available chain

growth models in literature have water partial pressure as a variable. In this article we propose a new chain growth model which includes the effect of water and predicts the C_{5+} and methane selectivities quite well.

Table 5.1: Kinetic studies of Co-based catalysts for Fischer-Tropsch synthesis

No.	Study	year	Catalyst	Reactor	T (C)	P (bar)	H_2/CO
1	Brötz (1949)	1949	$Co/MgO/ThO_2$/kieselguhr	FBR*	185 - 200	1	2
2	Anderson (1956)	1956	Co/ThO_2/kieselguhr	FBR	186 - 207	1	0.9 - 3.5
3	Yang et al. (1979)	1979	$Co/CuO/Al_2O_3$	FBR	235 - 270	1.7 - 55	1.0 - 3.0
4	Pannell et al. (1980)	1980	$Co/La_2O_3/Al_2O_3$	Berty (low conversion)	215	5.2 - 8.4	2
5	Outi et al. (1981)	1981	Co/Al_2O_3	FBR (low conversion)	250	1	0.2 - 4.0
6	Wang (1987)	1987	$Co/B/Al_2O_3$	FBR (low conversion)	170 - 195	1 - 2	0.25 - 4.0
7	Wojciechowski (1988)	1988	Co/kieselguhr	Berty	190	2 - 15	0.5 - 8.3
8	Sarup & Wojciechowski (1989)	1989	Co/kieselguhr	Berty	190	2 - 15	0.5 - 8.3
9	Withers et al. (1990)	1990	$Co/Zr/SiO_2$	CSTR**	240 - 280	30	1.0 - 2.0
10	Yates & Satterfield (1991)	1991	$Co/MgO/SiO_2$	Slurry	220 - 240	5 - 15	1.5 - 3.5
11	Iglesia et al. (1993)	1993	Co catalysts	FBR	200 - 210	1 - 30	1 - 10
12	Van Steen & Schulz (1999)	1999	$Co/MgO/ThO_2/SiO_2$	CSTR	190 - 210	2.7 - 6.2	Varied widely with water added
13	Zennaro et al. (2000)	2000	Co/TiO_2	FBR	200	8 - 16	1 - 4
14	Elbashir & Roberts (2004)	2004	Co/Al_2O_3	FBR - supercritical	230 - 260	60	0.5 - 2.0
15	Das et al. (2005)	2005	Co/SiO_2	CSTR	210	21.7	1 - 2.4
16	Storsæter et al. (2006)	2006	Co/Al_2O_3	Microreactor	210 ,220	1.85	10
17	Visconti et al. (2007)	2007	Co/Al_2O_3	FBR - micro reactor	210 - 235	8 - 25	1.8 - 2.7
18	Irankhah et al. (2007)	2007	$Co-Ru/Al_2O_3$	FBR	235 - 250	45 - 65	1.7 - 2.3
19	Botes et al. (2009)	2009	$CO/Pt/Al_2O_3$	Slurry	230	5 - 40	1.6 - 3.2
20	Atashi et al. (2010)	2010	$Co-Mn/TiO_2$	FBR - micro reactor	190 - 280	1.0 - 10	1.0 - 3.0
21	Bhatelia et al. (2011)	2011	$Ru/Co/Al_2O_3$	CSTR	205 - 220	14 - 24	1.4 - 2.1
22	Visconti et al. (2011)	2011	Co/Al_2O_3	FBR - micro reactor	210 - 236	8 - 26	1.8 - 2.8
23	Mansouri et al. (2013)	2013	$Co-Ce/SiO_2$	FBR - micro reactor	200 - 300	1	1.0 - 1.5
24	Nikparsaa et al. (2014)	2014	$Co-Ni/Al_2O_3$	FBR	250	30	2
25	Todic et al. (2014a, 2015, 2013)	2014	Co/Re	Slurry	205,210	15 - 25	1.4 - 2.1
26	Ma et al. (2014)	2014	Co/Al_2O_3	CSTR	205 - 230	14 - 25	1.0 - 2.5
27	Mosayebi & Haghtalab (2015)	2015	$Co-Ru/\gamma-Al_2O_3$	FBR	220 - 250	15 - 25	1.0 - 2.0
28	Azadi et al. (2015)	2015	$Co/\gamma-Al_2O_3$	Carberry spinning basket batch reactor	196 - 211	20	1.8 - 2.9
29	Mosayebi et al. (2016)	2016	$Co-Ru/\gamma-Al_2O_3$	FBR	200 - 240	10 - 30	1 - 3
30	Keyvanloo et al. (2016)	2016	$Co-Si/\gamma-Al_2O_3$	FBR	210 - 240	20	1.3 - 3.0

*FBR: Fixed bed reactor

**CSTR: Continuous stirred tank reactor

Table 5.2: Simple rate models proposed for Cobalt FTS

No.	Study	Rate model
1	Brötz (1949)	$r_{\mathrm{CO}} = \frac{aP_{\mathrm{H_2}}^2}{P_{\mathrm{CO}}}$
2	Anderson (1956)	$r_{\mathrm{CO}} = \frac{aP_{\mathrm{H_2}}^2 P_{\mathrm{CO}}}{1+bP_{\mathrm{H_2}}^2 P_{\mathrm{CO}}}$
3	Yang et al. (1979)	$r_{\mathrm{CO}} = aP_{\mathrm{H_2}} P_{\mathrm{CO}}^{-0.5}$
4	Pannell et al. (1980)	$r_{\mathrm{CO}} = aP_{\mathrm{H_2}}^{0.55} P_{\mathrm{CO}}^{-0.33}$
5	Outi et al. (1981)	$r_{\mathrm{CO}} = \frac{aP_{\mathrm{H_2}}^1 P_{\mathrm{CO}}^{0.5}}{(1+bP_{\mathrm{CO}}^{0.5})^3}$
6	Wang (1987)	$r_{\mathrm{CO}} = aP_{\mathrm{H_2}}^{0.66} P_{\mathrm{CO}}^{-0.5}$
7	Wojciechowski (1988)	$r_{\mathrm{CO}} = \frac{aP_{\mathrm{H_2}}^{0.5} P_{\mathrm{CO}}^1}{(1+bP_{\mathrm{CO}}^1+cP_{\mathrm{H_2}}^{0.5})^2}$
8	Sarup & Wojciechowski (1989)	$r_{\mathrm{CO}} = \frac{aP_{\mathrm{H_2}}^{0.5} P_{\mathrm{CO}}^{0.5}}{(1+bP_{\mathrm{CO}}^{0.5}+cP_{\mathrm{H_2}}^{0.5}+dP_{\mathrm{CO}})^2}$
9	Withers et al. (1990)	$r_{\mathrm{CO}} = \frac{aP_{\mathrm{H_2}}}{1+b\frac{P_{\mathrm{H_2O}}}{P_{\mathrm{CO}}P_{\mathrm{H_2}}}}$
10	Yates & Satterfield (1991)	$r_{\mathrm{CO}} = \frac{aP_{\mathrm{H_2}}^1 P_{\mathrm{CO}}^1}{(1+bP_{\mathrm{CO}}^1)^2}$
11	Iglesia et al. (1993)	$r_{\mathrm{CO}} = \frac{aP_{\mathrm{H_2}}^{0.6} P_{\mathrm{CO}}^{0.65}}{1+bP_{\mathrm{CO}}^1}$
12	Van Steen & Schulz (1999)	$r_{\mathrm{CO}} = \frac{kP_{\mathrm{H_2}}^{1.5}\frac{P_{\mathrm{CO}}}{P_{\mathrm{H_2O}}}}{(1+kP_{\mathrm{H_2}}(\frac{P_{\mathrm{CO}}}{P_{\mathrm{H_2O}}}))^2}$
13	Zennaro et al. (2000)	$r_{\mathrm{CO}} = \frac{aP_{\mathrm{H_2}}^{0.74} P_{\mathrm{CO}}^1}{(1+bP_{\mathrm{CO}}^1)^2}$
13	Zennaro et al. (2000)	$r_{\mathrm{CO}} = aP_{\mathrm{H_2}}^{0.74} P_{CO}^{-0.24}$
14	Elbashir & Roberts (2004)	$r_{\mathrm{CO}} = \frac{aP_{\mathrm{H_2}}^{0.5} P_{\mathrm{CO}}^{0.5}}{(1+bP_{\mathrm{CO}}^{0.5}+cP_{\mathrm{H_2}}^{0.5}+dP_{\mathrm{CO}})^2}$
15	Das et al. (2005)	$r_{\mathrm{CO}} = \frac{aP_{\mathrm{CO}}^{0.25} P_{\mathrm{H_2}}^{0.5}}{1+m\frac{P_{\mathrm{H_2O}}}{P_{\mathrm{H_2}}}}$
18	Irankhah et al. (2007)	$r_{\mathrm{CO}} = \frac{aP_{\mathrm{H_2}}^{0.5} P_{\mathrm{CO}}^{0.5}}{(1+bP_{\mathrm{CO}}^{0.5}+cP_{\mathrm{H_2}}^{0.5}+dP_{\mathrm{CO}})^2}$
19	Botes et al. (2009)	$r_{\mathrm{CO}} = \frac{aP_{\mathrm{CO}}^{0.5} P_{\mathrm{H_2}}^{0.75}}{(1+bP_{\mathrm{CO}}^{0.5})^2}$
20	Atashi et al. (2010)	$r_{\mathrm{CO}} = \frac{aP_{\mathrm{CO}}P_{\mathrm{H_2}}}{1+bP_{\mathrm{CO}}}$
20	Atashi et al. (2010)	$r_{\mathrm{CO}} = \frac{aP_{\mathrm{CO}}P_{\mathrm{H_2}}^2}{(1+2(bP_{\mathrm{CO}})^{0.5})^2}$
21	Bhatelia et al. (2011)	$r_{\mathrm{CO}} = \frac{aP_{\mathrm{H_2}}^{0.5} P_{\mathrm{CO}}}{(1+bP_{\mathrm{CO}}+cP_{\mathrm{H_2}}^{0.5}+mP_{\mathrm{H_2O}})^2}$
23	Mansouri et al. (2013)	$r_{\mathrm{CO}} = \frac{aP_{\mathrm{H_2}}}{(1+bP_{\mathrm{CO}})^2}$
24	Nikparsaa et al. (2014)	$r_{\mathrm{CO}} = \frac{aP_{\mathrm{H_2}}P_{\mathrm{CO}}}{(1+bP_{\mathrm{CO}}P_{\mathrm{H_2}}^{0.5})^2}$
26	Ma et al. (2014)	$r_{\mathrm{CO}} = \frac{aP_{\mathrm{CO}}^{0.31} P_{\mathrm{H_2}}^{0.88}}{1+m\frac{P_{\mathrm{H_2O}}}{P_{\mathrm{H_2}}}}$
30	Keyvanloo et al. (2016)	$r_{\mathrm{CO}} = \frac{aP_{\mathrm{CO}}^{0.5} P_{\mathrm{H_2}}}{(1+bP_{\mathrm{CO}}+cP_{\mathrm{H_2}}^{0.5})^2}$

5.2 Chain growth models

5.2.1 From literature

Only few detailed product distribution models have been proposed for Co-based FTS;(Visconti et al., 2007; Kwack et al., 2011; Visconti et al., 2011; Todic et al., 2013, 2014a, 2015; Mosayebi & Haghtalab, 2015; Mosayebi et al., 2016). Many of the chain growth models available are parts of micro kinetic models where chain growth probability changes with the propagation step. The growth factor is the ratio between two consecutive product formation rates which is a constant. However, what is often observed is a distribution that can be described by two or more growth factors. A possible model is to let the growth factor α_1 be the larger to produce paraffins, and the growth factor α_2, be the smaller to produce olefins. The FT reactions may be lumped into one reaction, and if all products with five and more carbons is lumped into a single C_{5+} component, the reaction can be written as:

$$CO + U \cdot H_2 \xrightarrow{r_{FT}} H_2O + \nu_1 C_1 + \nu_2 C_2 + \nu_3 C_3 + \nu_4 C_4 + \nu_{5+} C_{5+} \tag{5.7}$$

In addition, a known deviation from ideal ASF distribution is the enhanced production of methane, which can be accounted for by introducing an extra methanation reaction. How to calculate the stoichiometric coefficients U, ν_i and average carbon number of the lump is shown by Hillestad (2015). The stoichiometric product coefficients are $\nu_i = (1-\alpha)^2\alpha^{i-1}$ and $\nu_{5+} = (1-\alpha)\alpha^4$. The stoichiometric usage ratios of hydrogen, U, for production of paraffins and olefins are:

$$U_1 = 3 - \alpha_1 \tag{5.8}$$

$$U_2 = 2 + (1-\alpha_2)^2 \tag{5.9}$$

Depending on α_1 and α_2, the stoichiometric usage ratio will be slightly above 2. If the amount of H_2 in the feed is more than the stoichiometric usage ratio, CO will be the limiting reactant and the H_2/CO ratio will increase along the reactor. On the other hand, if the amount of H_2 is below the stoichiometric usage ratio, H_2 will be the limiting reactant and the H_2/CO ratio will decrease along the reactor.

A very simple chain growth model is suggested by Yermakova & Anikeev (2000) as an empirical relation between α and the compositions of H_2 and CO after testing several different equation forms:

$$\alpha = A\frac{y_{CO}}{y_{H_2} + y_{CO}} + B \tag{5.10}$$

Here, y_{CO} and y_{H_2} are the mol fractions of CO and H_2 in the gas phase. They fitted this model to their experimental data over an alumina-supported cobalt catalyst promoted with zirconium, and estimated constants A and B to be 0.2332 ± 0.0740 and 0.6330 ± 0.0420, respectively. This model lacks temperature dependency and Song et al. (2004) modified the model to:

$$\alpha = (A\frac{y_{CO}}{y_{H_2} + y_{CO}} + B)[1 - 0.0039(T - 533)] \tag{5.11}$$

They found the slope of temperature dependency by fitting equation 5.11 to various experimental data in the review paper by Van Der Laan & Beenackers (1999). However,

there is a concern over this temperature correlation in that the data in the mentioned reference are related to Fe and Ru catalysts which are different from the original catalyst for which equation 5.10 is developed. Lox & Froment (1993) proposed a chain growth model for an iron catalyst which is a function of temperature:

$$\alpha = \frac{k_1(T)P_{\mathrm{CO}}}{k_1(T)P_{\mathrm{CO}} + k_2(T)P_{\mathrm{H_2}} + k_3(T)} \tag{5.12}$$

Vervloet et al. (2012) derived a chain growth model for a cobalt catalyst:

$$\alpha = \frac{1}{1 + k_\alpha(\frac{C_{\mathrm{H_2}}}{C_{\mathrm{CO}}})^\beta \exp(\frac{\Delta E}{R}(\frac{1}{493.15} - \frac{1}{T}))} \tag{5.13}$$

The model does not take into account the effect of water. Kruit et al. (2013) and Becker et al. (2016) have used this model in their work to explain the deviations from the ASF distribution by using an α which is dependent on process conditions.

Ermolaev et al. (2015) used the following growth model in their fixed bed model with cobalt catalysts:

$$\alpha = \frac{1}{1 + \frac{k_\alpha}{P_{\mathrm{CO}}^{2/3} P_{\mathrm{H_2}}^{2/3}}.(1 + \frac{1}{1+k_\beta P_{\mathrm{H_2}}^{0.5}})} \tag{5.14}$$

Where

$$k_\alpha = 40.3 \exp(-9600(\frac{1}{T} - \frac{1}{488.15})) \tag{5.15}$$

$$k_\beta = 0.035 \exp(-4800(\frac{1}{T} - \frac{1}{488.15})) \tag{5.16}$$

All parameters, such as pre-exponential factors and activation energies, were obtained from experimental data of laboratory scale fixed bed reactor.

Extensions to the ASF model has been made by Frtsch et al. (2015) to account for deviations from ASF distribution. These extensions includes a description of enhanced product formation and re-adsorption. However, estimating several parameters from experimental data can be uncertain especially in case of deviations from ideal experimental conditions, such as diffusion limitations, existence of local hot spots or product accumulation in the reactor (Frtsch et al., 2015).

5.2.2 Our proposed model

In order to predict the product distribution, we have developed a chain growth model based on the experimental data of Yang et al. (2016). They performed a kinetic investigation on 40%Co/1%Re/γ-Al_2O_3 catalyst at reactor conditions of 210 - 240 °C, 20 - 40 bar and feed H_2/CO = 2.17. They studied the effect of operation temperature, pressure and gas-hourly space velocity on CO conversion, C_{5+} selectivity, CH_4 selectivity and stability during Fischer-Tropsch synthesis in a microchannel reactor. The model structure is based on the propagation probability being equal to the ratio of propagation rate and the sum

of propagation and termination rates. Empirical exponents are introduced and only one temperature parameter is estimated. The fitted model is:

$$\alpha = \frac{1}{1 + k_2(T)\frac{P_{\mathrm{H_2}}^{1.45}}{P_{\mathrm{CO}} P_{\mathrm{H_2O}}^{0.253}}} \tag{5.17}$$

$$k_2(T) = 0.0233 \exp(-1959(\frac{1}{T} - \frac{1}{483})) \tag{5.18}$$

The effects of temperature, partial pressures of H_2O, H_2 and CO are taken into account in this model. The growth probability decreases slightly with increasing total pressure, and increases with increasing H_2O partial pressure. With increase in H_2/CO ratio, the growth factor decreases.

A plug flow model is applied to simulate the 18 last experimental points from Yang et al. (2016). These points are from the same catalyst batch. Experimental CO conversion, C_{5+} and CH_4 selectivities range from 20 - 80 %, 76 - 88 % and 6 - 12 %, respectively (see Figure 5.1). The kinetic rate model suggested by Ma et al. (2014) is implemented and only one parameter of this rate model is adjusted, the level of k and not the activation energy, as the cobalt loading is different. The rate constant is given by:

$$k(T) = 0.0234 \exp(-\frac{104000}{R}(\frac{1}{T} - \frac{1}{483})) \tag{5.19}$$

A separate methanation reaction is added to account for the higher methane selectivity than predicted by the ASF distribution. The methanation reaction is found to be proportional to the methane formation rate from reaction 5.7 and is estimated to be:

$$r_{\mathrm{CH_4}} = 7.70 r_{\mathrm{FT}} (1-\alpha)^2 \cdot \exp(-\frac{36687}{R}(\frac{1}{T} - \frac{1}{483})) \tag{5.20}$$

The olefin production rate is set to 8% of paraffin production rate. To account for the production of olefins, the chain growth factor proposed by Todic et al. (2014a) is used:

$$\alpha_2 = \alpha_1 \exp(-0.27) \tag{5.21}$$

C_1 to C_4 carbon selectivities (S_{C_i}) are calculated as:

$$S_{\mathrm{C}_i} = i \times \frac{F_{\mathrm{C}_i}^{out} - F_{\mathrm{C}_i}^{in}}{F_{\mathrm{CO}}^{in} - F_{\mathrm{CO}}^{out}} \times 100 \qquad\qquad i = 1:4 \tag{5.22}$$

Where F_{C_i} is the molar flow of hydrocarbons containing i number of carbon atoms. C_{5+} selectivity is calculated as:

$$S_{\mathrm{C}_{5+}} = 100 - \sum_{i=1}^{4} S_{\mathrm{C}_i} \tag{5.23}$$

As a result, the reactor model predicts CO conversion, C_{5+} and CH_4 selectivities quite well, as shown in Figures 5.1 and 5.2.

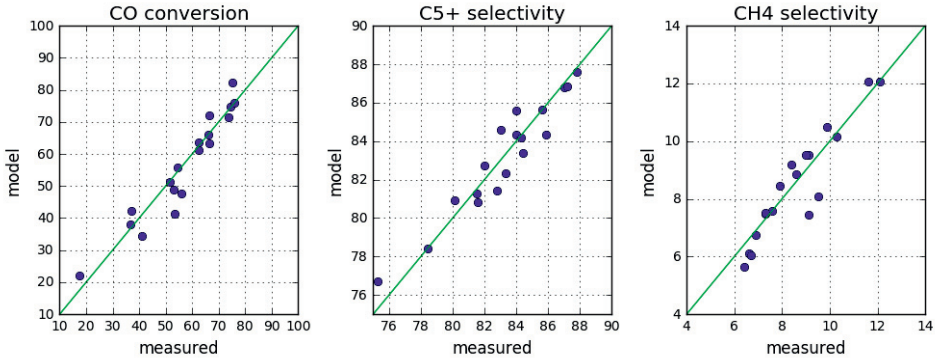

Figure 5.1: Parity plots of measured and estimated CO conversion, C_{5+} and CH_4 selectivities for the developed chain growth model.

5.3 Evaluation of kinetic models

In order to compare different kinetic models, they were implemented in a plug flow model. Our proposed chain growth model (eq. 5.17) is used to calculate selectivities toward C_{5+} and CH_4 as described in previous section. Olefin chain growth factor is calculated with eq. 5.21. The olefin production rate is set to 8% of paraffin production rate. To account for higher production of methane than predicted by ASF distribution, eq. 5.20 is also implemented. A total of 12 kinetic models mentioned in the work of Ma et al. (2014) is the basis for the present work. They fitted those models to their experimental data on a 25 %Co/Al_2O_3 catalyst and calculated parameter values for different kinetic rate models. Here we use the same parameter values so that the different rate models, presented in Table 5.3, are compared on the same basis.

For each reaction rate model, six different scenarios are investigated which are one over stoichiometric and two under stoichiometric H_2/CO ratios at the inlet of the reactor, each with and without added water. They are shown schematically in Figure 5.3. The trends observed for understoichiometric H_2/CO ratios of 2.0 and 1.5 are similar and therefore only results for one of them, namely H_2/CO = 2.0 are shown in the following figures. The reactor is operating at 27 bar and nearly isothermal conditions at 220 °C. Behaviours of rate models and chain growth model as function of H_2/CO ratio, H_2O/H_2 ratio and CO conversion are investigated along the reactor. The effect of CO conversion on C_{5+} selectivity is also studied.

5.3.1 Water addition

In practice, even after the water is knocked out before the FT reactor, the syngas will always contain some water. There has been numerous studies looking into the effects of added water on FTS. For these reasons, it is worthwhile to investigate how different rate models and our chain growth model (eq. 5.17) react to added water in the feed. 20% water is added for this investigation. Upon water addition, the total pressure and the flow rate

Table 5.3: Kinetic models used (parameter values from Ma et al. (2014))

Number*	Model	Study number in Table 1	Parameter values			
r_1	$r_{CO} = kP_{CO}^{a}P_{H_2}^{b}$	3,4,6,13	k,mol/g-cat/h/MPa^(a+b) 0.0137	a -0.35	b 0.81	
r_2	$r_{CO} = \frac{kP_{CO}^{0.65}P_{H_2}^{0.6}}{(1+K_1P_{CO})}$	11	k,mol/g-cat/h/MPa^(1.25) 0.6500	K1,MPa^(-1) 41.30		
r_3	$r_{CO} = \frac{kP_{CO}P_{H_2}^{0.74}}{(1+K_1P_{CO})^2}$	13	k,mol/g-cat/h/MPa 0.3080	K1,MPa^(-1) 3.90		
r_4	$r_{CO} = \frac{kP_{CO}^{0.5}P_{H_2}^{0.5}}{(1+K_1P_{CO}^{0.5}+K_2P_{H_2}^{0.5})^2}$	7,8	k,mol/g-cat/h/MPa 0.0976	K1,MPa^(-0.5) 2.36	K2,MPa^(-1) -0.67	
r_5	$r_{CO} = \frac{kP_{CO}P_{H_2}^{0.5}}{(1+K_1P_{CO}+K_2P_{H_2}^{0.5})^2}$	7,8	k,mol/g-cat/h/MPa^(1.5) 0.0782	K1,MPa^(-1) 1.95	K2,MPa^(-1) -0.48	
r_6	$r_{CO} = \frac{kP_{CO}P_{H_2}}{(1+K_1P_{CO})^2}$	10	k,mol/g-cat/h/MPa^(2) 0.2696	K1,MPa^(-1) 3.61		
r_7	$r_{CO} = \frac{kP_{CO}P_{H_2}^{2}}{(1+K_1P_{CO}P_{H_2}^{2})}$	2	k,mol/g-cat/h/MPa^(3) 0.1130	K1,MPa^(-3) 4.83		
r_8	$r_{CO} = \frac{kP_{CO}^{0.5}P_{H_2}}{(1+K_1P_{CO}^{0.5})^3}$	5	k,mol/g-cat/h/MPa^(1.5) 24.60	K1,MPa^(-0.5) 1.65		
r_9	$r_{CO} = \frac{k(P_{CO}P_{H_2}^{1.5}/P_{H_2O})}{(1+K_1P_{CO}P_{H_2}/P_{H_2O})^2}$	12	k,mol/g-cat/h/MPa^(2) 0.01470	K1,MPa^(-1) 0.19		
r_{10}	$r_{CO} = \frac{kP_{CO}P_{H_2}^{0.5}}{(1+K_1P_{CO}+K_2P_{H_2}^{0.5}+mP_{H_2O})^2}$	21	k,mol/g-cat/h/MPa^(1.5) 0.0560	K1,MPa^(-1) 1.61	K12,MPa^(-0.5) -0.51	m,MPa^(-1) -0.17
r_{11}	$r_{CO} = \frac{kP_{CO}^{0.5}P_{H_2}^{0.75}}{(1+K_1P_{CO}^{0.5})}$	19	k,mol/g-cat/h/MPa^(1.25) 1.36	K1,MPa^(-0.5) 8.16		
r_{12}	$r_{CO} = \frac{kP_{CO}^{0.31}P_{H_2}^{0.88}}{1+m\frac{P_{H_2O}}{P_{H_2}}}$	26	k,mol/g-cat/h/MPa^(0.57) 0.0133	m -0.24		

* Numbers in the following figures refer to these rates

Table 5.4: Inlet mol fractions for different scenarios

	Without water present			With water present		
Components	Over stoichiometric (H_2/CO = 2.5)	Under stoichiometric (H_2/CO = 2.0)	Under stoichiometric (H_2/CO = 1.5)	Over stoichiometric (H_2/CO = 2.5)	Under stoichiometric (H_2/CO = 2.0)	Under stoichiometric (H_2/CO = 1.5)
H_2	0.714	0.667	0.6	0.5714	0.53333	0.48
CO	0.286	0.333	0.4	0.2286	0.26666	0.32
H_2O	1 ppm*	1 ppm*	1 ppm*	0. 2	0.2	0.2

* Very low amount of water to avoid mathematical error in α model and some rates

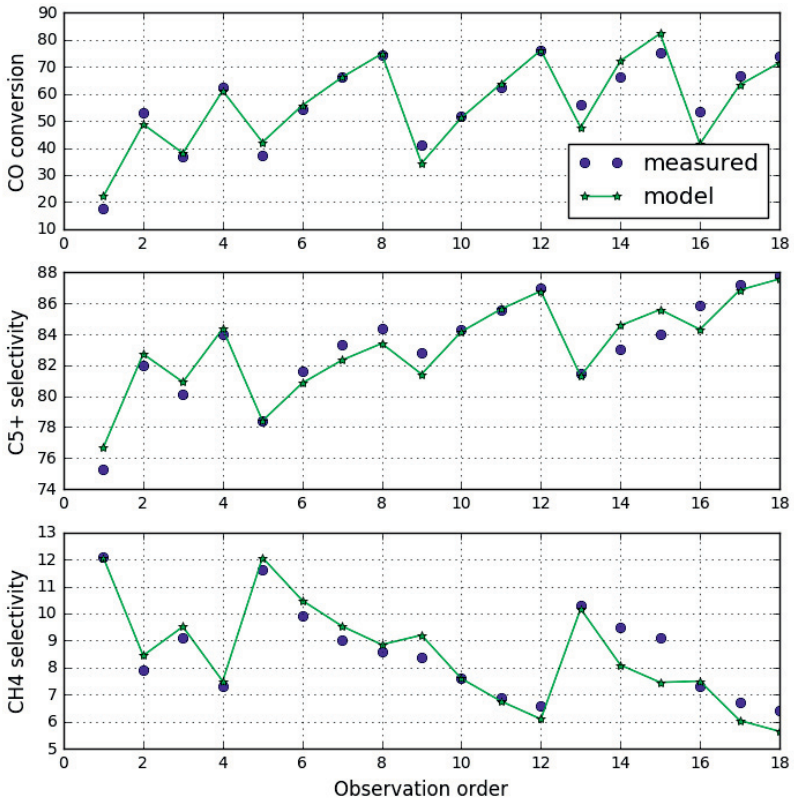

Figure 5.2: Order plot of measured and estimated CO conversion, C_{5+} and CH_4 selectivities for the developed chain growth model.

of synthesis gas are kept constant. Thus, the partial pressures of the reactants are reduced as water is introduced in the feed stream. The water flow rate is 20% of the syngas flow rate. Therefore the total flow rate with water addition is 20% higher than the case without water. Inlet compositions for different cases are shown in Table 5.4.

5.3.2 Behaviour of chain growth model

Behaviour of our chain growth model (eq. 5.17) versus CO conversion, H_2/CO ratio and H_2O/H_2 ratio is shown in Figure 5.4. The α behaviour as a function of these variables is the same with all kinetic models. It is clearly seen that water has positive effect on α model and increases C_{5+} selectivity. Having an under stoichiometric H_2/CO ratio at the inlet, the ratio decreases along the reactor; while and over stoichiometric H_2/CO ratio at the inlet, gives

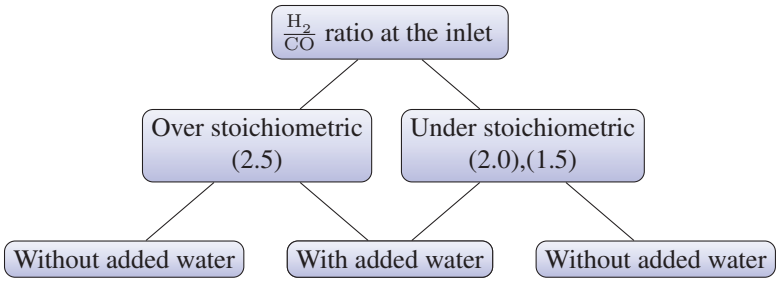

Figure 5.3: Simulation scenarios

the opposite effect. Lower H_2/CO ratios yields higher α values. In Figure 5.4, it worth to note the behaviour of α model versus CO conversion with overstiochiometric feed. Both curves increase up to CO conversion of about 80% and then they start to decrease. The reasons are attributed to counteracting effects of increasing H_2/CO ratio and water partial pressure on α. In Figure 5.4d, the effect of CO conversion on C_{5+} selectivity is shown. It follows the same trend as α model (Figure 5.4a).

5.3.3 Behaviour of kinetic rate models

In Figure 5.5, the response of kinetic models as a function of CO conversion along the reactor is plotted. All kinetic models follow the same trend, except r_9, r_{10} and r_{12} which have water term in their structure and with increase of CO conversion, water makes its impacts. r_9 has a bell shape in scenarios with no added water, mainly because of having two water terms in the denominator. r_{10} shows typical behaviour as the rest of the models in under stoichiometric cases, while it increases with conversion before a steep decline as conversion approaches 100% in over stoichiometric cases. r_{12} reaches a singularity point in its denominator at conversions of about 80% which makes it to go to infinity. r_1 goes to infinity at high conversions in over stoichiometric scenarios, because CO which is in the denominator of this rate model gets depleted. One point to mention is that in cases with under stoichiometric H_2/CO ratios at the inlet, none of the rate models reach 100% CO conversion, because H_2 gets depleted and becomes the limiting reactant.

In Figure 5.6, different rate models are plotted against the H_2/CO ratio along the reactor. Again all kinetic models follow more or less the same trend except r_9, r_{10} and r_{12}. In under stoichiometric scenarios, H_2/CO ratio decreases along the reactor. In over stoichiometric scenarios, H_2/CO ratio increases along the reactor.

In Figure 5.7, different rate models are plotted against the H_2O/H_2 ratio along the reactor. These reflect zones in which catalyst is prone to deactivation with high water partial pressure. Again all kinetic models follow more or less the same trend except r_9, r_{10} and r_{12}.

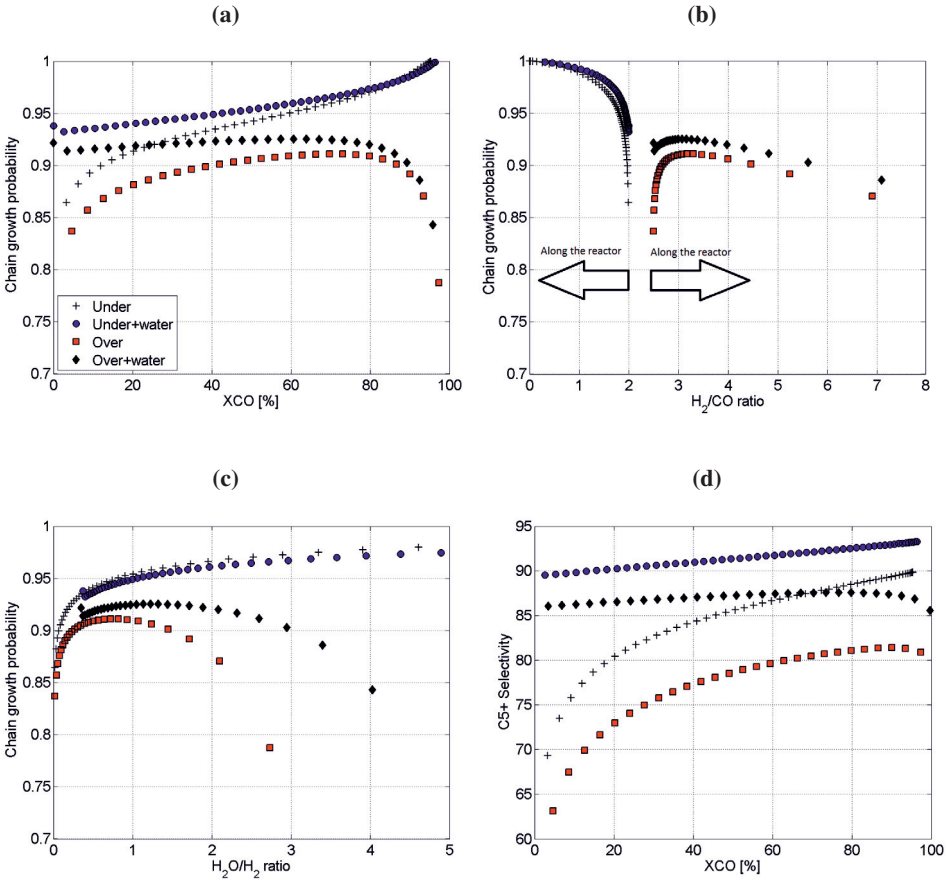

Figure 5.4: a, b & c: Chain growth probability as a function of CO conversion, H_2/CO and H_2O/H_2 ratio with under and over stoichiometric H_2 feed; d: C_{5+} selectivity versus CO conversion with under and over stoichiometric H_2 feed

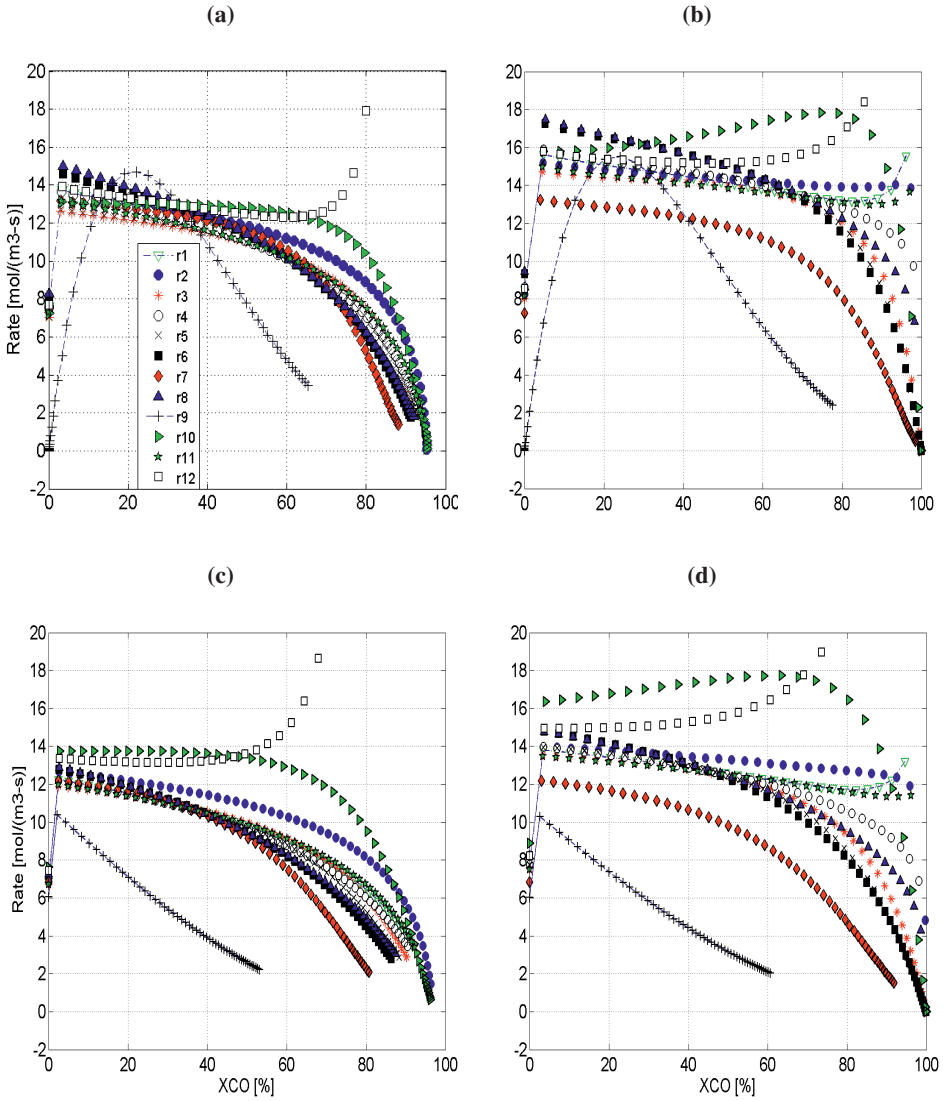

Figure 5.5: Reaction rates versus CO conversion for different rate models with under and over stoichiometric H_2 feed: a) Under stoichiometric with no added water; b) Over stoichiometric with no added water; c) Under stoichiometric with added water; d) Over stoichiometric with added water;

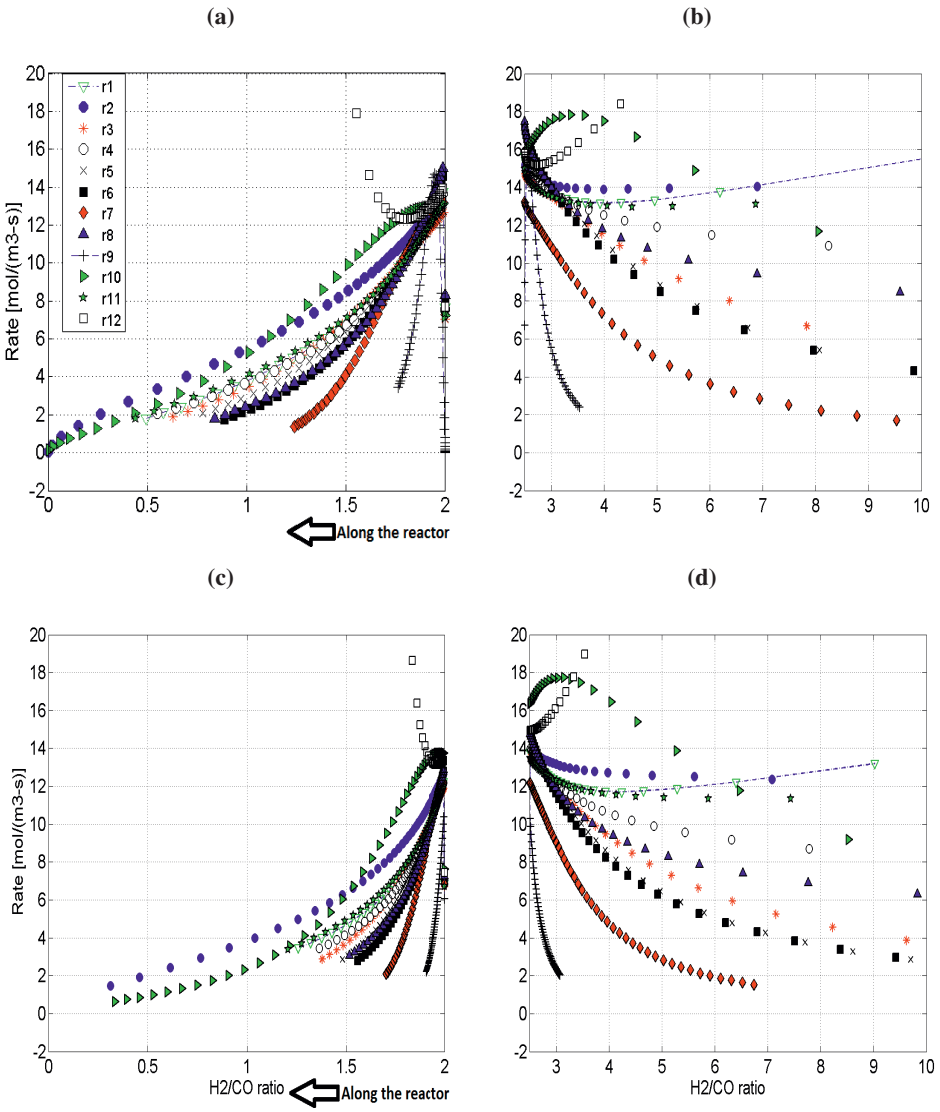

Figure 5.6: Reaction rates versus H_2/CO ratio for different rate models with under and over stoichiometric H_2 feed: a) Under stoichiometric with no added water; b) Over stoichiometric with no added water; c) Under stoichiometric with added water; d) Over stoichiometric with added water;

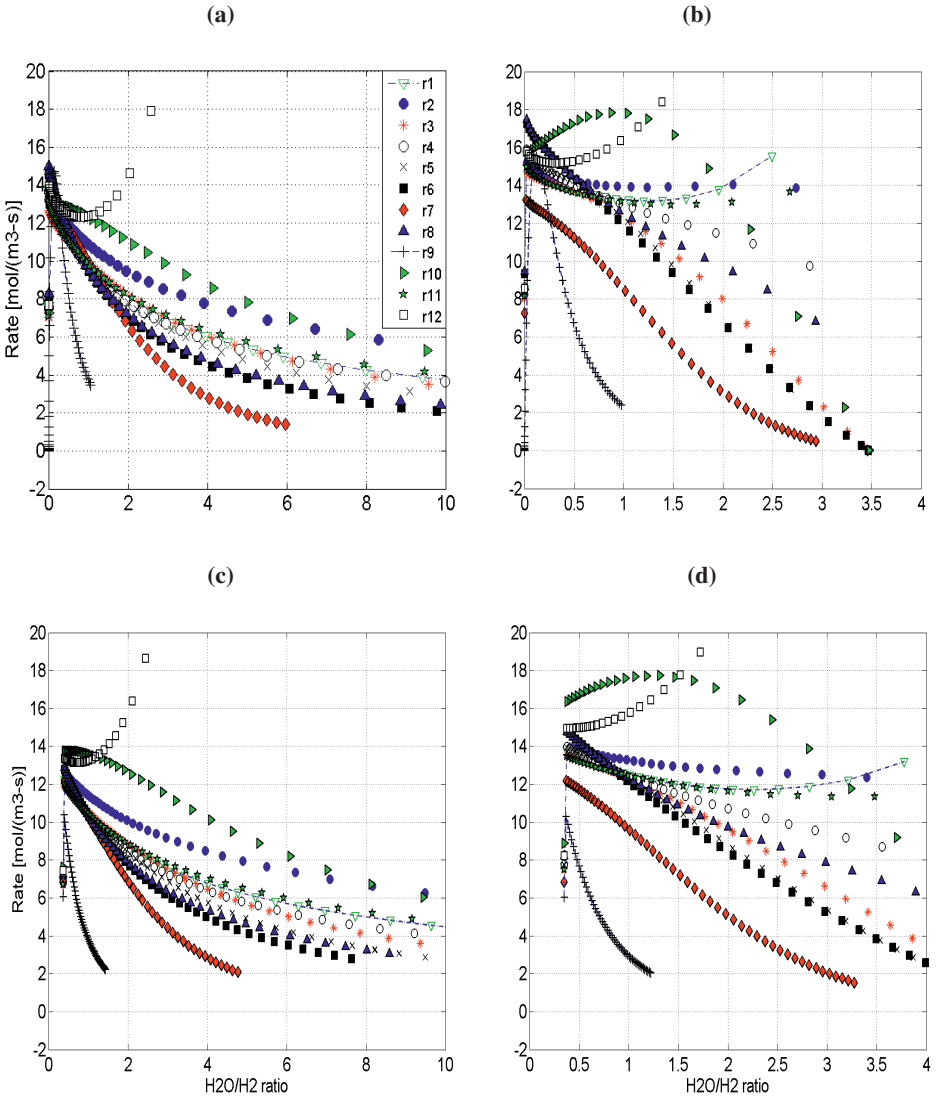

Figure 5.7: Reaction rates versus H_2O/H_2 ratio for different rate models with under and over stoichiometric H_2 feed: a) Under stoichiometric with no added water; b) Over stoichiometric with no added water; c) Under stoichiometric with added water; d) Over stoichiometric with added water;

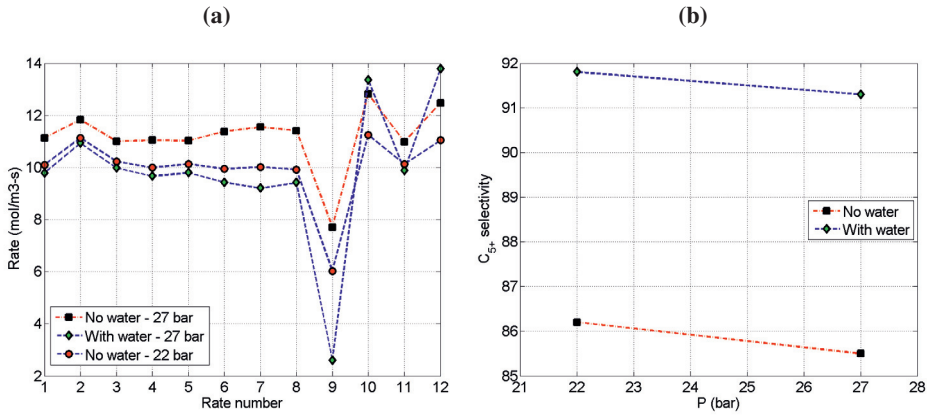

Figure 5.8: Effect of pressure and added water at constant CO conversion of 50% with under stoichiometric H_2/CO ratio feed on: a) FT rates; b) C_{5+} selectivity

5.3.4 Effect of pressure and added water on FT rate and C_{5+} selectivity at constant conversion (X_{CO}=50%)

In order to investigate the effect of pressure on different rates, another pressure level (22 bar) is used and compared with high pressure (27 bar) results. Since the trends for both understoichiometric and over stoichiometric H_2/CO ratio in the feed are similar, only results with understoichiometric feed are presented. The effect of added water on rate models are shown in Figure 5.8a. Because of direct effect of pressure, all rates decrease with decreasing pressure. For reaction rates r_1 to r_9, upon water addition, reaction rates decrease. The reason is that by water addition, syngas partial pressure is lowered to keep the total pressure constant. Among all reaction rates, only reaction r_9, r_{10} and r_{12} have water partial pressure present in their structure and water addition shows positive effect on r_{10} and r_{12}.

The effect of pressure and added water on C_{5+} selectivity is shown in Figure 5.8b. In our α model (eq. 5.17), C_{5+} selectivities decrease with increasing pressure. The effect of water on C_{5+} selectivities is positive. Added water increased C_{5+} selectivity by as much as 5%. The reason is that our proposed model (eq. 5.17) is strongly dependent on water.

5.4 Conclusions

A new chain growth model is proposed based on microchannel experimental data. This chain growth model together with Ma et al. (2014) kinetic model predicted the experimental data quite well. Twelve kinetic models are implemented in a plug flow reactor model and their behaviour to six different scenarios which are depicted in Figure 5.3 are investigated. These kinetic models are compared based on their response to CO conversion, H_2/CO ratio, H_2O/H_2 ratio and C_{5+} selectivities. The trends observed for under stoichiometric ratios of 2.0 and 1.5 are similar. r_9, r_{10} and r_{12} showed different behaviour than

the rest of the models, mainly because they have the water effect in their structure. r_{12}, reached a singularity point at CO conversions of about 80 %. If it is to be used for reactor design purposes, this should be taken into account. r_1 goes to infinity at very high conversions (more than 95%) in overstoichiometric scenarios, because CO which is in denominator gets depleted. Effects of pressure on rate models and C_{5+} selectivity is also investigated. Two pressure levels (22 and 27 bar) are used for this comparison. Higher pressure yields higher rates for all kinetic models. But the effect of pressure on C_{5+} selectivity is the opposite, higher pressure yields lower C_{5+} selectivity. Effect of added water is also investigated on kinetic models and C_{5+} selectivities. For all rate models except models r_{10} and r_{12}, added water decreased reaction rates, mainly because the syngas pressure is lowered upon water addition to keep the total pressure constant. Upon water addition, C_{5+} selectivities increased by about 5% for all rate models. This study can be an starting point for researchers to look closer to structures of kinetic models.

Chapter 6

Once-through Gas-to-Liquid Process with Verified Kinetics for Microchannel Fischer-Tropsch Reactors

This chapter is based on the published paper: "Conceptual design of an autonomous once-through gas-to-liquid process with microchannel Fischer-Tropsch reactors" in journal: Chemical Engineering Transactions, vol. ***52****, (2016), pp. 523-528.*

Converting remote natural gas to liquid fuel is one possible solution to the problem of transporting remote gas to the energy market. However, the high investment cost of gas-to-liquid (GTL) plants prevents large scale exploitation of remote gas reserves. A lean GTL is suggested based on an autothermal reformer with enriched air as oxidant and a once-through Fischer-Tropsch synthesis. In order to maximize the syngas conversion and the production of heavy hydrocarbons, a staged microchannel reactor path with distributed hydrogen feed and product withdraw is proposed. The hydrogen is produced by steam methane reforming in a heat exchange reformer (gas heated reformer). A verified kinetic model for the Fischer-Tropsch reactor is used. This kinetic model was fitted to kinetic data of a 40 %CO/Al_2O_3 catalyst which was used in a microchannel reactor. A new chain propagation model was also fitted to the data. The new kinetic and rate propagation models are believed to be specifically suitable for microchannel reactors. The chain propagation model in the process yields high C_{5+} selectivities. The process is autonomous in the sense that it is self-sufficient with power and water.

6.1 Introduction

Increase in energy demand and depleting easily accessible oil have turned industries focus on untapped resources that are unused for technical or economic reasons, such as associated gas or stranded gas reserves. Transportation of the gas is one of the biggest obstacles in exploiting these reserves. Converting natural gas to liquid fuels, gas-to-liquid (GTL), is one option in bringing remote natural gas to the market. By placing a GTL unit on a floating production vessel, many offshore remote gas reserves can be monetized and also reduce flaring. However, placing a GTL plant on a vessel faces its own challenges that an onshore plant does not. To mention a few are the need for operations autonomy in the sense that all production utilities, such as water and power, need to be available on board the ship. Pure oxygen streams may be problematic because of high explosion risk due to proximity with hydrocarbons. Also high columns with liquid inventory on board the ship may create problems. There have been some investigations looking at the feasibility of installing a gas-to-liquid (GTL) process on floating production storage and offloading (FPSO) vessel that are described by Ostadi et al. (2015).

Table 6.1: Specifications of the natural gas feeds; NG1 is used for all the results produced here, while NG2 is used to see the effect of heavier natural gas.

	NG1	NG2
Temperature [°C]	50	50
Pressure [bar]	30	30
Flow [MMscfd]	120.2	120.2
Molar flow [kmol/h]	6000	6000
Mole fraction		
CH_4	0.95	0.85
C_2H_6	0.02	0.067
C_3H_8	0.015	0.033
$n-C_4H_{10}$	0.01	0.022
$n-C_5H_{12}$	0.005	0.011
CO_2	0	0.017

6.2 The proposed process concept

The process configuration is the same as our previous study (Ostadi et al., 2015). The process flow diagram is shown in Figure 6.1. Here, the product upgrading process and the steam utility system are not shown. The specifications of natural gas feed are shown in Table 6.1. After sulfur removal, the natural gas is mixed with steam before entering the pre-reformer. Stream 100 is split into two streams, 101 and 102, the former to the ATR and the latter to the HER. The split ratio is 85 % to ATR and 15 % to HER. The energy required for the steam reforming reactions in the HER is provided by the hot outlet stream from the ATR. The outlet of the HER is cooled down before entering the high temperature water gas shift (WGS) reactor, shifting CO to CO_2 and H_2. After the WGS reactor, the stream is

cooled and water is knocked out before entering the membrane unit for separation of H_2. The hydrogen rich stream with 99 % purity is then compressed and distributed between the Fischer-Tropsch stages. The CO_2 rich stream, which also contains some H_2, CO and CH_4, is compressed and recycled to the ATR. By adding this stream, the H_2/CO ratio out of the ATR will be reduced, which is beneficial for the FT synthesis. Because of the under-stoichiometric H_2/CO ratio at the inlet of the first FT stage, this ratio continues to decrease along the reactor. In order to increase this ratio before the next stage, hydrogen is injected between the stages. The effluent stream from ATR after heat exchange with the HER, is further cooled to knock out water from the syngas. Without further compression the syngas stream is heated before entering the first Fischer-Tropsch stage. In order to increase the rate of the FT reactions, and also suppress catalyst deactivation, the gas outlet from FT reactors is cooled down and partly condensed where water and hydrocarbon products are separated from the gas. The tail gas, consisting of unconverted syngas, nitrogen and light gas components produced in the Fischer-Tropsch reactors, is used as fuel in the gas turbine to supply power to consumers.

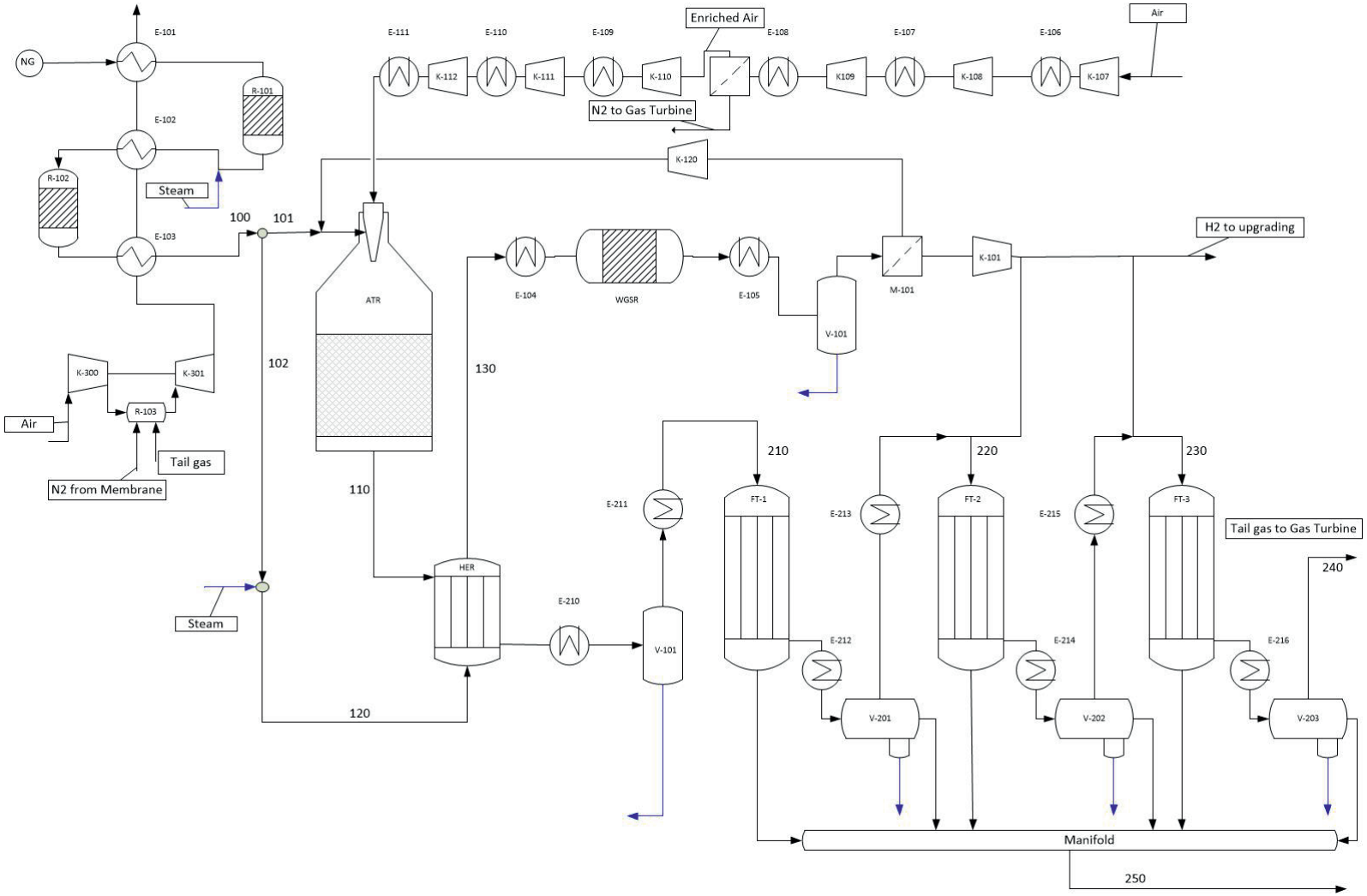

Figure 6.1: Process flow diagram of the proposed GTL plant. Heat integration and the steam system are not shown here.

6.2.1 Syngas production

An autothermal reformer is selected for syngas production. The main reasons are that the H_2/CO ratio can be adjusted to be close to the optimal ratio and the ease of scalability. A pre-reformer is used in front of the ATR to prevent coke formation on the ATR catalyst. With an air-blown ATR, it is practically impossible to recycle the unconverted syngas because of very high nitrogen concentrations. This is also the case with enriched air, and a once-through synthesis scheme is the only option to avoid high accumulation of nitrogen. PRISM membrane separators from Air Products are considered (AirProducts, 2015). Considering the large air flow through the membrane and therefore avoiding very large membrane modules, a PRISM membrane is chosen to have 34 % oxygen purity. An alternative to air or enriched air is to use pure oxygen. Pure oxygen from cryogenic air separation poses significant safety challenges offshore, in addition to large investment costs. Although having enriched air increases the volume of equipment after ATR, but considering the cost of having an air separation unit, it will be beneficial to have larger volumes than having an air separation unit.

6.2.2 Hydrogen production

When H_2/CO ratio is slightly under-stoichiometric, more C_{5+} products can be obtained and in order to compensate for the consumption of hydrogen, it is added between the stages. Part of the produced hydrogen is also sent to the product upgrading unit. Steam reforming with the use of a heat exchange reformer is applied to produce hydrogen with H_2/CO ratios of more than three. Apart from being a hydrogen generator, the HER provides efficient heat integration and avoids the use of a waste heat boiler. The heat exchange reformer is counter current and consists of 1000 steam reformer tubes of 10 cm diameter and 10 m long. Modeling of the heat exchange reformer is described in detail by Falkenberg & Hillestad (2015). The remaining CO is converted to CO_2 by the use of a water gas shift reactor. The WGS effluent is cooled down to 30 °C to remove most of the water before entering the membrane to produce a hydrogen rich and a CO_2 rich stream. The CO_2 rich stream is recycled back to the ATR to decrease the H_2/CO ratio at the outlet of the ATR. The membrane used here is a carbon membrane with no sweep gas on the permeate side. This will produce very pure hydrogen on the permeate side.

6.2.3 Fischer-Tropsch synthesis

The Fischer-Tropsch synthesis is staged with product withdrawal and hydrogen addition between the stages. This enables high conversion of syngas and high selectivity to higher hydrocarbons. Studies on the kinetics of FT synthesis show that nitrogen only dilutes syngas and therefore has no influence on the kinetics if the partial pressures of carbon monoxide and hydrogen are kept constant (Jess et al., 1999). Moreover, nitrogen plays an important role in the operation of multi-tubular reactors by facilitating removal of generated heat.

6.2.4 Microchannel reactor

Reactors with microchannels are suited for reactions that are highly exothermic or highly endothermic. Channels filled with FT catalyst powder and channels with coolant water are arranged in a cross flow configuration. We assumed a two-dimensional homogeneous model with no axial dispersion. Boiling water is used as coolant and its temperature is assumed to be constant along the axial direction. Table 6.2 shows the design parameters of the microchannel reactor model. Isothermal behaviour of microchannel FT reactors has been demonstrated by Deshmukh et al. (2010). The hot-oil-cooled microchannel reactors were isothermal to within 1 °C. This is also verified with our reactor model. With very high heat removal capability, single pass conversions near 80 % can be realized.

Table 6.2: Design parameters of microchannel reactor.

Catalyst bulk density [kg/m^3]	1200
Catalyst particle diameter [mm]	0.2
Catalyst void fraction	0.40
Cooling water temperature [°C]	220
Diameter of channel side [mm]	2×2

Table 6.3: Important stream information.

Stream	110	120	130	210	220	230	240	250
Temperature (°C)	1060	441.2	1052	210	210	210	30	191
Pressure (bar)	28.50	28.50	28.10	26.93	24.84	22.95	21.69	21.69
Mass flow (tonne/h)	476.90	63.89	63.89	399.10	307.80	273.10	255.2	57.44
Mass fractions								
CO	0.314	0	0.343	0.375	0.205	0.112	0.055	0.001
H_2	0.045	0.003	0.095	0.054	0.030	0.016	0.008	0
H_2O	0.165	0.727	0.428	0.002	0.001	0.001	0.001	0.002
CH_4	0.002	0.236	0.005	0.003	0.013	0.018	0.021	0
C_2-C_4	0	0	0	0	0.009	0.0014	0.017	0.001
C_{5+}^{p} (alkanes)	0	0	0	0	0.009	0.012	0.013	0.945
C_{5+}^{o} (alkenes)	0	0	0	0	0	0	0	0.046
CO_2	0.107	0.033	0.129	0.128	0.166	0.188	0.201	0.003
N_2	0.366	0	0	0.438	0.567	0.640	0.684	0.002

6.2.5 Kinetic rate and chain propagation models

Here, an alternative kinetic rate model and a model describing the product distribution of the Fischer-Tropsch synthesis are applied (Ostadi et al., 2016). The kinetic rate model,

Table 6.4: Overall plant results

Total CO conversion [%]	90.55
Total methane selectivity [%]	5.61
Carbon efficiency [%]	61
Catalyst volume [m^3]*	89
Reactor productivity [tonne/(h m^3)]	0.64
Surplus hydrogen [tonne/h]	5.96
C_{5+} production [tonne/h]	56.90
C_{5+} production [bbl/day]	12000

Table 6.5: Water balance

Water Stream [tonne/h]	
Steam demand	119.10
Retrieved water from syngas	96.4
Retrieved water from product	87.57
Excess water	64.86

Table 6.6: Power balance

Category	Power source/ sink	[MW]
Power sinks	Aircompression	129.9
	H_2 compression	4.5
	CO_2 recycle to ATR	0.2
Power sources	Gas Turbine	139.6
Excess power production		4.97

suggested by Ma et al. (2014), is verified against data from a microchannel laboratory reactor (Yang et al., 2016). In addition, a model describing the product distribution and methane selectivity is developed (Ostadi et al., 2016) and fitted to data generated by Yang et al. (2016). It is well known that the selectivity of methane is higher than predicted by the ASF distribution. To account for this fact, a separate methanation reaction rate is introduced. The methanation reaction rate, Equation 6.3, is found to be proportional to the rate of methane production by ASF model. ν_1 is the stoichiometric coefficient of methane according to ASF distribution. The data used for the fitting of the reaction rate is from 40 % CO/Al_2O_3 catalyst. To account for gradual deactivation of catalyst, 80 % of the activity of fresh catalyst is used to calculate the rate. The implemented kinetic rate model, Equation 6.1 and Equation 6.3, and the product distribution model, Equation 6.4, are as follows:

$$r_{FT} = k(T)\frac{P_{\mathrm{CO}}^{-0.31} P_{\mathrm{H_2}}^{0.88}}{1 - 0.24\frac{P_{\mathrm{H_2O}}}{P_{\mathrm{H_2}}}} \tag{6.1}$$

$$k(T) = 0.0133 \exp(-\frac{104000}{R}(\frac{1}{T} - \frac{1}{483})) \tag{6.2}$$

$$r_{\mathrm{CH_4}} = 7.70 r_{\mathrm{FT}}(1-\alpha)^2 \cdot \exp(-\frac{36687}{R}(\frac{1}{T} - \frac{1}{483})) \tag{6.3}$$

$$\alpha = \frac{1}{1 + k_2(T)\frac{P_{\mathrm{H_2}}^{1.45}}{P_{\mathrm{CO}} P_{\mathrm{H_2O}}^{0.253}}} \tag{6.4}$$

$$k_2(T) = 0.0233 \exp(-1959(\frac{1}{T} - \frac{1}{483})) \tag{6.5}$$

The production of alkanes and alkenes is described by two chain growth probabilities. The rate of production of alkenes is 70 % of that of alkanes. Since Fischer-Tropsch reaction can in theory produce infinite number of paraffins and olefins, the method suggested by Hillestad (2015) is used to handle infinite number of reactions and components. We have chosen to model alkane components individually up to C_{10} and a lump C^{p}_{11+} describing the tail distribution. While for alkenes, with less heavier components, we have chosen to model individual components up to C_4 and a lump C^{o}_{5+}. For the sake of brevity the lumps C^{p}_{5+} and C^{o}_{5+} are reported here, but they are made by adding individual components and the modeled lumps. This way of lumping is described in detail by Hillestad (2015). The kinetic model is implemented in a model of the microchannel reactor with the use of Aspen Custom Modeler (ACM) language. The model is further exported to Aspen HYSYS process simulator for simulation and optimization of the entire GTL plant.

6.3 Results

In our previous investigation two reactor stages with 2 meter reactor length was used (Ostadi et al., 2015). This distribution of volumes is not optimal. Here three stages are used to increase C_{5+} production in less volume. Following the method of systematic staging of reactors (Hillestad, 2010), we did an optimization of reactor path and came up with different lengths of reactors. Table 6.7 shows different design parameters for different FT stages. The first, second and third FT stages have 54, 27 and 19 % of the total volume. The proposed chain propagation model yields low methane selectivity and high C_{5+} selectivity. Methane selectivities are less than 6 % in all stages. The important streams information is shown in Table 6.3. The important results of the plant are shown in Table 6.4.

6.3.1 Water and power

The tail gas from the last FischerTropsch stage is used as fuel to the gas turbine for power production. Water balance and power balance are shown in Tables 6.5 and 6.6, respectively. The plant produces excess power of 4.97 MW and also excess water.

Table 6.7: Design parameters for different FT stages

	Stage 1	Stage 2	Stage 3
Channel Length [m]	0.8	0.6	0.5
Volume [m^3]	48	24	17
Inlet H_2/CO	2.0	2.0	2.0
H_2 addition between stage [kmol/h]	0	365.1	127.7
CH_4 selectivity [%]	5.95	5.39	4.26
CO conversion [%]	57.9	51.6	53.5
C_{5+} production [tonne/h]	35.65	13.99	7.26

6.3.2 Carbon and energy efficiencies

The carbon efficiency is defined as the fraction of the feed carbon components ending up as carbon of product components. The carbon efficiency is about 61 %. For the calculation of the energy efficiency, we look at the fraction of the natural gas feed heating value (LHV) that is converted to LHV of the product and hydrogen streams, in addition to power export, energy of steam and finally lost energy. The excess power from the gas turbine, adjusted with the Carnot efficiency to be comparable to thermal energies, is reported as Excess power. We should also keep this in mind that part of hydrogen will be transferred to products after the product upgrading. About 49 % of the natural gas LHV ends up in the product stream and about 12 % ends up as LHV of excess hydrogen. The amount of steam from the FT reactors is estimated to be 291.5 t/h. The amount of steam generated is calculated by heating and evaporating water from 20 °C and 23.19 bar. By using NG_2 in Table 1, we can see the effect of heavier natural gas. By use of NG_2, total CO conversion drops to 81.5 %, however, CH_4 selectivity and C_{5+} production remains the same. The carbon efficiency will also decrease to 54 %, which is because of lower conversion in the FT stages.

6.4 Conclusions

A novel process concept is proposed for converting natural gas to liquid hydrocarbon products. For the Fischer-Tropsch reactors, a verified kinetic rate and product distribution models of the Fischer-Tropsch synthesis are applied (Ostadi et al., 2016). The new and verified kinetic model yields higher reaction rates than what was used in our previous investigation (Ostadi et al., 2015). The new kinetic model along with the product distribution model is specifically suited for microchannel reactor and it gives us a more realistic view of the process in the large scale. With the proposed configuration, high once-through CO conversion, in the order of 90 % and more, is achieved. The carbon efficiencies for a once-through synthesis are calculated to be 61 % and the energy efficiency is about 49 %. Compared to our previous investigation, this study produces the same amount of C_{5+} but in 45 % less volume which means lower cost of the overall GTL plant.

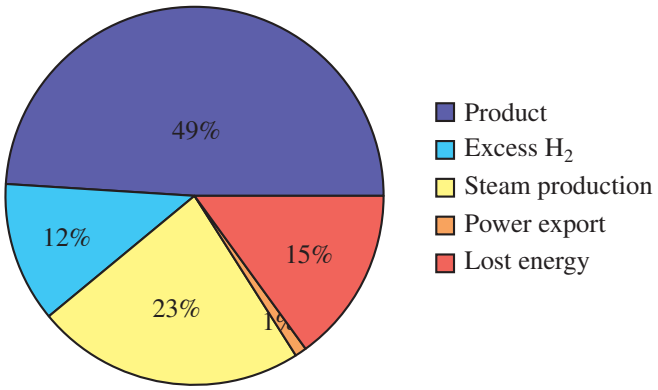

(a)

Figure 6.2: The relative distribution of energy content of the natural gas in different products streams of the GTL plant.

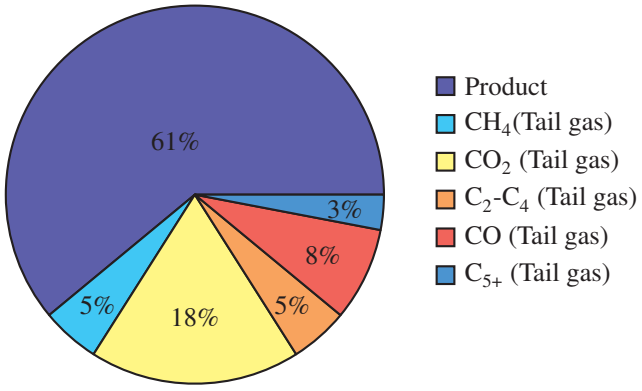

(a)

Figure 6.3: The relative distribution of carbon between the products stream and the tail gas.

Chapter 7

Combined Gas-to-Liquid and Ammonia Production

This chapter is based on the submitted paper: "Combined gas-to-liquid and ammonia production" to journal of Natural Gas Science and Engineering.

A novel process concept is proposed for cogeneration of Fischer-Tropsch products and ammonia. An autothermal reformer with enriched air as oxidant is applied for synthesis gas production, and because of the inert nitrogen, a once-through Fischer-Tropsch synthesis is necessary. In order to maximize the synthesis gas conversion and the production of heavy hydrocarbons in Fischer-Tropsch reactors, a staged reactor path with distributed hydrogen feed and product withdraw is applied. Hydrogen is produced by steam methane reforming in a heat exchange reformer (gas heated reformer), heat integrated with the hot effluent stream from the autothermal reformer. Part of this hydrogen stream is used in Fischer-Tropsch reactors and the rest are sent to product upgrading and the ammonia synthesis. Part of the nitrogen produced from the air membrane is used as feed to the ammonia process. The proposed ammonia process is simple as it does not require separate shift reactors and a CO_2 capture unit. The process is autonomous in the sense that it is self sufficient with power and water, and therefore well suited for production in remote locations such as a floating production unit. The total investment of 12000 bbl/d (57 tonnes/h) GTL plant combined with 24 tonnes/h ammonia plant is estimated to be around 900 million USD, of which the ammonia process counts only for 7 %. The extra ammonia production will increase total revenues by 50 %, which makes the combined process commercially attractive.

7.1 Introduction

Steadily increasing energy consumption worldwide and depletion of easily accessible oil have turned attentions to untapped resources, such as associated and stranded gas reserves. Converting natural gas to liquid fuels is one possibility to monetize these reserves. In two previous articles (Ostadi et al., 2015; Ostadi & Hillestad, 2016), we proposed a once-through GTL plant that produces liquid fuels from natural gas which is suitable for deployment on a floating vessel. Through ammonia cogeneration, the process becomes more profitable and thus more appealing for commercialization. Since the proposed GTL process produces pure hydrogen, only relatively small changes or additions are needed to build an ammonia production unit.

Cogeneration of chemicals has been practised in industry as a means to increase efficiency and profitability of processing plants. Cogeneration of ammonia with GTL products is not a new concept and has been discussed in numerous patents such as Kresnyak (2016); Zhou et al. (2003); Price & Tindall (2005) and Pedersen & Yakobson (2007).

In Kresnyak's design (Kresnyak, 2016), nitrogen is taken from an air separation unit (ASU) and hydrogen from hydrogen separation unit which takes in portion of the syngas from autothermal reformer (ATR) or partial oxidation (POX) reactor to produce hydrogen rich stream. The hydrogen separation unit can be pressure swing adsorption (PSA), membrane or liquid absorption technology or a combination of them. Zhou et al. (2003) used the Fischer-Tropsch (FT) effluent stream containing unreacted hydrogen and inert nitrogen for the ammonia synthesis. All hydrocarbons are separated from the FT effluent stream and the unconverted CO is shifted to CO_2. The inlet stream to ammonia process contains H_2, N_2 and CO_2. It is believed that CO_2 is a poison for the ammonia synthesis and presence of CO_2 in the inlet stream is strange. In Price & Tindall (2005)'s design, nitrogen is taken from an ASU. Hydrogen is extracted from a portion of the FT syngas stream by means of PSA or a membrane unit. FT syngas is produced by ATR or steam methane reformer (SMR). In case of using SMR, water gas shift (WGS) reactor is used to shift CO to H_2 before the hydrogen extraction. In Pedersen & Yakobson (2007)'s design, the effluent of FT unit which contains significant amounts of gaseous hydrocarbons are reformed in a steam reformer to produce additional amount of hydrogen. The CO in the tail gas from the FT unit is shifted to produce H_2 which, after extraction, e.g., in a H_2 membrane, and purification is combined with N_2 from the ASU in H_2 to N_2 ratio of 3 for ammonia production. At their Sasolburg plant in South Africa, Sasol is producing ammonia and GTL products. In their process, nitrogen comes from the air separation unit, while hydrogen is recovered from the FT tail gas to produce ammonia (Dry & Steynberg, 2004).

In our design, hydrogen is produced in a separate path by heat exchange reformer (HER), while nitrogen comes from the high pressure side of air separation membrane. The proposed process will produce about 576 tonnes/day of ammonia and about 12,000 bbl/day of hydrocarbon products. This process is still self sufficient in power and water and can export an excess power of about 17.6 MW. Total investment cost for the combined processes is estimated to be around 900 million USD, from which the ammonia synthesis has only 7% of the share.

7.2 The proposed process concept

The natural gas feed specification is the same as the one used in Ostadi & Hillestad (2016). The integration of the ammonia into the GTL plant is chosen to be as simple as possible. In the proposed design, the integration between GTL and ammonia processes is limited to hydrogen and nitrogen feeds to the ammonia process and exchange of power and steam between the two processes. A simplified block flow diagram of the combined GTL with ammonia production is shown in Figure 7.1.

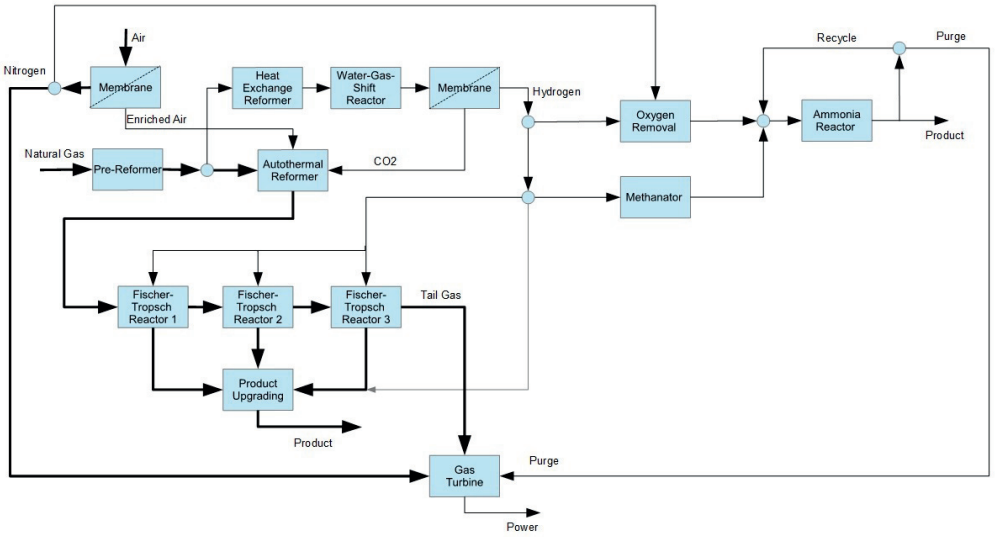

Figure 7.1: Block flow diagram of the proposed process concept; water and steam are not shown.

7.2.1 The gas-to-liquid process

The GTL process is the same as the process described by Ostadi & Hillestad (2016), and a brief description of the process is provided here. The process flow diagram of the combined GTL-ammonia process is shown in Figure 7.2. Sulfur is first removed from the natural and then it is mixed with steam before entering the pre-reformer. The pre-reformed natural gas is then split into two streams,with split ratio of 85% and 15%. The former enters the ATR and the latter enters the HER. Air is compressed and separated in an air separation membrane to supply enriched-air to the ATR. The main reasons for not using a cryogenic air separation unit onboard a floating production storage and offloading (FPSO) vessel are twofold; safety and space issues. Moreover, with ship movement, the liquid inventory of distillation columns may be a problem.

The energy required for the steam reforming reactions in the HER is provided by the hot outlet stream from the ATR. The outlet of the HER is cooled down before entering the high temperature water gas shift reactor, where CO is shifted to CO_2 and H_2. After the WGS reactor, the stream is cooled and water is knocked out before entering the hydrogen

membrane unit. The permeate is hydrogen with 99 % purity, which is further compressed and distributed between the FT stages and the ammonia process. The retentate, mainly CO_2 with some H_2, CO and CH_4, is compressed and recycled to the ATR. By recycling this stream to the ATR, the H_2/CO ratio will be reduced, which is beneficial for the FT synthesis. The H_2/CO ratio in the feeds to the FT reactors is under-stoichiometric, because the yield to higher hydrocarbons is favoured. The stoichiometric usage ratios of hydrogen, U, for production of paraffins and olefins are $U_1 = 3 - \alpha_1$ and $U_2 = 2 + (1 - \alpha_2)^2$, respectively (Hillestad, 2015). Where α_1 and α_2 are chain growth factors for paraffins and olefins, respectively. Depending on α_1 and α_2, the stoichiometric usage ratio will be slightly above 2. With under-stoichiometric H_2/CO feed ratio, it will decrease along the reactors, and to compensate for this, hydrogen must be fed between the stages.

The hot syngas from the ATR is heat exchanged with the HER, and is further cooled to knock out water. Without further compression the syngas is heated and fed to the first FT stage. The FT reactors are microchannel reactors (Ostadi & Hillestad, 2016). In order to increase the hydrocarbon production and also suppress catalyst deactivation, the gas is inter-cooled and products, including water, are withdrawn between each FT stage. The tail, consisting of unconverted syngas, nitrogen and light gas components produced in the FT reactors, is used as fuel in the gas turbine to supply power to the plant and ancillary users.

7.2.2 The ammonia process

Oxygen removal unit

The best nitrogen source for the ammonia process is the nitrogen rich stream from the air separation membrane, where the nitrogen purity is 95% and at a pressure of 16 bar. The remaining is 4.5% oxygen and 0.5% argon. Only 10% of this stream is used in ammonia process and the rest is sent to gas turbine for power production and turbine blades cooling. Oxygen and oxygen containing compounds are poisons for the ammonia synthesis catalyst, and therefore the feed to ammonia reactor should be free of any oxygen containing compounds. The limits for concentrations of these compounds are in ppm range. To remove the oxygen, it is reacted with hydrogen to produce water. A small stream of hydrogen is mixed with the the nitrogen stream in an oxygen removal vessel with or without a catalyst. The heat of reaction is used to produce high pressure steam, and subsequently the temperature is reduced to 30 °C and water is knocked out.

Methanation reaction

The permeate stream from the H_2/CO_2 separation membrane has 0.84% CO_2 which needs to be removed as it is poisonous for ammonia catalyst. A methanation step is applied to convert CO_2 to methane which is an inert for the ammonia catalyst. The impurities such as methane are not completely removed from the feed to ammonia reactor since they are not directly harmful to the ammonia catalyst and are expensive to remove. The rest of the hydrogen stream is cooled to 30 °C to separate the water produced in methanation reactor.

The methanation reactor converts carbon oxides to extinction (less than 10 ppm) at 250-350 °C over a nickel containing catalyst. The process is simple, reliable and inexpen-

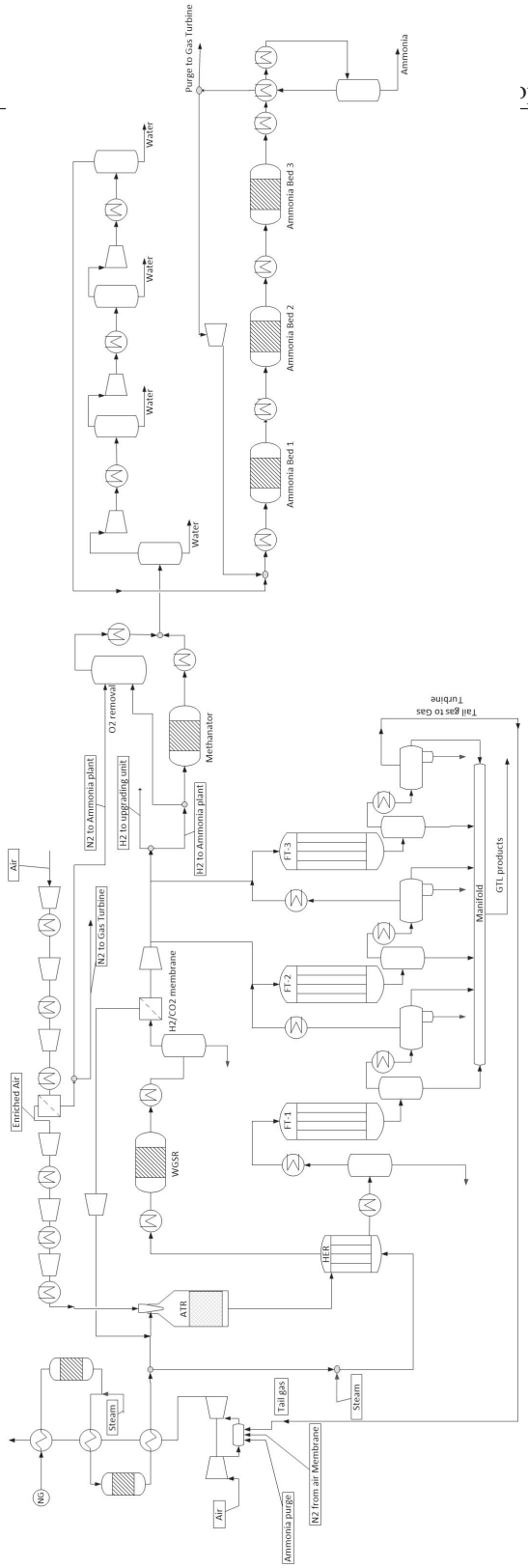

Figure 7.2: Process flow diagram of the combined GTL - ammonia process

sive both in investment and in operating cost (Dybkjær & Nielsen, 1995). It will cause a certain loss of hydrogen; in addition, due to production of methane, it causes an increased loss with purge gas from the synthesis loop. The gas from a methanation reactor unit will contain water. Moreover, the gas from oxygen removal unit will also contain water. This water must be removed before the gas reaches the ammonia synthesis catalyst. The advantages of simplicity and low cost outweigh the disadvantages of hydrogen consumption and production of additional inerts in the make-up gas to the synthesis loop (Appl, 2007).

7.2.3 Ammonia Synthesis

The synthesis gas is compressed to 223 bar in three stages of compression with intercooling and separation of water in between. Syngas compressors are driven by steam turbines which are reliable and low-maintenance devices. They are easy to control and have nonsparking operation which makes them suitable for use in explosive atmospheres or highly corrosive environments. Fresh syngas has an H_2/N_2 ratio of 3.0 which is the stoichiometric ratio of ammonia reaction. After combining the fresh syngas with the recycled stream from the ammonia reactor, the H_2/N_2 ratio increases to about 3.1. The combined stream is heated to 350 °C before entering the first bed. After the third bed, the product stream is cooled to 30 °C. In order to separate ammonia from the product stream, a closed refrigeration loop is used. Part of the produced ammonia is used as refrigerant and the lowest temperature that the product stream can reach is -25 °C (ammonia boils at atmospheric pressure at -33 °C). After refrigeration, liquid ammonia is separated from the unconverted reactants and is sent to storage tanks. Because the conversion is limited by equilibrium and is 30% which is relatively low, a recycle of unconverted syngas is required to have an economically feasible process. Due to presence of inert components such as argon and methane, it is necessary to have a purge stream to avoid inert accumulation. About 5 % of the product gas is purged. The recycle stream, containing 1.7% ammonia, is fed to the last stage of the last syngas compressor. Liquid ammonia from the separator contains small amount of dissolved gases which will be partly released by pressure reduction in ”let down” tank to about 20 bar.

Catalyst

Most commercial ammonia catalysts are based on metallic iron, mostly produced from magnetite, Fe_3O_4, which is promoted with alkali metals such as aluminum, calcium, or magnesium (Kirk-Othmer, 2004). Osmium (Os) and ruthenium (Ru) catalysts have also been applied. The ruthenium catalyst is found to be more active than the Fe catalyst, so it can operate at milder conditions (Rossetti et al., 2006). On the other side, Ru is more expensive with a shorter lifetime than the Fe catalyst (Klinsrisuk et al., 2015). Here, the iron catalyst is selected because of the extensive industrial experience with it. A number of compounds including H_2O, H_2S and halogens are strong poisons for the ammonia catalyst. A common feature of the poisons is that they are adsorbed at least as strongly on the surface as some of the reaction intermediates (Stoltze & Nielsen, 1995). Oxygen-containing compounds such as H_2O, CO and CO_2 are poisonous for ammonia catalysts due to reversible adsorption of oxygen species on the active sites (Dybkjær & Nielsen, 1995). The adsorption equilibrium is such that at temperatures below about 350 °C, near to complete

coverage and therefore almost complete deactivation of the catalyst is obtained even at concentrations of oxygen containing compounds about or below 1 ppm (Oudar, 1985). Such low concentrations are very difficult and expensive to achieve, and as a consequence, the risk of poisoning sets a practical lower limit to the catalyst temperature and thereby the operating pressure (Dybkjær & Nielsen, 1995).

Reaction kinetics

Different rate equations are available in the literature for ammonia production. Appl (2000) and Hansen (1995) give a description of available kinetic models. An early and also one of the most used kinetic models for ammonia production with iron catalysts is the one proposed by Temkin and Pyznev (Rossetti et al., 2006). The model used here, is one that Dyson & Simon (1968) modified.

$$r_{\mathrm{NH_3}} = 2k \left[K_a^2 a_{\mathrm{N_2}} \left(\frac{a_{\mathrm{H_2}}^3}{a_{\mathrm{NH_3}}^2} \right)^{\alpha} - \left(\frac{a_{\mathrm{NH_3}}^2}{a_{\mathrm{H_2}}^3} \right)^{1-\alpha} \right] \tag{7.1}$$

Where a_i are component activities and α is a constant between 0.5 and 0.75 (Dyson & Simon, 1968). In this work $\alpha = 0.5$ is used. The activity of a component is given as $a_i = \frac{f_i}{f_i^0}$, where f_i^0 is the reference fugacity taken to be 1 atm. The fugacity coefficients of nitrogen, hydrogen and ammonia are used for calculating the rate equation. Dyson & Simon (1968) used the equation of Gillespie & Beattie (1930) to calculate the equilibrium constant. In order to make this equation suitable for implementation in HYSYS, it has to be fitted by an Arrhenius type temperature function. The fitted model matches the original model very well in the temperature range used in this study. Both k and K_a are of the same function $A \exp(-\frac{E}{RT}) \cdot T^{\beta}$, and the parameters are given in Table 7.1.

Table 7.1: Rate equation constants

	A	E	β
k	$8.849 \cdot 10^{14}$	17056	0
K_a	2.531	40893	−1.93672

The ammonia converter

Commercial ammonia converters can be classified into two main groups (Appl, 2007). To the first group belongs the tube cooled converters, which have catalyst beds with cooling tubes running through them, or catalysts are inside tubes and cooling medium on the shell side. The cooling medium is mostly the reactor feed gas. The second group are reactors where the volume is divided into several beds in which the reaction runs adiabatically. Between individual beds heat is removed by injection of colder synthesis gas (quench converters) or by indirect cooling with synthesis gas or via steam generation (indirectly cooled multibed converters).

In reactors with indirect cooling, all gas passes through all catalyst beds. In contrast to quench cooling where part of the gas only passes through some beds. This means that at

identical conditions, a higher conversion can be obtained in the same number of catalyst beds in the indirectly cooled converter than in the quench cooled converter. Indirectly cooled converters are used in almost all large, new ammonia plants constructed today (Appl, 2007).

The simulated reactor is of the second group which is composed of three beds with indirect cooling between the beds. Each bed is simulated with a plug flow reactor model in HYSYS, and the inter cooling between the beds is simulated by use of heat exchangers. These heat exchangers are used to preheat synthesis gas and at the same time cool the beds. Constant pressure drop of 2 bar is considered for each of of the catalytic beds. The total once-through nitrogen conversion over all three beds is 30 %.

Ammonia separation

Ammonia is recovered from the effluent of the reactor by cooling to condensation followed by separation of the liquid from the gas. Refrigeration to -25 °C has been used which corresponds to cooling by evaporation of ammonia at about atmospheric pressure.

Optimization of ammonia synthesis

In order to maximize production from the synthesis loop, there are several variables which have great influence on ammonia production. Variables considered are bed inlet temperatures, operating pressure, purge ratio and volume of each bed. Sequential quadratic programming (SQP) method of optimization available within HYSYS optimizer is used for optimizing the ammonia loop. Since N_2 conversion to NH_3 can not reach 100% due to equilibrium limitations, reactor volume in the three beds need to be optimized. As shown in Figure 7.3, NH_3 production reach a plateau in total volume of 55 m^3. Therefore this is used as the total volume of the three beds. Specifications of the ammonia reactor is shown in Table 7.2. It is worthwhile to have a look at the optimum reactor volume distributions. The third bed is the largest followed by the second and the first bed. However, in the Fischer Tropsh section of the GTL plant, the volume distribution is the opposite, with the first reactor having the largest volume, followed by the second reactor and then the third reactor. The reason is that if we have larger volume in first ammonia bed, we get more conversion to ammonia, and we will have less conversion in the next two beds because of equilibrium limitation. Moreover, in FT case, there is inter-cooling and product separation between reactor stages, however in ammonia beds there is only inter-cooling.

7.3 Results and discussion

Design parameters for different FT stages are shown in Table 7.3. The GTL overall results are shown in Table 7.4.

7.3.1 Water and power

If the process concept is to be deployed on an FPSO, it needs to be self sufficient with water and power. The GTL process alone is self sufficient with water and power, with

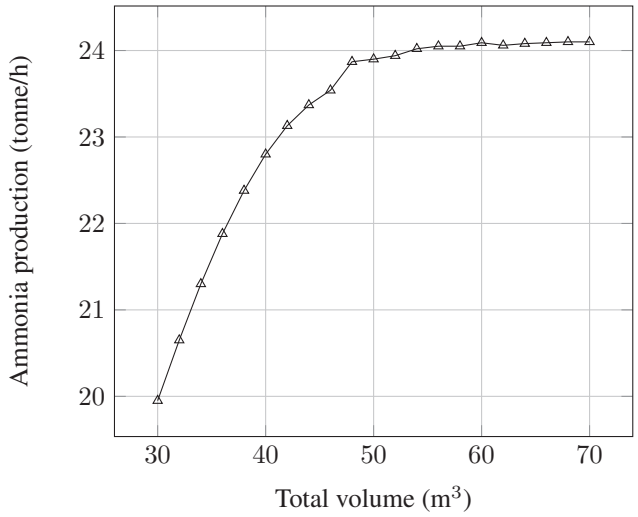

Figure 7.3: The production of ammonia with different total volume in 3 ammonia beds

Table 7.2: Design parameters for the ammonia reactor

Specification	Bed 1	Bed 2	Bed 3
Reactor type	Adiabatic	Adiabatic	Adiabatic
Volume (m^3)	10.38	14.52	30.1
Length (m)	5.87	8.22	17.03
Diameter (m)	1.5	1.5	1.5
Bed voidage	0.33	0.33	0.33
Particle density (kg/m^3)	2500	2500	2500
Bulk density (kg/m^3)	1675	1675	1675
Inlet temperature (°C)	350	350.3	384.9
Inlet H_2/N_2 ratio	3.15	3.17	3.18
Once-through N_2 conversion (%)	14.63	4.41	14.24

Table 7.3: Design parameters for different FT stages

	Stage 1	Stage 2	Stage 3
Channel length [m]	0.8	0.6	0.5
Number of channels [million]	15	10	8.5
Volume [m^3]*	48	24	17
Inlet H_2/CO	2.0	2.0	2.0
H_2 addition between stages [kmol/h]	0	365.1	127.7
CH_4 selectivity [%]	5.95	5.39	4.26
CO conversion [%]	57.9	51.6	53.5
C_{5+} production [tonne/h]	35.65	13.99	7.26

* After optimization of volume distribution

Table 7.4: Overall GTL plant results

Total CO conversion [%]	90.55
Total methane selectivity [%]	5.61
Carbon efficiency [%]	61
Catalyst volume [m^3]*	89
Reactor productivity [tonne/(h m^3)]	0.64
Surplus hydrogen [tonne/h]	5.96
C_{5+} production [tonne/h]	56.90
C_{5+} production [bbl/day]	12000

* Considerable reduction of catalyst volume (71 m^3) is achieved by optimization of volume distribution compared to our previous study (Ostadi et al., 2015)

Table 7.5: Combined GTL - ammonia power balance

Category	Power source/sink		[MW]
Power sinks	GTL	Air compression	129.9
		H_2 compression	4.5
		Recycle compression	0.2
	Ammonia	Syngas and recycle compression	8.6
		Refrigeration compression	3.5
Power sources	Gas Turbine		145.5
	Steam Turbine		18.4
Excess power production			17.6

excess power of 5 MW (Ostadi & Hillestad, 2016). Power and water balance in the GTL plant are shown in Table 7.5 and Table 7.6, respectively. The combined GTL and ammonia process is still self sufficient with water and power. By addition of the purge stream from ammonia synthesis to the gas turbine, power production is increased by about 6 MW, despite the fact that 10% of nitrogen stream from air membrane is sent to ammonia synthesis. Heat from cooling FT reactors are used to produce MP steam. In ammonia process by cooling effluents from oxygen removal unit and methanation reactor, HP and MP steam are produced. The produced steam is used to run an steam turbine which drives ammonia syngas compressor shaft. Simulation flowsheet of the steam cycle of the plant is shown in Figure 7.4. The steam cycle provides the process with HP, MP and LP steam.

Table 7.6: Combined GTL - ammonia water balance

Water stream [tonne/h]		
GTL	Steam demand	119.1
	Retrived water from syngas	96.4
	Retrived water from product	87.6
Ammonia	Retrived water	2.0
Excess water		66.9

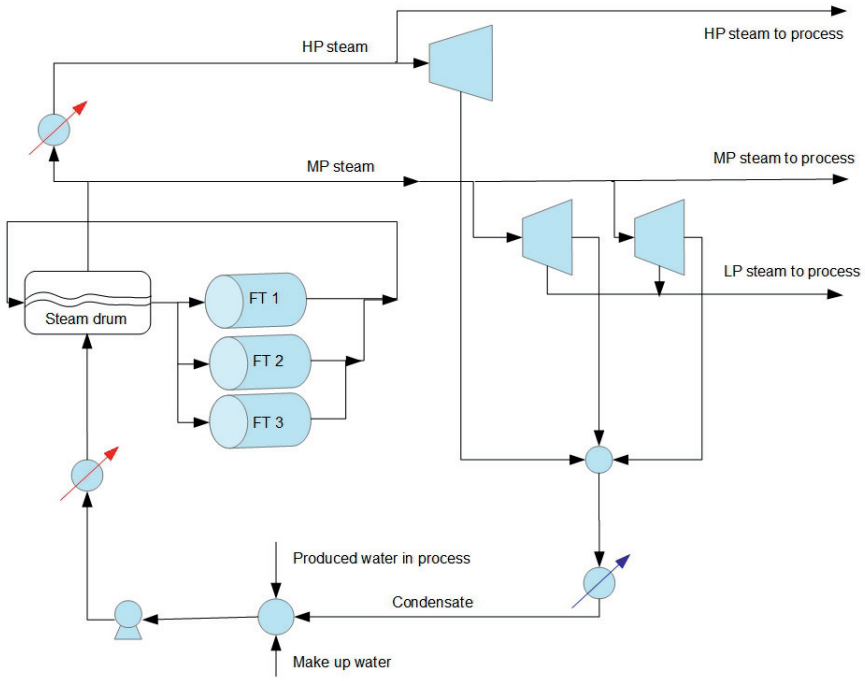

Figure 7.4: Process flow diagram of steam cycle

7.3.2 Cost Estimation

Cost estimation is done based on cost correlations from two different sources, namely Towler & Sinnott (2013) and Turton et al. (2012). Since there are no historical data on the cost of microchannel reactors, the cost estimation is done based on the cost of material and the cost of labour assumed to be equal to 7 times the material cost. The cost of catalysts and pressure vessels containing the microchannel reactors are also taken into account. The purchased cost of the microchannel reactors, including microchannels, pressure vessels and catalysts, is estimated to be 56 million USD and installed cost to be 310 million USD. Installed costs include piping, equipment erection, instrumentation and control, electrical and lagging and paint. The microchannel reactors constitute 40 % of the total fixed capital costs when civil, structure, buildings, the upgrading unit and the ship are not included. If the process is to be on an FPSO the product upgrading process will be relatively simple because the oil need to be refined onshore. The total capital investment for the combined GTL - ammonia process including offsites, design and engineering and contingency add up to approximately 900 million USD. Note that civil, structures, buildings, the upgrading unit and the FPSO are not included in this estimate. Ammonia process alone will constitute 7% of this amount which is about 65 million USD. The main reason for the relatively low cost is that cryogenic air separation and conventional steam reformers are avoided. By

producing ammonia in addition to GTL products, the sale revenues of the plant increases by about 50% based on ammonia price of 500 USD/tonne and GTL product price of 50 USD/bbl, which makes it more appealing for commercialization.

7.4 Conclusion

In order to increase the profitability of the GTL process, cogeneration of ammonia is proposed. The total capital investment of a combined GTL and ammonia plant producing 12000 bbl/day of GTL products and 576 tonnes/day of ammonia without considering the FPSO, buildings and structures or the upgrading unit is estimated to approximately 900 million USD. Ammonia process alone will constitute 7% of this amount. The process is autonomous as it is self sufficient with power and water and therefore well suited for production in remote locations. Through ammonia cogeneration with GTL products, the sale revenues of the plant increases by about 50% which makes it commercially more attractive. The whole process is a low-cost process and addition of ammonia production makes it more profitable. The main reason for the low cost is that cryogenic air separation and the costly steam methane reformer and CO_2 capture units are avoided.

Chapter 8

Enriched-air or Pure Oxygen as Oxidant for Gas-to-Liquid Process with Microchannel Reactors

This chapter is based on the submitted paper: "Enriched-air or pure oxygen as oxidant for gas-to-liquid process with microchannel reactors" to Chemical Engineering & Technology.

The syngas production step is the most costly step in a gas to liquid plant. It is common practice to use oxygen as oxidant in the reforming step. However, by the introduction of microchannel reactors with their remarkable heat transfer characteristics, high active catalyst site exposure to reactants and therefore high once-through conversions, the use of enriched-air maybe justified. The purpose of this chapter is to analyse the merits of using enriched-air versus pure oxygen in the reforming step of a gas to liquid plant utilizing an autothermal reformer (ATR), while microchannel reactors are used in the once-through Fischer-Tropsch (FT) step. Pure oxygen is provided by a cryogenic Air Separation Unit (ASU) and enriched-air by use of air separation membranes. To make the two cases comparable, the total once-through CO conversion is kept the same. By using pure oxygen less FT reactor volume is required which means lower reactor cost at the expense of having a costly cryogenic ASU to produce pure oxygen. The operating cost of ASU is lower than air membrane, while its installed cost is higher. Due to safety and space issues of having a cryogenic ASU offshore, the only viable option is the use of enriched-air, while in an onshore setting, the use of oxygen is more attractive.

8.1 Introduction

There are several routes for syngas generation from any carbonaceous feedstock. All technologies used for synthesis gas technologies are based either on steam reforming, partial oxidation, or a combination of the two as in Autothermal Reformer (ATR) (Dybkjær & Aasberg-Petersen, 2016). The preparation of synthesis gas is one of the most capital intensive part of a GTL-complex and may account for 30% to 50% of the total investment including cryogenic Air Separation Unit (ASU). The main reason for this high estimate is the high cost of ASU.

ATR operation at low steam to carbon ratio as low as 0.6 has become the state-of-the-art synthesis gas technology for Fischer-Tropsch applications (Aasberg-Petersen et al., 2004). ATR is a relatively simple piece of equipment with a burner and a catalyst bed in a brick-lined pressure vessel (Rostrup-Nielsen, 2002). In almost all GTL plants that utilize ATR, oxygen is used as oxidant such as in Oryx GTL plant in Qatar. Oxygen-blown ATR is the preferred technology for large-scale GTL plants (Rostrup-Nielsen, 2002). Oxygen-blown ATR has also been commercially used in methanol synthesis (Wilhelm et al., 2001). Air-blown secondary reforming is well established, being commonly utilized for syngas production for ammonia plant. Use of air to produce FT syngas has also been suggested by several authors, but have not been commercially-deployed yet. Syntroleum Corporation in their offshore GTL process design, used air in the reforming step to produce syngas (Hutton & Holmes, 2005; Loenhout et al., 2006). Syntroleum and ARCO have demonstrated a GTL process that utilizes an air blown ATR and moving bed Fischer-Tropsch reactor (Schubert et al., 2000; Agee, 1997). Jess et al. (1999) proposed a once-through GTL plant in which syngas is generated through partial oxidation of natural gas and air. Their proposed plant was successfully operated in a semi-technical scale (Jess et al., 2001).

Dybkjær & Christensen (2001) did a comparison of air-blown and oxygen-blown ATRs. They concluded that it is not economically feasible to have air as oxidant due to large volume of inert nitrogen (about 50 vol% in the dry synthesis gas) and compression power needed to produce enriched-air. But on the other side, the advantages of using air are reduced or eliminated investments related to production of oxygen.

It is a common practice to have recycle loop in the FT step with nitrogen-free syngas, because of low per pass conversion of CO. However, with presence of large amount of nitrogen in syngas in case of using enriched-air, having recycle loop is not feasible. By use of microchannel reactors, with their high heat and mass transfer properties, high once-through conversions of up to 90% is achievable and there will be no need for having recycle loop. Then the question is which oxidant is better suited for a GTL process with microchannel reactors.

In this study, the GTL plant utilizes 120 MMscfd of natural gas and produces about 58 tonne/h or more than 12000 bbl/day of hydrocarbon products. Natural gas specifications are the same as the one used by Ostadi et al. (2015). Simulations were carried out using HYSYS V8.6 process simulator. Modeling of Fischer-Tropsch reactor and Heat Exchange Reformer (HER) are done using Aspen Custom Modeler. Water-Gas-Shift (WGS) reactor, Pre-reformer and ATR are simulated using the Gibbs reactor model present in HYSYS. Peng-Robinson equation of state is used as the thermodynamic model to calculate thermodynamic properties. All chemical properties were provided by Aspen Properties V8.6.

8.2 Model building

8.2.1 Process layout

A simplified process flow diagram of the proposed process concept for oxygen blown and enriched-air blown ATR is shown in Figure 8.1. A pre-refomer is used in front of the ATR to prevent coke formation on the ATR catalyst. In the pre-reformer almost all higher hydrocarbons are converted to methane and carbon oxides. The pre-reformed natural gas is then split into two streams, with split ratio of 85% and 15%. The former enters the ATR and the latter enters the HER. This is to have one path for production of syngas and one path for production of hydrogen. Outlet temperature of ATR is kept constant at 1060 °C by adjusting the amount of oxidant. The energy required for the steam reforming reactions in the HER is provided by the hot outlet stream from the ATR. The outlet of the HER is cooled down to 350 °C before entering the high temperature WGS reactor, where CO is shifted to CO_2 and H_2. After the WGS reactor, the stream is cooled and water is knocked out and then it enters the hydrogen separation membrane. The permeate is hydrogen with 99 % purity, which is further compressed and distributed between the FT stages and the upgrading unit. The retentate, mainly CO_2 with some H_2, CO and CH_4, is then compressed and recycled back to the ATR. By recycling this stream to the ATR, the H_2/CO ratio in the effluent of the ATR will reduce, which is beneficial for the FT synthesis as it increases the selectivity to heavier hydrocarbons. The stoichiometric usage ratios of hydrogen, U, for production of paraffins and olefins are $U_1 = 3 - \alpha_1$ and $U_2 = 2 + (1 - \alpha_2)^2$, respectively (Hillestad, 2015). Where α_1 and α_2 are chain growth factors for paraffins and olefins, respectively. Depending on α_1 and α_2, the stoichiometric usage ratio will be slightly above 2.0. Having an under-stoichiometric H_2/CO feed ratio to FT reactor is beneficial for the selectivity to heavier hydrocarbons, however this ratio will decrease along the reactor and hydrogen must be fed between the stages to compensate for this reduction. In both cases with oxygen blown and enriched-air blown ATR, the H_2/CO ratio out of ATR is already undrestoichiometric (arround 2.0), however the H_2/CO ratio in the feed to the second and third stages are set to 2.0 by means of hydrogen addition. This value is chosen for simplicity and it does not mean that it is the optimum value. FT products are cooled to 50 °C and liquid products and water are separated at the end of each FT stage.

Oxygen blown ATR

Pure oxygen is used as oxidant which is provided by a cryogenic ASU. With oxygen as oxidant, it is possible to have recycle loop in the FT step, however, due to high once-through conversion and also being able to compare with enriched-air case, it is decided not to include recycle loop.

Enriched-air blown ATR

With an air-blown ATR, it is practically impossible to recycle the unconverted syngas because of very high nitrogen concentrations. This is also the case with enriched-air, and a once-through synthesis scheme is the only option to avoid high accumulation of nitrogen.

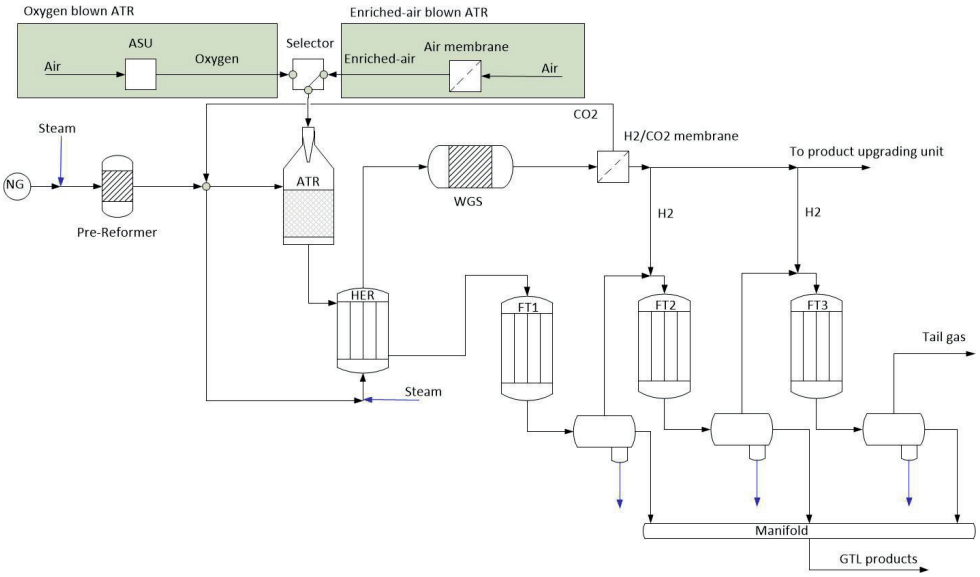

Figure 8.1: Process flow diagram of the GTL plant with either oxygen blown or enriched-air blown ATR

PRISM membrane separators from Air Products are considered (AirProducts, 2015). With these membranes, enriched-air with oxygen concentrations ranging from 25 to 50% can be obtained. Considering the large air flow through the membrane and therefore avoiding a very large membrane modules, a PRISM membrane is chosen to have 34% oxygen purity. Long durability and simple startup of the separator are highlighted by the producer. Air is fed to the membrane at 16 bar and 100 °C. The enriched-air is on the permeate side at a pressure of 1 bar and needs to be re-pressurized before entering the ATR. Furthermore, the nitrogen stream which is on the retentate side has a pressure of 16 bar which can be used for power production. Three compressors are used before the air membrane and three compressors are used after the air membrane. Inter-cooler is used between the air compressors in order to avoid excessive air temperatures. Compressors are powered by electricity.

8.2.2 Fischer-Tropsch synthesis

Microchannel reactors, with numerous parallel channels with small dimensions are suited for highly endothermic or highly exothermic reactions due to intensified heat transfer characteristics. Channels filled with FT catalyst powder and channels with boiling water (as coolant) are arranged in a cross flow configuration. The temperature of boiling water is assumed to be constant along the axial direction. Our simulations are based on channels with a dimension of 2×2 mm^2 and a length of 1 meter. The reactor consists of several thousands of these repeating units. A two-dimensional homogeneous model with no axial dispersion is assumed. Particles with diameter of 0.2 mm are applied in the reaction

channels. Because of the small diameter a reasonable assumption is that there will be no mass transfer limitation inside the particles, equivalent to setting the effectiveness factor equal to unity for all reactions (Rytter et al., 2007). The FT kinetic model and the chain propagation model for simulating microchannel reactors are taken from our previous work (Ostadi et al., 2016).

8.3 Bases for comparison of the two cases

Both cases of oxygen and enriched-air have once-through configuration with product cooling and separation between FT stages. These two cases are shown in the same process flow diagram in Figure 8.1. Unit operations used for the two cases are the same except that their sizes will be different. In order to make the two cases comparable, the total CO conversion is the same in both cases. Moreover, the same amount of pre-reformed natural gas is sent to HER, therefore equal amount of hydrogen is produced in both cases and consequently the sizes of the WGS reactors and H_2/CO_2 separation membranes are equal. Furthermore, reactor volume distributions in all FT stages are almost the same in both cases. Finally, superficial gas velocity at the inlet of each FT stage which affects the pressure drop in channels is the same in both cases.

8.4 Results and discussion

The results for enriched-air and oxygen cases are shown in Table 8.1 and Table 8.2, respectively. The H_2/CO ratio to the first FT stage in enriched-air case is lower than the oxygen case, mainly due to presence of inert nitrogen which has cooling effect in the ATR. This ratio is an important variable which affects the selectivity to heavier hydrocarbons. Moreover, nitrogen has cooling effect in FT reaction and contributes in the dissipation of produced heat. As a result, temperature in FT channels in enriched-air case is slightly lower than FT channels in oxygen case. This also affects the selectivity to heavier hydrocarbons. These reasons justify production of 1 tonne/hr more C_{5+} products in enriched-air case. In oxygen case, more of the lighter hydrocarbons is produced. Syngas flow to the first FT stage in enriched-air case is 34% more than the oxygen blown case. This difference in syngas flow increases to 67% and 115% in second and third FT stages, respectively. The reason is due to hydrogen addition and inert nitrogen flow. In enriched-air case, nitrogen concentration in syngas increases from 25.9 % in the first FT stage to 53.5 % in the third stage. In terms of hydrogen addition, there is 9% more hydrogen addition between FT stages in enriched-air case than oxygen blown case. The reason is mainly due to more hydrogen deficient syngas to the first FT stage in enriched-air case than oxygen case.

All cost estimations reported are based on cost correlations in Towler & Sinnott (2013) and Turton et al. (2012). Since there are no historical data and correlations on the cost of microchannel reactors, the cost estimation is done based on the cost of material and the cost of labour assumed to be equal to 7 times the material cost. Stainless steel is assumed to be used for production of channels. The cost of catalysts and pressure vessels containing the microchannel reactors are also taken into account. The resulting installed cost estimate for every m^3 of catalyst volume is around 3.48 million USD.

Table 8.1: Fischer-Tropsch synthesis with enriched-air blown ATR

	FT1	**FT2**	**FT3**	**Total**
Reactor volume (m^3)	52.2	31.28	21	104.48
Volume distribution (%)	50	29.9	20.1	
Cost of reactor (million USD)	20.76	12.44	8.35	41.56
CO conversion (%)	53.02	51.33	49.45	88.45
C_{5+} (tonne/hr)	34.2	15.9	7.6	57.7
Hydrogen addition (kmol/hr)	0	294	139	433
Syngas flow (kmol/hr)	23588	15210	11411	
Nitrogen in syngas (mol %)	25.9	40.0	53.5	
H_2/CO at the FT inlet	2.01	2.0	2.0	

Table 8.2: Fischer-Tropsch synthesis with oxygen blown ATR

	FT1	**FT2**	**FT3**	**Total**
Reactor volume (m^3)	42.0	22.0	12.4	76.4
Volume distribution (%)	55.0	28.8	16.2	
Cost of reactor (million USD)	16.70	8.75	4.93	30.39
CO conversion (%)	53.00	51.39	49.45	88.46
C_{5+} (tonne/hr)	33.6	15.6	7.4	56.6
Hydrogen addition (kmol/hr)	0	235	163	398
Syngas flow (kmol/hr)	17578	9109	5307	
H_2/CO at the FT inlet	2.028	2.0	2.0	

Table 8.3: Comparison of GTL plant with enriched-air blown ATR and oxygen blown ATR

	Oxidant	
	Oxygen	**Enriched-air**
Reactor volume	1	1.37
Cost of reactor	1	1.37
CO conversion	1	1
Power for oxidant	1	2.21
C_{5+} production (tonne/hr)	1	1.02
Hydrogen addition (kmol/hr)	1	1.09
Syngas flow to the first FT stage (kmol/hr)	1	1.34
Installed cost of equipment to produce oxidant	1	0.86
Cost of equipment downstream ATR excluding FT reactors	1	1.15

The specific power need for oxygen production is assumed to be 0.4 kWh/kg O_2 (Dybkjær & Christensen, 2001). The cost of electricity needed to drive compressors is calculated to 0.1 USD/kWh (Ulrich & Vasudevan, 2006).

Comparison of enriched-air blown and oxygen blown GTL plants are shown in Table 8.3. As expected, more reactor volume is needed in the enriched-air case, namely 37%. The corresponding cost of reactor is also 37 % more for the enriched-air case. By considering FT reactors alone, the pressure drop is 2 bar higher in enriched-air case mainly due to larger volume of syngas passing through reactor than in oxygen case. The installed cost of equipment to produce enriched-air is 14% lower than the oxygen case.

The installed cost of FT reactor and oxidant production equipment and operating cost of oxidant production are shown in Table 8.4. This Table shows that installed cost for enriched-air is about 18.6% higher than the oxygen and the operating cost for producing enriched-air is 2.21 times higher than oxygen case. Therefore, it is concluded that the Net Present Value (NPV) of the oxygen case is higher than the enriched-air case and as a result, it will be the preferred choice. The use of oxygen as oxidant is more attractive in an onshore setting, while the only viable option offshore is the use of enriched-air, because of limitations of having a cryogenic ASU offshore, mainly due to safety and space issues. As mentioned before, nitrogen stream from the air membrane has a pressure of 16 bar and it can be de-pressurized in an expansion turbine to generate power. Even by considering this generated power, the NPV will still be in favour of the oxygen case.

Nitrogen is not entirely inert in partial oxidation processes as it can be involved in reaction mechanisms that can form ammonia, nitrogen oxides and hydrogen cyanide (Aasberg-Petersen et al., 2004). The concentration of these compounds depend on the amount of nitrogen in the natural gas and in the oxidant and they are normally in ppm range (Aasberg-Petersen et al., 2004). However, Jess et al. (1999) did not make note of the production of nitrogen oxides and hydrogen cyanide in their partial oxidation reformer which utilized air and natural gas. There are several studies suggesting that these compounds will result in cobalt catalyst deactivation in FT synthesis (Ordomsky et al., 2016; Pendyala et al., 2016).

Table 8.4: Installed cost of FT reactor and oxidant production equipment and operating cost of oxidant production

	Oxidant	
	Oxygen	**Enriched-air**
Installed cost (FT reactor and oxidant production equipment in million USD)	366	450
Operating cost of oxidant production (million USD/year)	34.7	76.6

8.5 Conclusion

Process simulation of a once-through gas to liquid process with two different oxidants (enriched-air and oxygen) and utilizing microchannel reactors for FT synthesis is performed. Economic analysis indicates that installed cost of FT reactor and oxidant production equipment in enriched-air case is 18.6% higher than the case with oxygen. Moreover, the operating cost is 2.21 times higher in enriched-air case. This results in a higher net present value (NPV) for the oxygen case which makes it commercially more attractive. Due to offshore limitations such as safety and space issues, having a cryogenic ASU is problematic, therefore enriched-air will be the preferred choice offshore. Furthermore, possibility of formation of NH_3 and HCN in ATR adds to the favorability of using oxygen as oxidant over enriched-air.

Chapter 9

Path Optimization of the Fischer-Tropsch Synthesis with Cobalt Catalyst and Microchannel Reactors

This chapter is based on the paper: "Path optimization of the Fischer-Tropsch synthesis with cobalt catalyst and microchannel reactors" planned for submission to journal of Chemical Engineering Science.

In chapter 4, a new process configuration for a once-through GTL plant suited for a floating production unit is proposed. In that chapter, the reactor path of the Fischer-Tropsch synthesis is not optimized. Here, we have optimized the total reactor volume of the FT synthesis and the volume distribution between stages, in addition to hydrogen distribution and coolant temperature. Systematic staging or the path optimization method, described in an earlier paper (Hillestad, 2010), is applied here. The productivity is maximized subject to constraints on a maximum reactor temperature and a minimum conversion. Considerable reduction of reactor volume is obtained by path optimization.

9.1 Introduction

Today gas-to-liquid process technologies are deployed large scale only in places where the natural gas price is low. The main reason is that the capital investment of existing process technologies are very high, and requires a low natural gas price and a relativity high product price in order to be profitable. There is a large incentive to make existing process technologies more cost effective. The proposed GTL process configuration (Os-

tadi et al., 2015) is simple and lean as it does not require a cryogenic air separation unit. Enriched air, produced by PRISM membranes (AirProducts, 2015), is used as oxidant to the autothermal reformer. Air, enriched air and oxygen have been used as the oxidant in the reformer in literature. Jess et al. (1999) and Loenhout et al. (2006) considered using air in the reformer which produces a nitrogen rich syngas. Choi et al. (1997) used enriched air in their once-through natural gas Fischer-Tropsch plant. In their design, the 40% enriched air was produced by diluting an oxygen rich stream coming from the air separation plant. Because of large amount of inert nitrogen in the syngas, the Fischer-Tropsch reactors constitute a major part of the total investment cost and a once-through conversion is required. Once-through configuration for Fischer-Tropsch synthesis has been investigated by several authors (Jess et al., 1999; Kreutz, 2008; Rafiee & Hillestad, 2012). It is of interest to minimize the FT reactor size and at the same time maintain a high production of higher hydrocarbons and high CO conversion. Process intensification by use of microchannel technology has gained growing attention in recent years. There has been numerous investigations regarding different aspects of microchannel reactors in industrial applications (Kolb, 2013; Venvik & Yang, 2017; Deshmukh et al., 2010; Leviness et al., 2014). Microchannel technology has shown to have high reactor productivity defined as production per unit volume of catalyst. Velocys is one of the pioneers of commercializing microchannel technology (Leviness et al., 2011; Deshmukh et al., 2010). Velocys together with Toyo Engineering and Mitsui Ocean Development & Engineering Co are working on commercializing Micro-GTL technology which is applicable for small scale gas reserves. CompactGTL is another leading company in modular small scale GTL. Together with Petrobras, they built a fully integrated small scale GTL facility using associated gas. SBM Offshore together with CompactGTL is cooperating on offshore projects to increase productivity and to reduce flaring. The concept utilizes CompactGTL technology for conversion of associated gas into syncrude. Sectioning of chemical engineering processes in chemical engineering has been investigated in several studies. Androulakis & Reyes (1999) studied the role of oxygen distribution and product removal in a staged plug flow reactor which runs the oxidative coupling of methane (OCM). Diakov & Varma (2004) studied the effect of the oxygen feed in a packed bed membrane for methanol oxidative dehydrogenation. Maretto & Krishna (2001) proposed a multi-stage FT slurry reactor concept. The multi-stage design results in increased syngas conversion and reactor productivity. Guillou et al. (2008) studied the effect of hydrogen distribution between stages in a microchannel FT reactor. Systematic staging design method of Hillestad (2010) has been applied in several studies. Manenti (2014) applied the method to methanol and methanol/DME synthesis process. Rafiee & Hillestad (2013) considered staging of the FT synthesis utilizing cobalt catalyst. Staging of FT synthesis with product separation and addition of hydrogen between each stage has also been studied (Rytter, 2010; Rafiee & Hillestad, 2012). Product separation and hydrogen addition between stages resulted in increased heavy hydrocarbon production.

9.2 The path optimization method

The state-of-the-art reactor design methods can be classified into heuristics, attainable region methods, rigorous optimization approaches such as superstructure optimization,

dynamic opptimizaion approach and the systematic staging of reactors (Peschel et al., 2011). Systematic staging or the path optimization method, described in an earlier paper (Hillestad, 2010), is applied here. Extensions of the method is implemented, such as the possibility of product separation between stages. Also pressure drop over a packed bed, modelled by Ergun's equation, is taken into account.

The method will not be explained in detail here, but the total reactor volume of the FT synthesis as well as the volume distribution between stages, in addition to hydrogen distribution and coolant temperature are subject to optimization. After optimization of volume distribution, number of channels or cross sectional area are calculated such that the superficial gas velocity at the inlet of each stage is constant and equal to 0.4 $\mathrm{m/s}$. By knowing the cross sectional area at each stage and the volume distribution, the length of each stage is determined.

Figure 9.1 depicts the structure of the process to be optimized. Between each reactor stage there is a heat exchanger where the hot effluent is heat exchanged with cold gas from the separator. The pinch temperature is on the hot side and the temperature approach is set to 10 °C. The inlet temperature of all the stages is set to 210 °C. In addition, there is a cooler taking the temperature down to ca 30 °C for the C_{5+} products and water to be condensed to liquid and separated.

A back-mixing flow on each reactor stage indicates that the mixing structure is also optimized. The two extreme mixing structures are segregated flow (plug flow) and completely mixed flow. If the back-mixing flow in the Figure 9.1 is very large, the stage will be completely mixed, and if it is zero it will be plug flow. There may also be intermediate mixing. In the reference Hillestad (2010), it is explained how the model is formulated and how the design function defining the mixing is represented in the model.

The catalyst volume of each stage is also optimized. Not only the distribution of volume, but also the total volume may be subject to optimization. The coolant temperatures may be different on each stage and they are subject to optimization. Furthermore, the catalyst activity or catalyst dilution at each stage may change. The activity is a number between 0 and 1 relative to the kinetics, 1 being the undiluted catalyst describing the intrinsic kinetics. Here, the maximum catalyst activity is set to 0.75 because of highly active catalyst data used in kinetic model fitting (see section 9.2.1). Lastly the distributed hydrogen feed is also optimized. As indicated by Figure 9.1, these are point feeds. What is not subject to optimization here is the specific heat transfer area. The specific heat transfer area is given by the selected geometry of a channel. The cross section of a channel is quadratic $2 \times 2\ \mathrm{mm}^2$ and only two sides will be exposed to the coolant. The specific heat transfer area is therefore 1000 $\mathrm{m}^2/\mathrm{m}^3$.

Defining an objective function is not trivial. As explained by Hillestad (2010), objective functions can be defined as maximization of heavy hydrocarbon production, reactor productivity, energy efficiency and return on investment (ROI), to name a few. Here the objective function is to maximize the concentration of heavy hydrocarbons at the end of the path, which is hydrocarbons with at least 5 number of carbons (C_{5+}).

9.2.1 Kinetic model

A kinetic model is the basis for the development of a reactor design. In order to do a good and realistic design of a Gas-to-Liquid (GTL) plant, it is necessary to have kinetic

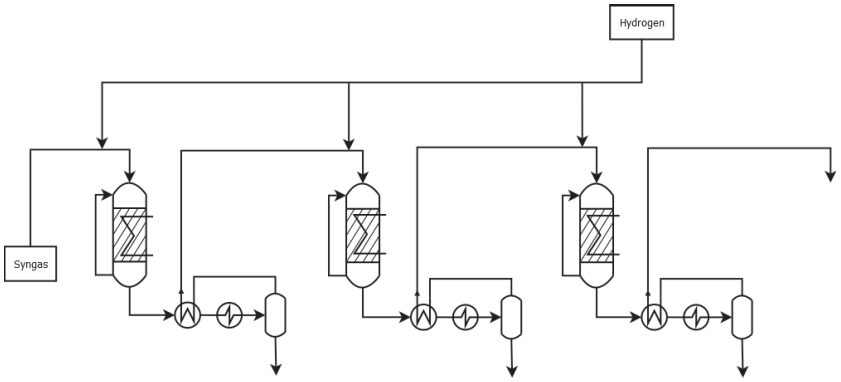

Figure 9.1: The structure of the path to be optimized. The catalyst volume (size) of each stage and the mixing structure indicated by the back-mixing are optimized, in addition to the coolant temperature, catalyst activity and feed of hydrogen to each stage.

models that accurately capture major variations of reaction rates and selectivities subject to changes in process parameters.

In chapter 5, we have fitted Ma et al. (2014) kinetic model and our own chain growth model to microchannel experimental data of Yang et al. (2016). The chain growth model includes the effect of water and predicts the C_{5+} and methane selectivities quite well. The model is able to explain the effects of temperature and composition on the reaction rates and selectivities. It is based on experiments done in a microchannel reactor over a range of operating conditions which fits to our design conditions. The same models are implemented here. However, the production of alkenes are neglected as they will constitute a small fraction of the products and also in this manner, the optimization variables will be reduced.

Fischer-Tropsch reaction can theoretically produce hydrocarbons with infinite number of carbons. In order to model this product distribution, a method for handling infinite number of reactions and components described by Hillestad (2015) is used. The method provides an accurate product distribution without violating the element balances. Here we have chosen to model alkanes individually up to C_4, and the tail distribution of the alkanes by the C_{5+} lump.

9.2.2 Microchannel reactors

The main differences between a microchannel reactor and a shell and tube fixed bed reactor are firstly the dimension of a channel is far smaller than the diameter of a tube, and the catalyst particles in a channel are also far smaller than what is possible in a tube. Here the channel dimension is chosen $2 \times 2\ \mathrm{mm}^2$, while a tube for a FT reactor is typically one inch or 25.4 mm. The consequence of this is that the volume specific heat transfer area is increased by a factor more than six. This characteristic makes microchannel reactors suitable for highly endothermic or highly exothermic reactions. The catalyst particle diameter in a microchannel is here chosen 0.2 mm while a catalyst particle in a tube is typically 3 mm. The consequence of this is that mass transfer limitation inside the particle

is practically eliminated and all active sites are exposed to the syngas. For a catalyst pellet of 3 mm diameter and with the kinetic model described by Todic et al. (2014a, 2015) and diffusivities given by Erkey et al. (1990), the effectiveness factor is calculated to be 0.20-0.25 along the length of a tube, while for particle of 0.2 mm the effectiveness factor is close to one.

9.2.3 Synthesis gas

The synthesis gas is generated by the process model described in chapter 4. The total flow rate, temperature, pressure and composition are given in Table 9.1. Two different syngas compositions are considered to take into account different upstream configurations which produce syngas.

Table 9.1: Two different syngas compositions are tested; syngas 1 with H_2/CO= 2 and syngas 2 with H_2/CO=1.8

	Syngas 1	Syngas 2
Temperature [°C]	210	210
Pressure [bar]	26.93	26.93
Molar flow [kmol/h]	23560	22560
Mass flow [kg/h]	399100	399100
Mass fraction		
CO	0.3751	0.3751
H_2	0.0541	0.0486
H_2O	0.0001	0.0001
CH_4	0.0027	0.0027
CO_2	0.1283	0.1283
N_2	0.4397	0.4452
H_2/CO molar ratio	2.00	1.80

9.3 Results and discussion

In all cases three FT stages are considered. Only three stages because there is a cost associated with cooling separation and heating the syngas between each stage, and not less because high conversion per pass is required. The mixing structure is optimized in all cases, but with microchannel all cases show that it is optimal with plug flow, i.e. without back-mixing or dispersion. The reason for this is because of the almost isothermal conditions inside a microchannel. If temperature hot-spots are encountered, we may see that back mixing is beneficial, since back-mixing will level out the hot-spots. However, with a microchannel reactor this is not seen as a problem.

In the following cases the maximum allowed reactor temperature along the path is set to 220 °C. The reason is that the catalyst lifetime is prolonged when the temperature is kept

low, and 220 °C is a reasonable limit. Catalyst deactivation increases exponentially with temperature. Each calculated temperature along the path becomes an inequality constraint in the optimization.

The results of maximizing the total production outtake with different values of the maximum allowed total volume are shown in Table 9.2. The total reactor volume V_{R} will end up at the maximum in all cases, which is logical as long as there is sufficient CO left. The cases are identified by the maximum value of $\sigma = V_{\mathrm{R}}/W_0$, which is selected to be 1.0, 0.75 and 0.4. For the highest values of 1.0 and 0.75 the total volumes are large enough to obtain a high conversion, and we see that the optimal coolant temperature profile is lower than the other. Testing the solution by increasing the temperature will increase production of the first stage, while the total production will decrease. Sometimes, the optimization suggests lower activity (catalyst dilution) with increased temperature, which has the same effect on the production distribution. Lower temperature is preferred because of less catalyst deactivation. In all cases, the optimal distribution of volume is the same: largest volume in the first stage and smallest volume in the last stage. Addition of hydrogen is beneficial as it increases the C_{5+} production. Moreover, removing C_{5+} and water at the end of each stage, increases the reaction rate because partial pressures of CO and H_2 increases. This positively affects the C_{5+} production. In all the cases, the optimal designs have over stoichiometric H_2/CO ratios in the reactor. This is not in accordance to what we expect that under stoichiometric H_2/CO ratio is beneficial for heavy hydrocarbon production. We believe that this anomaly is related to the Ma et al. (2014) rate expression which is considerably affected by the H_2 partial pressure. When Ma et al. (2014) rate expression is replaced with Todic et al. (2015, 2014a) rate expression, the optimal designs have decreasing H_2/CO ratios in the reactor.

9.4 Conclusion

This chapter demonstrates the application of path optimization method of Hillestad (2010) on FT synthesis part of a GTL plant. Through optimization of reactor path, increase in C_{5+} production and decrease in reactor volume is achieved. In other words, reactor productivity is enhanced by use of this method. We do not claim that the reported results are the global optimum, because of very non-linear nature of the optimization problem and high possibility for existence of many local minima.

Table 9.2: The result of maximizing production with syngas 1 subject to a maximum reactor temperature of 220 °C. V is the catalyst volume, T_{cool} is the coolant temperature, $W_{\mathrm{H_2}}$ is the feed of hydrogen, a is the catalyst activity, X_{CO} is the CO conversion, $W_{\mathrm{C_{5+}}}$ is the production outtake of C_{5+} lump, $\frac{W}{W_0}$ is the mass flow rate along the path relative to the inlet flow, L is the channel length and N_{chan} is the number of channels.

	Case	Stage	V m^3	T_{cool} [°C]	$W_{\mathrm{H_2}}$ [T/h]	a [-]	X_{CO} [-]	$W_{\mathrm{C_{5+}}}$ [T/h]	$\frac{W}{W_0}$ [-]	L [m]	N_{chan} million
Syngas 1	C-1.0	1	42.9	216.3	4.06	0.75	42.2	26.4	1.01	1.72	6.23
		2	35.2	217.9	0	0.75	53.8	20.2	0.85	1.68	5.24
		3	32.7	217.1	0	0.75	92.8	15	0.72	1.83	4.46
		Total	110.8		4.06		97.2	61.6			
	C-0.75	1	32.1	217	4.62	0.75	33.6	20.1	1.01	1.29	6.23
		2	28	218	3.8	0.75	49.4	18.8	0.895	1.27	5.51
		3	23	216.9	0	0.75	82.2	12.9	0.774	1.21	4.77
		Total	83.1		8.42		94	51.8			
	C-0.4	1	17.7	218.1	2.5	0.75	18.4	10.8	1	0.71	6.2
		2	15.3	219	2.2	0.75	20.2	9.6	0.94	0.66	5.82
		3	12.4	219	1.7	0.75	21	7.5	0.88	0.57	5.45
		Total	45.4		6.4		48.5	27.9			
Syngas 2	C-1.0	1	42.6	216.25	5.91	0.75	41.5	26	1.01	1.7	6.25
		2	35.7	217.95	0	0.75	53	20.6	0.86	1.7	5.3
		3	33.6	217.49	0	0.75	91.3	15.7	0.74	1.8	4.5
		Total	110.8		5.91		97.6	62.3			
	C-0.75	1	34.6	217.1	4.98	0.75	33.8	21	1.01	1.39	6.24
		2	31.9	218.1	4.6	0.75	53.1	21.2	0.9	1.44	5.52
		3	16.6	216.8	1.7	0.75	74.7	9.3	0.76	0.88	4.72
		Total	83.1		11.28		92.1	51.5			
	C-0.4	1	16.8	218.3	2.42	0.75	16.1	9.8	1	0.68	6.2
		2	14.85	219	2.14	0.75	17.3	8.93	0.95	0.63	5.86
		3	13.79	219	1.98	0.75	19.8	8.13	0.9	0.62	5.53
		Total	45.4		6.54		44.3	26.86			

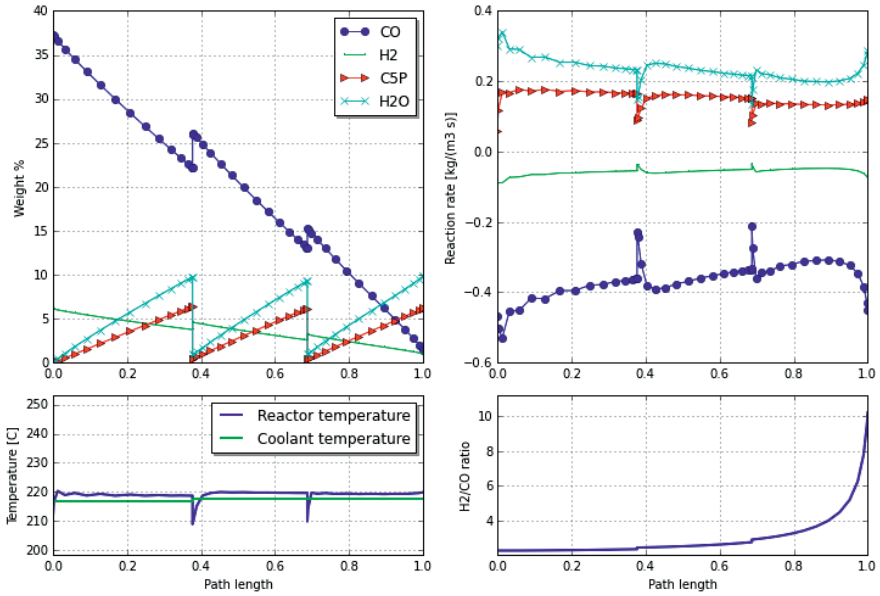

Figure 9.2: The case C-1.0 with Syngas 1

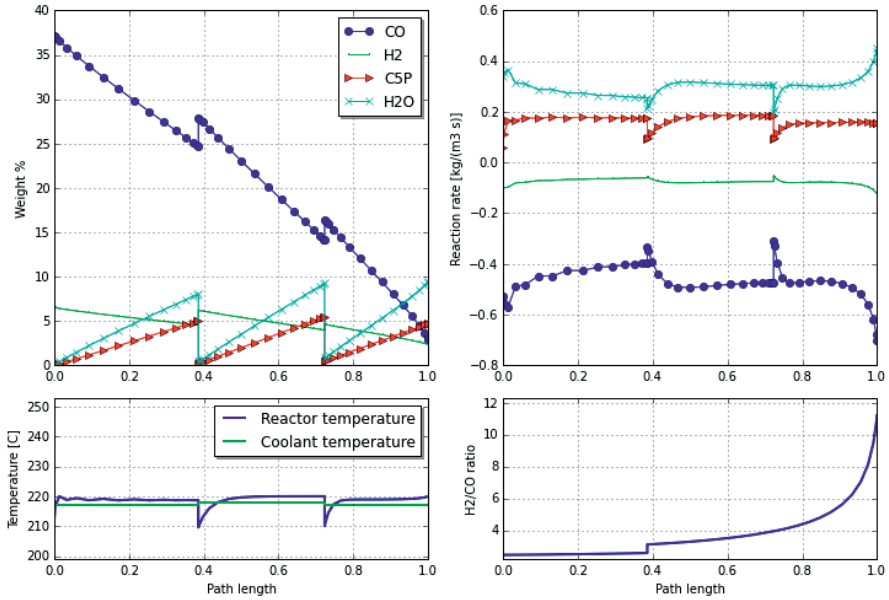

Figure 9.3: The case C-0.75 with Syngas 1

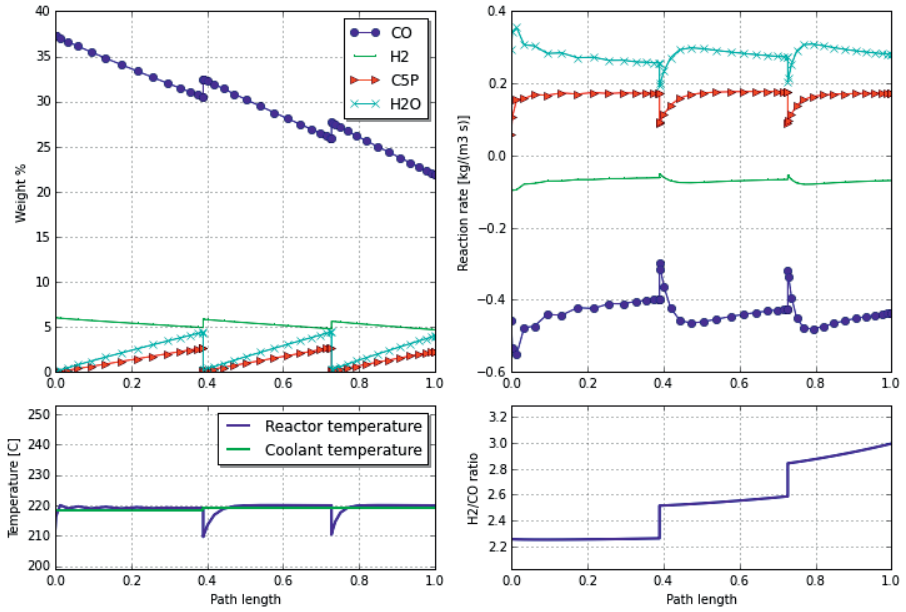

Figure 9.4: The case C-0.4 with Syngas 1

Chapter 10

Conclusions and Recommendations for Future Work

10.1 Concluding remarks

A novel process concept is proposed in chapter 4 for converting natural gas to liquid hydrocarbon products. The synthesis section is staged and hydrogen is fed between the stages to make up for the hydrogen consumption. Products and water are removed between the stages. This enables a high CO conversion in a once-through configuration. The process produces syngas and hydrogen in two parallel paths. Hydrogen is produced in a heat exchange reformer, heat integrated with the hot outlet from the ATR. The process does not require cryogenic air separation or fired heaters. With the proposed configuration, high once-through CO conversion, in the order of 90 % and more, is achieved. Conventional fixed bed and microchannel reactor models for the FT synthesis are developed and tested separately in process simulations. The carbon efficiencies for a once-through synthesis are calculated to be 57 and 62 % for the fixed bed and microchannel reactors, respectively. The part of the energy that ends up in the product is 45 and 50 % for the fixed bed and microchannel reactors. However, the fixed bed alternative produces more energy as steam and power for export. A natural gas with heavier gas gives more products and less excess hydrogen. As long as there is sufficient excess hydrogen for upgrading, the heavier natural gas NG2 gives a more favorable energy distribution. The process is autonomous as it is self-sufficient with power and water. The total investment of a 12000 bbl/day plant without considering the ship, buildings and structures or the upgrading unit is estimated to approximately 500 million USD with fixed bed reactors. Even when everything is not counted in the total cost, the proposed process concept is estimated to be less expensive than existing projects. The main reason for the low cost is that cryogenic air separation and the costly steam methane reformer are avoided.

In chapter 5, a new chain growth model is proposed based on microchannel experimental data. This chain growth model together with Ma et al. (2014) kinetic model predicted

the experimental data quite well. Twelve kinetic models are implemented in a plug flow reactor model and their behaviour to six different scenarios which are depicted in Figure 5.3 are investigated. These kinetic models are compared based on their response to CO conversion, H_2/CO ratio, H_2O/H_2 ratio and C_{5+} selectivities. The trends observed for under stoichiometric ratios of 2.0 and 1.5 are similar. r_9, r_{10} and r_{12} showed different behaviour than the rest of the models, mainly because they have the water effect in their structure. r_{12}, reached a singularity point at CO conversions of about 80 %. If it is to be used for reactor design purposes, this should be taken into account. r_1 goes to infinity at very high conversions (more than 95%) in overstoichiometric scenarios, because CO which is in denominator gets depleted. Effects of pressure on rate models and C_{5+} selectivity is also investigated. Two pressure levels (22 and 27 bar) are used for this comparison. Higher pressure yields higher rates for all kinetic models. But the effect of pressure on C_{5+} selectivity is the opposite, higher pressure yields lower C_{5+} selectivity. Effect of added water is also investigated on kinetic models and C_{5+} selectivities. For all rate models except models r_{10} and r_{12}, added water decreased reaction rates, mainly because the syngas pressure is lowered upon water addition to keep the total pressure constant. Upon water addition, C_{5+} selectivities increased by about 5% for all rate models. This study can be an starting point for researchers to look closer to structures of kinetic models.

In chapter 6, the verified kinetic rate and product distribution models of the Fischer-Tropsch synthesis are applied (Ostadi et al., 2016). The new and verified kinetic model yields higher reaction rates than what was used in chapter 4. The new kinetic model along with the product distribution model is specifically suited for microchannel reactor and it gives us a more realistic view of the process in the large scale. With the proposed configuration, high once-through CO conversion, in the order of 90 % and more, is achieved. The carbon efficiencies for a once-through synthesis are calculated to be 61 % and the energy efficiency is about 49 %. Compared to our previous investigation, this study produces the same amount of C_{5+} but in 45 % less volume which means lower cost of the overall GTL plant.

In chapter 7, in order to increase the profitability of the GTL process, cogeneration of ammonia is proposed. The total capital investment of a combined GTL and ammonia plant producing 12000 bbl/day of GTL products and 576 tonnes/day of ammonia without considering the FPSO, buildings and structures or the upgrading unit is estimated to approximately 900 million USD. Ammonia process alone will constitute 7% of this amount. The process is autonomous as it is self sufficient with power and water and therefore well suited for production in remote locations. Through ammonia cogeneration with GTL products, the sale revenues of the plant increases by about 50% which makes it commercially more attractive. The whole process is a low-cost process and addition of ammonia production makes it more profitable. The main reason for the low cost is that cryogenic air separation and the costly steam methane reformer and CO_2 capture units are avoided.

In chapter 8, process simulation of a once-through gas to liquid process with two different oxidants (enriched-air and oxygen) and utilizing microchannel reactors for FT synthesis is performed. Economic analysis indicates that installed cost of FT reactor and oxidant production equipment in enriched-air case is 18.6% higher than the case with oxygen. Moreover, the operating cost is 2.21 times higher in enriched-air case. This results in a higher net present value (NPV) for the oxygen case which makes it commercially more

attractive. Due to offshore limitations such as safety and space issues, having a cryogenic ASU is problematic, therefore enriched-air will be the preferred choice offshore. Furthermore, possibility of formation of NH_3 and HCN in ATR adds to the favorability of using oxygen as oxidant over enriched-air.

In the last chapter, the path optimization method of Hillestad (2010) on FT synthesis part of a GTL plant is performed. Through optimization of reactor path, increase in C_{5+} production and decrease in reactor volume is achieved. In other words, reactor productivity is enhanced by use of this method. It is highly recommended to use this method on other processes too. We do not claim that the reported results are the global optimum, because of very non-linear nature of the optimization problem and high possibility for existence of many local minima.

10.2 Directions for future work

The following points are suggested for future research work:

- More research can be done to find ways to increase the energy and carbon efficiencies of the proposed process in chapter 4.
- By advancement of technologies in production of process equipment, it may be possible to reduce the footprint of the proposed process even more.
- Modelling of the Heat Exchange Reformer (HER) can be done in MATLAB CAPE-OPEN, because of its robustness and easier implementation than in Aspen Custom Modeller (ACM). Moreover, it will make it easier to do sensitivity studies.
- Our chain growth model in chapter 5 is based on 18 experimental data points. It is of utmost importance to validate the model on a larger set of experimental data.
- In chapter 5, we have investigated the structures of 12 kinetic models. It will be rewarding to look into more kinetic models and come up with better structures.
- Path optimization is done with microchannel reactor with Ma et al. (2014) rate expression and our proposed chain growth model in chapter 9. This method can be used on fixed bed reactor and other kinetic models.

Bibliography

Aasberg-Petersen, K., Christensen, T., Dybkjær, I., Sehested, J., Ostberg, M., Coertzen, R., M., M. J., Keyser, & Steynberg, P., A. (2004). Chapter 4 - Synthesis gas production for FT synthesis. *Studies in Surface Science and Catalysis*, *152*, 258 – 405.

Agee, M. A. (1997). Gas to Liquids (GTL) Conversion: A New Option for Monetizing Natural Gas. *ASME Turbo Asia Conference*, (pp. 1–10).

AirProducts (2015). Stainless steel nitrogen membrane separator. *white paper*.

AmsterChem (2017). `http://www.amsterchem.com/`. Accessed: 2017-04-17.

Anderson, R. B. (1956). Deactivation of cobalt based Fischer-Tropsch catalysts: A review. *Catalysis*, *4*, 247– 283.

Anderson, R. B., Friedel, R. A., & Storch, H. H. (1951). Fischer-Tropsch Reaction Mechanism Involving Stepwise Growth of Carbon Chain. *The Journal of Chemical Physics*, *19*(3), 313.

Androulakis, I. P., & Reyes, S. C. (1999). Role of distributed oxygen addition and product removal in the oxidative coupling of methane. *AIChE Journal*, *45*, 860868.

Appl, M. (2000). *Ullmann's Encyclopedia of Industrial Chemistry*. Wiley-VCH Verlag GmbH and Co. KGaA.

Appl, M. (2007). *Ammonia: Catalysis and Manufacture*. Wiley-VCH Verlag GmbH.

AspenTechnology (2011). *Aspen HYSYS customization guide*. Aspen Technology Inc., Burlingtin, MA, USA.

Atashi, H., Siami, F., Mirzaei, A. A., & Sarkari, M. (2010). Kinetic study of Fischer-Tropsch process on titania-supported cobalt–manganese catalyst. *Journal of Industrial and Engineering Chemistry*, *16*, 952–961.

Azadi, P., Brownbridge, G., Kemp, I., Mosbach, S., Dennis, J. S., & Kraft, M. (2015). Microkinetic Modeling of the Fischer-Tropsch Synthesis over Cobalt Catalysts. *ChemCatChem*, *7*, 137–143.

Baten, J. V., & Szczepanski, R. (2011). A thermodynamic equilibrium reactor model as a cape-open unit operation. *Computers and Chemical Engineering*, *35*(7), 1251 – 1256.

Baxter, I. (2010). Modular GTL as an Offshore Associated Gas Solution. *Deep Offshore Technology International*, (pp. 1–19).

Becker, H., Guttel, R., & Turek, T. (2016). Enhancing internal mass transport in Fischer-Tropsch catalyst layers utilizing transport pores. *Catalysis Science & Technology*, *6*, 275–287.

Bey, O., & Eigenberger, G. (2001). Gas flow and heat transfer through catalyst filled tubes. *International Journal of Thermal Sciences*, *40*, 152–164.

Bhatelia, T., Ma, W., Davis, B., Jacobs, G., & Drabukur, G. (2011). Kinetics of the fischer-Tropsch reaction over a Ru-promoted Co/Al_2O_3 catalyst. *Chemical Engineering Transactions*, *25*, 707–712.

Borg, Ø., Storsæter, S., Eri, S., Wigum, H., Rytter, E., & Holmen, A. (2006). The effect of water on the activity and selectivity for g-alumina supported cobalt Fischer-Tropsch catalysts with different pore sizes. *Catalysis Letters*, *107*, 95–102.

Botes, F. G. (2009). Influences of Water and Syngas Partial Pressure on the Kinetics of a Commercial Alumina-Supported Cobalt Fischer-Tropsch Catalyst. *Industrial & Engineering Chemistry Research*, *48*, 1859–1865.

Botes, F. G., van Dyk, B., & McGregor, C. (2009). The Development of a Macro Kinetic Model for a Commercial $Co/Pt/Al_2O_3$ Fischer-Tropsch Catalyst. *Ammonia Plant Safety and Related Facilities*, *48*, 10439–10447.

Bouchy, C., Hastoy, G., Guillon, E., & Martens, J. A. (2009). Fischer-Tropsch waxes upgrading via hydrocracking and selective hydroisomerization. *Oil and Gas Science and Technology*, *64*(1), 91–112.

Brötz, W. (1949). Zur Systematik der Fischer-Tropsch Katalyse. *Zeitschrift fr Elektrochemie und angewandte physikalische Chemie*, *53*, 301–306.

Carson, N., Hawker, P., Whitley, N., Wright, A., Dunleavy, J., & Tomlinson, D. (2010). Presentation to Analysts/ Investors. *(white paper) Johnson Matthey*, (pp. 139–148).

Chaumette, P., Verdon, C., & Boucot, P. (1995). Influence of the hydrocarbons distribution on the heat produced during Fischer-Tropsch synthesis. *Topics in Catalysis*, *2*(1-4), 301–311.

Choi, G., Kramer, S., Tam, S., Fox, J., Carr, N., & Wilson, G. (1997). Design/economics of a once-through Fischer-Tropsch plant with power co-production. *paper presented at the Coal Liquefaction and Solid Fuels Contractors Review Conference, Pittsburgh, 34 September*.

COLaN (2017). `http://ww.colan.org/`. Accessed: 2017-04-23.

Dalai, A. K., & Davis, B. H. (2008). Fischer-Tropsch synthesis: A review of water effects on the performances of unsupported and supported Co catalysts. *Applied Catalysis A: General*, *348*, 1–15.

Das, T. K., Conner, W. A., Li, J., Jacobs, G., Dry, M. E., & Davis, B. H. (2005). Fischer-Tropsch Synthesis: Kinetics and Effect of Water for a Co/SiO_2 Catalyst. *Energy & Fuels*, *19*, 1430–1439.

Deshmukh, S. R., Tonkovich, A. L. Y., Jarosch, K. T., Schrader, L., Fitzgerald, S. P., Kilanowski, D. R., Lerou, J. J., & Mazanec, T. J. (2010). Scale-up of microchannel reactors for Fischer-Tropsch synthesis. *Industrial and Engineering Chemistry Research*, *49*, 10883 –10888.

Diakov, V., & Varma, A. (2004). Optimal Feed Distribution in a Packed-Bed Membrane Reactor: The Case of Methanol Oxidative Dehydrogenation. *Industrial & Engineering Chemistry Research*, *43*, 309–314.

Douglas, J. (1988). *Conceptual design of chemical processes*. McGraw-Hill, New York.

Dry, E., M, & Steynberg, P., A (2004). *Studies in Surface Science and Catalysis: Fischer-Tropsch Technology, Elsevier*, vol. 152, chap. 5 - Commercial FT Process Applications, (pp. 406 – 481).

DWSIM (2017). `http://dwsim.inforside.com.br/wiki/index.php?title=Main_Page`. Accessed: 2017-04-17.

Dybkjær, I., & Aasberg-Petersen, K. (2016). Synthesis gas technology large-scale applications. *The Canadian Journal of Chemical Engineering*, *94*, 607–612.

Dybkjær, I., & Christensen, T. S. (2001). Syngas for Large Scale Conversion of Natural Gas to Liquid Fuels. *Studies in Surface Science and Catalysis*, *136*, 435–440.

Dybkjær, I., & Nielsen, A. (1995). *Ammonia: Catalysis and Manufacture*. Springer Berlin Heidelberg.

Dyson, D. C., & Simon, J. M. (1968). Kinetic Expression with Diffusion Correction for Ammonia Synthesis on Industrial Catalyst. *Industrial & Engineering Chemistry Fundamentals*, *7*, 605–610.

Elbashir, N. O., & Roberts, C. B. (2004). Reaction pathway and kinetic modeling of Fischer-Tropsch synthesis over an alumina supported cobalt catalyst in supercritical-hexane. *American Chemical Society, Division of Petroleum Chemistry*, *49*, 157–160.

Elvidge, C. D., Zhizhin, M., Baugh, K., Hsu, F.-C., & Ghosh, T. (2016). Methods for global survey of natural gas flaring from visible infrared imaging radiometer suite data. *Energies*, *9*(1).

Ergun, S., & Orning, A. A. (1949). Fluid Flow through Randomly Packed Columns and Fluidized Beds. *Industrial & Engineering Chemistry*, *41*, 1179–1184.

Erkey, C., Rodden, J. B., & Akgerman, A. (1990). Diffusivities of synthesis gas and n-alkanes in fischer-tropsch wax. *Energy & Fuels*, *4*(3), 275–276.

Ermolaev, V. S., Gryaznov, K. O., Mitberg, E. B., Mordkovich, V. Z., & Tretyakov, V. F. (2015). Laboratory and pilot plant fixed-bed reactors for Fischer-Tropsch synthesis: Mathematical modeling and experimental investigation. *Chemical Engineering Science*, *138*, 1–8.

Falkenberg, M., & Hillestad, M. (2015). Modeling, simulation and design of three different concepts for offshore methanol production. *Submitted for publication*.

Fonseca, A., Bidart, A., Passarelli, F., Nunes, G., & Oliveira, R. (2012). Offshore gas-to-liquids : Modular solution for associated gas with variable CO2 content. *World gas conference*, (pp. 1–15).

Frtsch, D., Pabst, K., & Gro-Hardt, E. (2015). The product distribution in Fischer-Tropsch synthesis: An extension of the ASF model to describe common deviations. *Chemical Engineering Science*, *138*, 333–346.

Gillespie, L. J., & Beattie, J. A. (1930). The Thermodynamic Treatment of Chemical Equilibria in Systems Composed of Real Gases. I. An Approximate Equation for the Mass Action Function Applied to the Existing Data on the Haber Equilibrium. *Physical Review*, *36*, 743–753.

Guettel, R., & Turek, T. (2010). Assessment of micro-structured fixed-bed reactors for highly exothermic gas-phase reactions. *Chemical Engineering Science*, *65*(5), 1644–1654.

Guillou, L., Paul, S., & Le Courtois, V. (2008). Investigation of H_2 staging effects on CO conversion and product distribution for Fischer-Trospch synthesis in a structured microchannel reactor. *Chemical Engineering Journal*, *136*, 66–76.

Hansen, J. B. (1995). *Kinetics of Ammonia Synthesis and Decomposition on Heterogeneous Catalysts*, (p. 150). Ed. Anders Nielsen. Springer Science and Business Media.

He, X. (2011). *Developement of hollow fiber carbon membranes for CO_2 separation*. Ph.D. thesis, PhD Thesis, Norwegian University of Science and Technology, Department of Chemical Engineering.

Hillestad, M. (2010). Systematic staging in chemical reactor design. *Chemical Engineering Science*, *65*(10), 3301–3312.

Hillestad, M. (2015). Modeling the fischertropsch product distribution and model implementation. *Chemical Product and Process Modeling*, *10*(3), 147–159.

Hutton, W. J., & Holmes, J. (2005). Floating Gas to Liquids - A Solution to Offshore Stranded Gas. *18th World Petroleum Congress*.

Iglesia, E., Sebastian, C. R., & Stuart, L. S. (1993). *Reaction-transport selectivity models and the design of Fischer-Tropsch catalysts*, (p. 199). Computer-Aided Design of Catalysts, Marcel Dekker, New York.

Irankhah, A., Haghtalab, A., Farahani, E. V., & Sadaghianizadeh, K. (2007). Fischer-Tropsch Reaction Kinetics of Cobalt Catalyst in Supercritical Phase. *Journal of Natural Gas Chemistry*, *16*, 115–120.

Jager, B. (1997). Developments in fischer-tropsch technology. *Studies in Surface Science and Catalysis*, *107*, 219 – 224.

Jess, A., Hedden, K., & Popp, R. (2001). Diesel Oil from Natural Gas by Fischer-Tropsch Synthesis Using Nitrogen-Rich Syngas. *Chemical Engineering and Technology*, *24*, 27–31.

Jess, A., Popp, R., & Hedden, K. (1999). FischerTropsch-synthesis with nitrogen-rich syngas: fundamentals and reactor design aspects. *Applied Catalysis A: General*, *186*, 321–342.

Keyvanloo, K., Lanham, S. J., & Hecker, W. C. (2016). Kinetics of Fischer-Tropsch synthesis on supported cobalt: Effect of temperature on CO and H2 partial pressure dependencies. *Catalysis Today*, *270*, 9–18.

Kim, H. J., Choi, D. K., Ahn, S. I., Kwon, H., Lim, H. W., Denholm, D., Park, T., & Zhang, L. (2014a). OTC 24113 GTL FPSO : An Alternative Solution to Offshore Stranded Gas. *Oil and Gas Facilities*, *June 2014*, 41–51.

Kim, W. S., Yang, D. R., Moon, D. J., & Ahn, B. S. (2014b). The process design and simulation for the methanol production on the FPSO (floating production, storage and off-loading) system. *Chemical Engineering Research and Design*, *92*, 931–940.

Kirk-Othmer (2004). chap. Ammonia. Kirk-Othmer Encyclopedia of Chemical Technology; Published by Wiley InterScience.

Klinsrisuk, S., Tao, S., & Irvine, J. T. S. (2015). *Membrane Reactors for Energy Applications and Basic Chemical Production*, chap. 18 - Membrane reactors for ammonia production, (pp. 543 – 563). Woodhead Publishing.

Kolb, G. (2013). Review: Microstructured reactors for distributed and renewable production of fuels and electrical energy. *Chemical Engineering and Processing: Process Intensification*, *65*, 1–44.

Kresnyak, S. (2016). Process for co-producing commercially valuable products from byproducts of Fischer-Tropsch process for hydrocarbon fuel formulation in a GTL environment. Patent US 9,315,452.

Kreutz, L. E. L. G.-. W. R., T.G (2008). FischerTropsch Fuels from Coal and Biomass . *Proc. 25th Annual Pittsburg Coal Conference, Pittsburgh, PA,29 Sept-3 Oct*.

Krishnamoorthy, S., Tu, M., Ojeda, M. P., Pinna, D., & Iglesia, E. (2002). An investigation of the effects of water on rate and selectivity for the Fischer-Tropsch synthesis on cobalt-based catalysts. *Journal of Catalysis*, *211*, 422–433.

Kruit, K. D., Vervloet, D., Kapteijn, F., & van Ommen, J. R. (2013). Selectivity of the Fischer-Tropsch process: deviations from single alpha product distribution explained by gradients in process conditions. *Catalysis Science & Technology*, *3*, 2210–2213.

Krupiczka, R. (1967). Analysis of thermal conductivity in granular materials. *International Journal of Chemical Engineering*, *7*, 122–144.

Kwack, S. H., Bae, J. W., Park, M. J., Kim, S. M., Ha, K. S., & Jun, K. W. (2011). Reaction modeling on the phosphorous-treated ru/co/zr/sio2 fischer-tropsch catalyst with the estimation of kinetic parameters and hydrocarbon distribution. *Fuel*, *90*, 1383–1394.

Leviness, S., Deshmukh, S. R., Richard, L. A., & Robota, H. J. (2014). Velocys FischerTropsch synthesis thechnology-New advances on state- of-the-art. *Top catalysis*, *57*, 518–525.

Leviness, S., Tonkovich, A., Mazanec, T., & Jarosch, K. (2011). Improved Fischer-Tropsch economics enabled by microchannel technology. *white paper*, (pp. 1–7).

Li, J., Jacobs, G., Das, T., & Davis, B. H. (2002a). Fischer-Tropsch synthesis: effect of water on the catalytic properties of a ruthenium promoted Co/TiO_2 catalyst. *Applied Catalysis A: General*, *233*, 255–262.

Li, J., Jacobs, G., Das, T., Zhang, Y., & Davis, B. H. (2002b). Fischer-Tropsch synthesis: effect of water on the catalytic properties of a Co/SiO2 catalyst. *Applied Catalysis A: General*, *236*, 67–76.

Li, J., Zhan, X., Zhang, Y., Jacobs, G., Das, T., & Davis, B. H. (2002c). Fischer-Tropsch synthesis: effect of water on the deactivation of Pt promoted Co/Al_2O_3 catalysts. *Applied Catalysis A: General*, *228*, 203–212.

Loenhout, V., Zeelenberg, L., Gerritse, A., Roth, G., Sheehan, E., & Jannasch, N. (2006). Commercialization of Stranded Gas With a Combined Oil and GTL FPSO. *Offshore Technology Conference*.

Lögdberg, S., Boutonnet, M., Walmsley, J. C., S, J., Holmen, A., & A, B. E. (2011). Effect of water on the space-time yield of different supported cobalt catalysts during FischerTropsch synthesis. *Applied Catalysis A: General*, *393*, 109–121.

Lögdberg, S., Lualdi, M., Jrs, S., Walmsley, J. C., Blekkan, E. A., Rytter, E., & Holmen, A. (2010). On the selectivity of cobalt-based Fischer-Tropsch catalysts: Evidence for a common precursor for methane and long-chain hydrocarbons. *Journal of Catalysis*, *274*, 84–98.

Lowe, C., Gerdes, K., Stupin, W., Hook, B., & Marriott, P. (2001). Impact of syngas generation technology selection on a GTL FPSO. *Studies in surface science and catalysis*, (pp. 57–62).

Lox, E. S., & Froment, G. F. (1993). Kinetics of the Fischer-Tropsch reaction on a precipitated promoted iron catalyst 2. Kinetic modeling. *Industrial & Engineering Chemistry Research*, *32*, 71–82.

Ma, W., Jacobs, G., Ji, Y., Bhatelia, T., Bukur, D. B., Khalid, S., & Davis, B. H. (2011). Fischer-Tropsch synthesis: Influence of CO conversion on selectivities, H_2/CO usage ratios, and catalyst stability for a ru promoted Co/Al_2O_3 catalyst using a slurry phase reactor. *Top Catalysis*, *54*, 757–767.

Ma, W., Jacobs, G., Sparks, D. E., Spicer, R. L., Davis, B. H., Klettlinger, J. L. S., & Yen, C. H. (2014). Fischertropsch synthesis: Kinetics and water effect study over 25 *Catalysis Today*, *228*, 158–166.

Malhotra, A., Macris, A., & Gosnell, J. (2004). Increase Hydrogen Production Using KBRs KRES Technology. *National Petrochemical and Refiners Association*, (pp. 1–14).

Manenti, L.-G. A. R.-A. Z. . P. C., F (2014). Systematic staging design applied to the fixed-bed reactor series for methanol and one-step methanol/dimethyl ether synthesis. *Applied Thermal Engineering*, *70*, 1228–1237.

Mansouri, M., Atashi, H., Mirzaei, A. A., & Jangi, R. (2013). Kinetics of the Fischer-Tropsch synthesis on silica-supported cobalt-cerium catalyst. *International Journal of Industrial Chemistry*, *4*, 1–10.

Marano, J. J., & Holder, G. D. (1997). Characterization of fischer-tropsch liquids for vapor-liquid equilibria calculations. *Fluid Phase Equilibria*, *138*(1), 1 – 21.

Maretto, C., & Krishna, R. (2001). Design and optimisation of a multi-stage bubble column slurry reactor for FischerTropsch synthesis. *Catalysis Today*, *66*, 241–248.

Masanobu, S., Kato, S., Nakamura, A., Sakamoto, T., Yoshikawa, T., Sakamoto, A., Uetani, H., Kawazuishi, K., & Sao, K. (2004). Development of Natural Gas Liquefaction FPSO. *23rd internationa conference on offshore mechanics and arctic engineering*, (pp. 1–10).

Morales-Rodriguez, R., Gani, R., Dechelotte, S., Vacher, A., & Baudouin, O. (2008). Use of CAPE-OPEN standards in the interoperability between modelling tools (MoT) and process simulators (Simulis Thermodynamics and ProSimPlus). *Chemical Engineering Research and Design*, *86*(7), 823–833.

Mosayebi, A., & Haghtalab, A. (2015). The comprehensive kinetic modeling of the Fischer-Tropsch synthesis over Co@Ru/g-Al2O3 core–shell structure catalyst. *Chemical Engineering Journal*, *259*, 191–204.

Mosayebi, A., Mehrpouya, M. A., & Abedini, R. (2016). The development of new comprehensive kinetic modeling for Fischer-Tropsch synthesis process over Co-Ru/γ-Al_2O_3 nano-catalyst in a fixed-bed reactor. *Chemical Engineering Journal*, *286*, 416–426.

Nikparsaa, P., Mirzaeia, A. A., & Atashib, H. (2014). Effect of reaction conditions and Kinetic study on the Fischer-Tropsch synthesis over fused Co-Ni/Al_2O_3 catalyst. *Journal of Fuel Chemistry and Technology*, *42*, 710–718.

Ordomsky, V. V., Carvalho, A., Legras, B., Paul, S., Virginie, M., Sushkevich, V. L., & Khodakov, A. Y. (2016). Effects of co-feeding with nitrogen-containing compounds on the performance of supported cobalt and iron catalysts in FischerTropsch synthesis. *Catalysis Today*, *275*, 84 – 93.

Ostadi, M., Dalane, K., Rytter, E., & Hillestad, M. (2015). Conceptual design of an autonomous once-through gas-to-liquid process comparison between fixed bed and microchannel reactors. *Fuel Processing Technology*, *139*, 186–195.

Ostadi, M., & Hillestad, M. (2016). Conceptual design of an autonomous once-through gas-to-liquid process with microchannel Fischer-Tropsch reactors. *Chemical Engineering Transactions*, *52*, 523–528.

Ostadi, M., Rytter, E., & Hillestad, M. (2016). Evaluation of kinetic models for FischerTropsch cobalt catalysts in a plug flow reactor. *Chemical Engineering Research and Design*, *114*, 236 – 246.

Oudar, J. (1985). Deactivation and poisoning of catalysts. *CRC Press*, *20*, 259.

Outi, A., Rautavuoma, I., & Van der Baan, H. S. (1981). Kinetics and mechanism of the Fischer-Tropsch hydrocarbon synthesis on a cobalt on alumina catalyst. *Applied Catalysis*, *1*, 247–272.

Pannell, R., Kibby, C. L., & Kobylinski, T. P. (1980). *Proceedings of the Seventh International Congress on Catalysis, Tokyo*, *47*, 447–459.

Pedersen, S., P, & Yakobson, L., D (2007). Process for the production of ammonia and Fischer-Tropsch liquids. Patent US 7,300,642.

Pendyala, V. R. R., Jacobs, G., Bertaux, C., Khalid, S., & Davis, B. H. (2016). FischerTropsch synthesis: Effect of ammonia on supported cobalt catalysts. *Journal of Catalysis*, *337*, 80–90.

Perry, R. H., & Green, D. W. (2008). *Perry's chemical engineers' handbook*. McGraw-Hil: New York.

Peschel, A., Karst, F., Freund, H., & Sundmacher, K. (2011). Analysis and optimal design of an ethylene oxide reactor. *Chemical Engineering Science*, *66*, 6453–6469.

Price, G., J, & Tindall, A., B (2005). Natural gas conversion to hydrocarbons and ammonia. Patent US 6,900,247.

Rafiee, A., & Hillestad, M. (2012). Staging of the Fischer-Tropsch reactor with an iron based catalyst. *Computers and Chemical Engineering*, *39*, 75 – 83.

Rafiee, A., & Hillestad, M. (2013). Staging of the Fischer-Tropsch Reactor with a Cobalt-Based Catalyst. *Chemical Engineering & Technology*, *36*, 1729–1738.

Rao, V. U. S., Stiegel, G. J., Cinquegrane, G. J., & Srivastava, R. D. (1992). Iron-based catalysts for slurry-phase Fischer-Tropsch process: Technology review. *Fuel processing technology*, *30*, 83–107.

Rossetti, I., Pernicone, N., Ferrero, F., & Forni, L. (2006). Kinetic Study of Ammonia Synthesis on a Promoted Ru/C Catalyst. *Industrial & Engineering Chemistry Research*, *45*, 4150–4155.

Rostrup-Nielsen, J. R. (2002). Syngas in perspective. *Catalysis Today*, *71*(34), 243 – 247.

Rytter, E. (2010). Gas to liquids plant with consecutive Fischer-Tropsch reactors and hydrogen make-up. Patent US 2010/0137458 A1.

Rytter, E., Eri, S., Skagseth, T. H., Schanke, D., Bergene, E., Myrstad, R., & Lindvåg, A. (2007). Catalyst Particle Size of Cobalt/Rhenium on Porous Alumina and the Effect on FischerTropsch Catalytic Performance. *Industrial & Engineering Chemistry Research*, *46*, 9032–9036.

Rytter, E., & Holmen, A. (2015). Deactivation and Regeneration of Commercial Type Fischer-Tropsch Co-CatalystsA Mini-Review. *Catalysts*, *5*(2), 478–499.

Sarup, B., & Wojciechowski, B. W. (1989). Studies of the Fischer-Tropsch synthesis on a cobalt catalyst II. Kinetics of carbon monoxide conversion to methane and to higher hydrocarbons. *The Canadian Journal of Chemical Engineering*, *67*, 62–74.

Schanke, D., Hilmen, A. M., Bergene, E., Kinnari, K., Rytter, E., Adnanes, E., & Holmen, A. (1995). Study of the deactivation mechanism of Al_2O_3-supported cobalt Fischer-Tropsch catalysts. *Fuel processing technology*, *34*, 269–284.

Schanke, D., Lian, P., Eri, S., Rytter, E., Sannaes, B. H., & Kinnari, K. J. (2001). Optimisation of Fischer-Tropsch reactor design and operation in GTL plants. *Studies in Surface Science and Catalysis*, *136*, 239–244.

Schubert, P. F., Freerks, R., Thomlinson, H. L., & Russell, B. (2000). Fischer-Tropsch Diesel Fuel Preparation and Testing. *Preprints of symposia- division of fuel chemistry american chemical society*, *45*, 592–597.

Schulz, H., Claeys, M., & Harms, S. (1997). Effect of water partial pressure on steady state Fischer-Tropsch activity and selectivity of a promoted cobalt catalyst. *Studies in Surface Science and Catalysis*, (pp. 193–200).

Schulz, H., Vein Steen, E., & Claeys, M. (1994). Selectivity and mechanism of Fischer-Tropsch synthesis with iron and cobalt catalysts. *Studies in Surface Science and Catalysis*, (pp. 455–460).

Song, H., Ramkrishna, D., Trinh, S., & Wright, H. (2004). Operating strategies for fischer-tropsch reactors: A model-directed study. *Korean Journal of Chemical Engineering*, *21*, 308–317.

Spath, P. L., & Dayton, D. C. (2003). Preliminary Screening – Technical and Economic Assessment of Synthesis Gas to Fuels and Chemicals with Emphasis on the Potential for Biomass-Derived Syngas. *National Renewable Energy Laboratory*, (December), 1–160.

Steynberg, A. P., Dry, M. E., Davis, B. H., & Breman, B. B. (2004). *Chapter 2 - Fischer-Tropsch Reactors*, vol. Volume 152, (pp. 64–195). Elsevier.

Stoltze, P., & Nielsen, A. (1995). Structure and Surface Chemistry of Industrial Ammonia Synthesis Catalysts. *Ammonia: Catalysis and Manufacture, Springer Berlin Heidelberg*, (p. 85).

Storsæter, S., Borg, Ø., Blekkan, E. A., & Holmen, A. (2005). Study of the effect of water on Fischer-Tropsch synthesis over supported cobalt catalysts. *Journal of Catalysis*, *231*, 405–419.

Storsæter, S., Chen, D., & Holmen, A. (2006). Microkinetic modelling of the formation of C_1 and C_2 products in the Fischer-Tropsch synthesis over cobalt catalysts. *Surface Science*, *600*, 2051–2063.

Thomsen, S. G., Han, P. A., Loock, S., & Ernst, W. (2006). The first industrial experience with the Haldor Topsøe exchange reformer. *Ammonia Plant Safety and Related Facilities*, *47*, 259–266.

Todic, B., Bhatelia, T., Froment, G. F., Ma, W., Jacobs, G., Davis, B. H., & Bukur, D. B. (2013). Kinetic model of Fischer-Tropsch synthesis in a slurry reactor on Co-Re/Al2O3 catalyst. *Industrial and Engineering Chemistry Research*, *52*, 669–679.

Todic, B., Ma, W., Jacobs, G., Davis, B. H., & Bukur, D. B. (2014a). Co-insertion mechanism based kinetic model of the fischertropsch synthesis reaction over re-promoted co catalyst. *Catalysis Today*, *228*, 32 – 39.

Todic, B., Ma, W., Jacobs, G., Davis, B. H., & Bukur, D. B. (2014b). Effect of process conditions on the product distribution of FischerTropsch synthesis over a Re-promoted cobalt-alumina catalyst using a stirred tank slurry reactor. *Journal of Catalysis*, *311*, 325–338.

Todic, B., Ma, W., Jacobs, G., Davis, B. H., & Bukur, D. B. (2015). Erratum: CO-insertion mechanism based kinetic model of the Fischer-Tropsch synthesis reaction over Re-promoted Co catalyst. *Catalysis Today*, *242*(Part B), 386.

Tonkovich, A. L., Jarosch, K., Arora, R., Silva, L., Perry, S., McDaniel, J., Daly, F., & Litt, B. (2008). Methanol production FPSO plant concept using multiple microchannel unit operations. *Chemical Engineering Journal*, *135*, 2–8.

Towler, G., & Sinnott, R. (2013). *Chemical Engineering Design (Second Edition), Butterworth-Heinemann*.

Tsakoumis, N. E., Rnning, M., Borg, Ø., Rytter, E., & Holmen, A. (2010). Deactivation of cobalt based Fischer-Tropsch catalysts: A review. *Catalysis Today*, *154*, 162–182.

Turton, R., Bailie, R., Whiting, B., W, Shaeiwitz, A., J, & Bhattacharyya, D. (2012). *Analysis, Synthesis, and Design of Chemical Processes (Fourth Ediition)*. Prentice Hall, New Jersey.

Ulrich, G. D., & Vasudevan, T., P (2006). How to estimate utility costs . *Chemical Engineering, Available from http://www.che.com/*.

Van Baten, J. (2009). Rapid prototyping of unit operation models using generic tools and cape-open. *2009 AIChE Annual Meeting*.

Van Baten, J., & Pons, M. (2014). Cape-open: Interoperability in industrial flowsheet simulation software. *Chemie-Ingenieur-Technik*, *86*(7), 1052–1064.

Van Der Laan, G. P., & Beenackers, A. A. C. M. (1999). Kinetics and selectivity of the fischer-tropsch synthesis: A literature review. *Catalysis Reviews*, *41*, 255–318.

Van Steen, E., & Schulz, H. (1999). Polymerisation kinetics of the Fischer-Tropsch CO hydrogenation using iron and cobalt based catalysts. *Applied Catalysis A: General*, *186*, 309–320.

Vannice, M. (1977). The catalytic synthesis of hydrocarbons from H_2CO mixtures over the group viii metals. *Journal of Catalysis*, *50*(2), 228 – 236.

VDI (2010). *VDI Heat Atlas, 2nd eddition*. Springer, Berlin.

Venvik, H. J., & Yang, J. (2017). Catalysis in microstructured reactors: Short review on small-scale syngas production and further conversion into methanol, DME and Fischer-Tropsch products. *Catalysis Today*, *285*, 135–146.

Vervloet, D., Kapteijn, F., Nijenhuis, J., & Van Ommen, J. R. (2012). Fischer-Tropsch reaction-diffusion in a cobalt catalyst particle: aspects of activity and selectivity for a variable chain growth probability. *Catalysis Science & Technology*, *2*, 1221–1233.

Visconti, C. G., Tronconi, E., Lietti, L., Forzatti, P., Rossini, S., & Zennaro, R. (2011). Detailed kinetics of the fischer-tropsch synthesis on cobalt catalysts based on H-assisted CO activation. *Topics in Catalysis*, *54*, 786–800.

Visconti, C. G., Tronconi, E., Lietti, L., Zennaro, R., & Forzatti, P. (2007). Development of a complete kinetic model for the FischerTropsch synthesis over Co/Al2O3 catalysts. *Chemical Engineering Science*, *62*(18-20), 5338–5343.

Wang, J. (1987). *Physical, chemical and catalytic properties of borided cobalt Fischer-Tropsch catalysts*. Ph.D. thesis, Ph.D. Thesis, Brigham Young University, Provo, UT.

Wen, D., & Ding, Y. (2006). Heat transfer of gas flow through a packed bed. *Chemical Engineering Science*, *61*, 3532–3542.

Wilhelm, D. J., Simbeck, D. R., Karp, A. D., & Dickenson, R. L. (2001). Syngas production for gas-to-liquids applications: technologies, issues and outlook. *Fuel Processing Technology*, *71*(13), 139–148.

Withers, H. P., Eliezer, K. F., & Mitchell, J. W. (1990). Slurry-phase Fischer-Tropsch synthesis and kinetic studies over supported cobalt carbonyl derived catalysts. *Industrial & Engineering Chemistry Research*, *29*, 1807–1814.

Wojciechowski, B. W. (1988). The Kinetics of the Fischer-Tropsch Synthesis. *Catalysis Reviews*, *30*, 629–702.

Yang, C. H., Massoth, F. E., & Oblad, A. G. (1979). Kinetics of CO + H_2 reaction over Co-Cu-Al_2O_3 catalyst. *Hydrocarbon Synthesis from Carbon Monoxide and Hydrogen, American Chemical Society*, *178*, 35–46.

Yang, J., Eiras, S. B., Myrstad, R., Venvik, H. J., Pfeifer, P., & Holmen, A. (2016). Fischer-Tropsch Synthesis on Co-based Catalysts in a Microchannel Reactor, effect of temperature and pressure on selectivity and stability. *Chemical Engineering Journal*, *223*, 259–266.

Yates, I. C., & Satterfield, C. N. (1991). Intrinsic kinetics of the Fischer-Tropsch synthesis on a cobalt catalyst. *Energy & Fuels*, *5*, 168–173.

Yermakova, A., & Anikeev, V. I. (2000). Thermodynamic Calculations in the Modeling of Multiphase Processes and Reactors. *Industrial & Engineering Chemistry Research*, *39*, 1453–1472.

Zennaro, R., Tagliabue, M., & Bartholomew, C. H. (2000). Kinetics of Fischer-Tropsch synthesis on titania-supported cobalt. *Catalysis Today*, *58*, 309–319.

Zhou, P., Lu, Y., & Rueter, M. (2003). Integrated process for the production of hydrocarbon liquids and ammonia. Patent US 6,586,480.

Appendices

Appendix A

MATLAB as a CAPE-OPEN unit operation in HYSYS

A.1 What is CAPE-OPEN

CAPE-OPEN is a collection of open software interface standards that describe the interaction between flowsheet software components (Douglas, 1988). These set of standards facilitate interoperability between process simulators and cover most aspects of process simulation activities: Unit operations, Thermodynamics, Physical properties, Numerics, etc. COLaN is a non-profit organization and is responsible for setting the standards (COLaN, 2017).

All process simulators have built-in models and if a user wants to add a user defined model, they should obey the custom interface (Figure A.1). These custom interfaces differ between different process simulators. Therefore if user writes a custom model for process simulator A, it can not be used in process simulator B, unless it obeys the custom interface of process simulator B.

If a unit operation is CAPE-OPEN compliant, it can be used in any process simulation software that are CAPE-OPEN compliant (Figure A.2). End-user can plug any CAPE-OPEN compliant property package or unit operation (PMC) into any CAPE-OPEN compliant process modelling environment (PME) (Figure A.3).

Most process simulation software (like Aspen HYSYS, Aspen Plus, VMGsim, etc) have CAPE-OPEN sockets which means they accept CAPE-OPEN unit operations and property packages. There are two process simulation software that are completely based on CAPE-OPEN and are free to download and use: COCO (AmsterChem, 2017) and DWSIM which is open source (DWSIM, 2017).

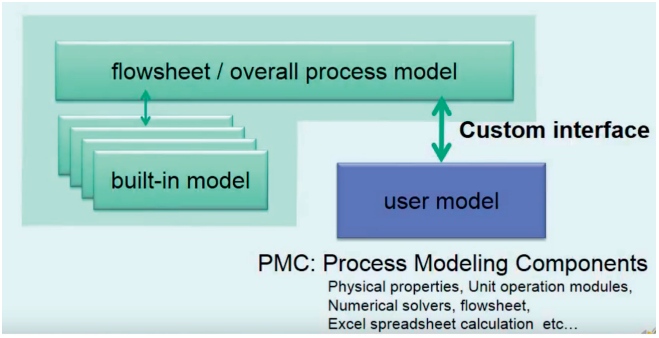

Figure A.1: Process simulator structure

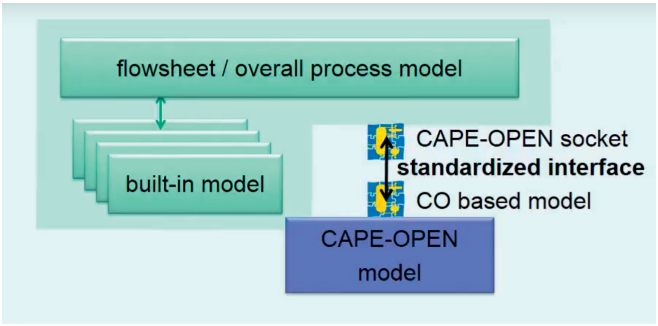

Figure A.2: Process simulator interface with CAPE-OPEN

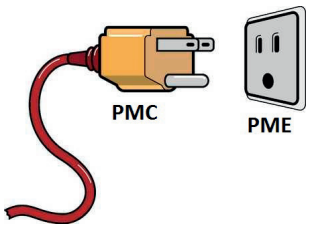

Figure A.3: Plug and play feature of CAPE-OPEN

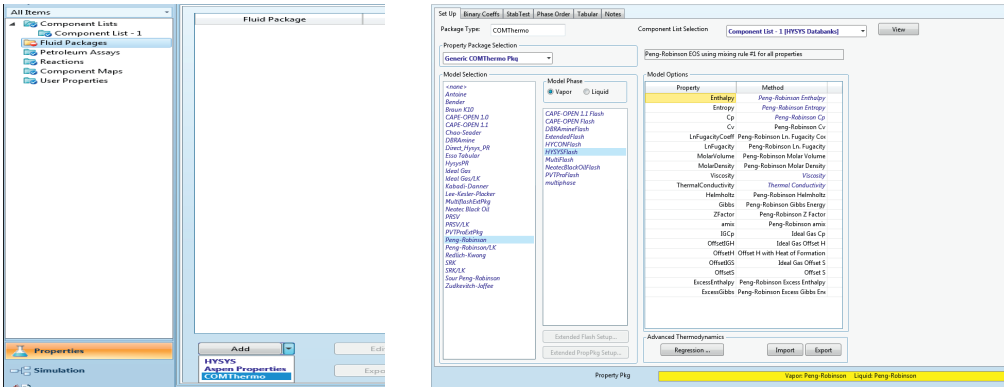

(a) **(b)**

Figure A.4: a) Step 2: Choose COMThermo fluid package type, b) Step 3: Choose Equation of State

A.2 MATLAB CAPE-OPEN Unit Operation

It is a CAPE-OPEN compliant unit operation downloadable from `http://www.amsterchem.com/`. You need to request a license from the website (free for non-commercial use). This website has other CAPE-OPEN compliant unit operations and also a completely CAPE-OPEN based process modelling environment named COCO.

A.3 Use of CAPE-OPEN in HYSYS

A.3.1 Create CAPE-OPEN fluid package from HYSYS:

In order to use a CAPE-OPEN unit operation in HYSYS, the streams (ports) connected to that unit operation need to have CAPE-OPEN fluid package (this is the case with the latest version of HYSYS which is 8.9. This requirement may change in future versions). Therefore we need to create our CAPE-OPEN fluid package. Here we create it in HYSYS, but it is not the only way to create a CAPE-OPEN fluid package. We need to do it once if we want to use the same components in all our simulations. The following steps need to be taken to create CAPE-OPEN fluid package in HYSYS:

1- Add your components

2- Choose COMThermo fluid package type (FigureA.4a)

3- Choose Equation of State for both liquid and vapour phases (FigureA.4b)

4- Export the created fluid package (FigureA.5a)

5- Give it a name and save it as ”COMThermo Property Package (.ctf)” in this folder (FigureA.5b) :

`C:\ProgramFiles(x86)\CommonFiles\Hyprotech\COMThermo\CTFFiles`

Now our CAPE-OPEN fluid package is created and we can use it in HYSYS. With following steps the created CAPE-OPEN fluid package be used to do simulations in HYSYS or any other CAPE-OPEN compliant process simulator.

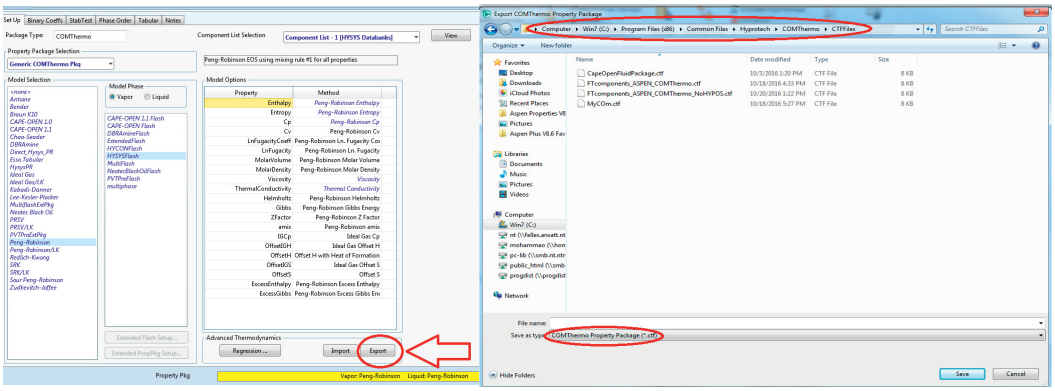

(a) **(b)**

Figure A.5: a) Step 4: Export the created fluid package, b) Step 5: Save it as ”COMThermo Property Package (.ctf)”

1- Choose COMThermo fluid package type (FigureA.6a)

2- Choose CAPE-OPEN property package both for Vapour and Liquid phases (FigureA.6b)

3- Choose the fluid package that you created under Aspen COM Thermo (FigureA.7a)

4- Click on ”Extended PropPkg Setup” (FigureA.7b)

5- Click on ”Finish Setup...” and then click ”OK” (FigureA.8a)

6- Go to simulation environment

7- Choose CAPE-OPEN unit Operation (FigureA.8b)

8- Choose MATLAB CAPE-OPEN unit operation (FigureA.9a)

9- The resulting unit operation will look like FigureA.9b

You can enter your MATLAB code as in Figure A.10. There are a few commands to communicate between MATLAB and HYSYS which are given in the product website (AmsterChem, 2017). An example MATLAB code of a mixer is shown in Figure A.11.

There are some example codes provided by `Amsterchem.com` which can be loaded into MATLAB CAPE-OPEN Unit Operation. These examples can be found in the installation folder of Matlab CAPE-OPEN Unit Operation:

```
C:\ProgramFiles\MatlabCAPE-OPENUnitOperation\Examplemodels
```

A.4 Sending model to another user

Requirements for the other user to be able to run your simulation:

- HYSYS and MATLAB CAPE-OPEN unit operation should be installed
- The same fluid package (.ctf file) should be used

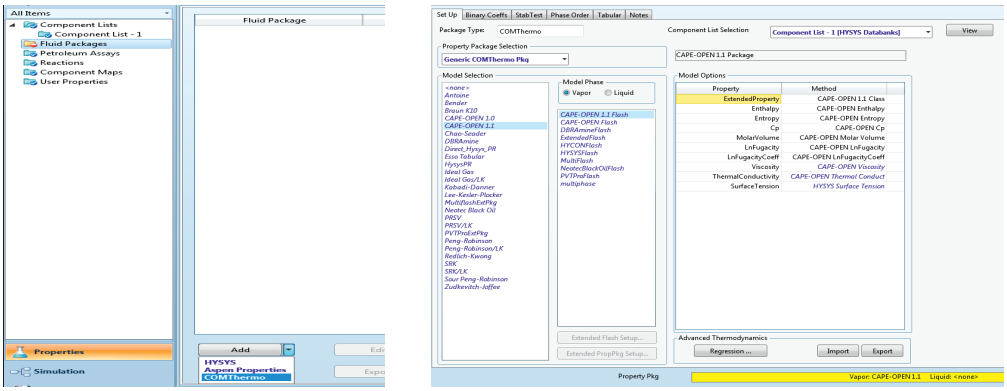

(a) **(b)**

Figure A.6: a) Step 1: Choose COMThermo fluid package type, b) Step 2: Choose CAPE-OPEN property package both for Vapour and Liquid phases

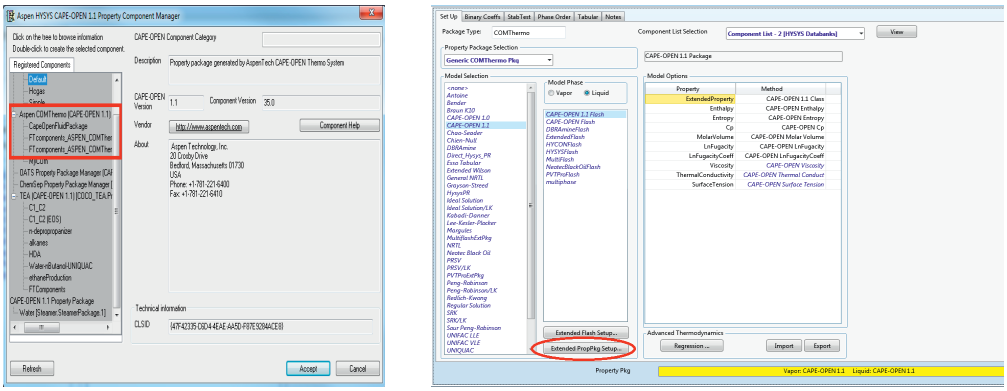

(a) **(b)**

Figure A.7: a) Step 3: Choose the fluid package that you created under Aspen COM Thermo, b) Step 4: Click on "Extended PropPkg Setup"

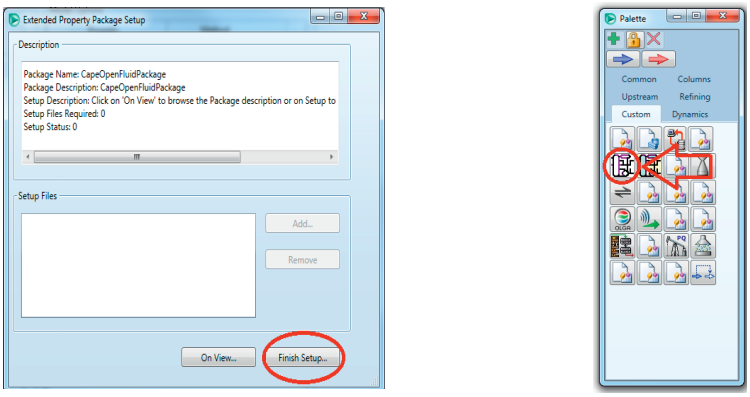

(a) **(b)**

Figure A.8: a) Step 5: Click on ”Finish Setup...” , b) Step 7: Choose CAPE-OPEN unit Operation

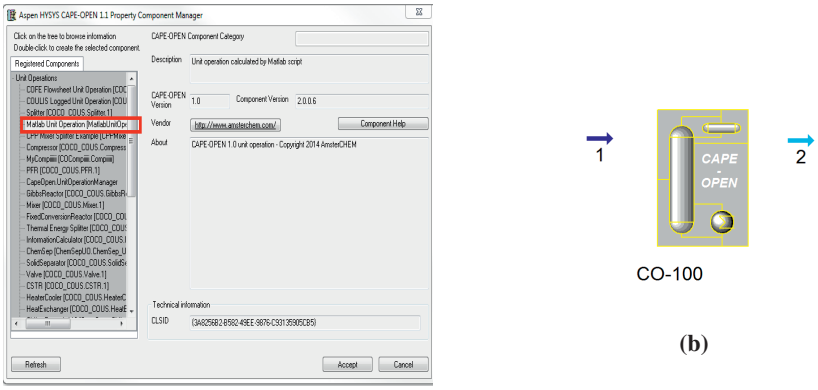

(a) **(b)**

Figure A.9: a) Step 8: Choose MATLAB CAPE-OPEN unit operation, b) Resulting unit operation

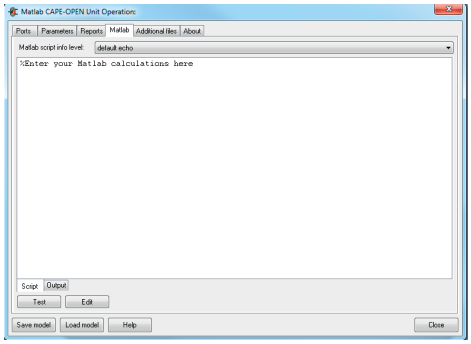

Figure A.10: Enter your MATLAB code

```
1
2     %Simple mixer code
3
4 -   ft1=getFeedProp(1,'totalflow');  %Total molar flow port 1 [kmol / s]
5 -   ft2=getFeedProp(2,'totalflow');  %Total molar flow port 2 [kmol / s]
6 -   z1=getFeedProp(1,'fraction');  %Mol fractions port 1
7 -   z2=getFeedProp(2,'fraction');  %Mol fractions port 2
8 -   f1=z1*ft1;   % Component molar flows port 1 [kmol / s]
9 -   f2=z2*ft2;   % Component molar flows port 2 [kmol / s]
10
11
12 -  h1=getFeedProp(1,'enthalpy');     %[J / mol]
13 -  h2=getFeedProp(2,'enthalpy');     %[J / mol]
14 -  p1=getFeedProp(1,'pressure');     %Pa
15 -  p2=getFeedProp(2,'pressure');     %Pa
16 -  p=min(p1,p2);
17 -  f=f1+f2;
18 -  h=(h1*f1+h2*f2)/f;
19 -  totF=sum(f);
20 -  setProduct(1,totF,f/totF,'pressure',p,'enthalpy',h)   % assign values to outlet port
```

Figure A.11: Example MATLAB code in MATLAB CAPE-OPEN

A.5 Useful links

Useful links:

- AmsterChem: `http://www.amsterchem.com/matlabunitop.html`
- COLaN: `http://www.colan.org/`
- CAPE-OPEN Forum for discussions about CAPE-OPEN standards: `http://www.cape-open-forum.org/viewforum.php?f=5`